Fast Contrast Enhanced Imaging with Projection Reconstruction

by

Dana Ceceilia Peters

A dissertation submitted in partial fulfillment
of the requirements for the degree of

Doctor of Philosophy
(Physics)

at the
UNIVERSITY OF WISCONSIN – MADISON
1999

Fast Contrast Enhanced Imaging with Projection Reconstruction

Dana C. Peters

Under the supervision of Professor Charles A. Mistretta

Abstract

The use of contrast agents has lead to great advances in magnetic resonance angiography (MRA). Here we present the first application of projection reconstruction to contrast enhanced MRA. In this research the limited angle projection reconstruction (PR) trajectory is implemented to acquire higher resolution images per unit time than with conventional Fourier transform (FT) imaging. It is well known that as the FOV is reduced in conventional spin-warp imaging, higher resolution per unit time can be obtained, but aliasing may appear as a replication of outside material within the FOV. The limited angle PR acquisition also produces aliasing artifacts. This method produced artifacts which were unacceptable in X-ray CT but which appear to be tolerable in MR Angiography. Resolution throughout the FOV is determined by the projection readout resolution and not by the number of projections. As the number of projections is reduced, the resolution is unchanged, but low intensity artifacts appear. This thesis presents the outcome of using limited angle PR for contrast-enhanced angiography.

Acknowledgments

My research in MRI began after I left the Space Physics group. I can still remember how exciting and uncertain that time was. I thank Professors Hakki Ogelman and Loyal Durand for their support then. Viji and Samar in the physics department helped me then and throughout. Tom Eiler, Daniel Lewis and Suzanne Way helped me with their imagination and spirit and love of adventure.

My interest in medical physics originated with a physics colloquium by John Cameron. I asked to work in the biomagnetism lab, and that began an immense journey that ended with research in MRI. I thank Professor James Sorenson for his excellent course on MRI. I thank Professor Wakai for encouraging me to speak to Chuck Mistretta.

I first met my advisor, Professor Charles A. Mistretta, on a day of a total solar eclipse, which could not too greatly signal the experience ahead. His creativity and endless ideas are wonderful. He encouraged me to believe in my ideas and work, and taught by example how to be human and a scientist together. He taught me how to put meaning and purpose and care into talks and papers and interactions with people.

I am greatly indebted to Frank Korosec for teaching me how to perform MR research. He has incredible clarity and great interest in all developments in MR, and his advice during a scan was often the determining factor of its success. His presence in our MR lab raises the level of carefulness, and accuracy and truth.

Dr. Thomas Grist was the main investigator for many research projects. I thank Tom for his high standards for images, his appreciation for high spatial and temporal resolution and his readiness to try the most experimental ideas. Working with him was very productive and creative time, because of his energy for discovery.

Kris Wedding, a friend and fellow graduate student, was the first (and probably only!) "progressive" physicist I have met. I have valued the friendship and incisive ideas of Yousef Mazaheri. Richard Frayne has taught me much about MR angiography. Tim Carroll's seriousness about physics and humour about life helped in ways I cannot now trace. I am indebted to Karl Vigen, who I feel can make any idea a reality on the MR scanner. I thank Orhan Unal for sharing his great knowledge about computers.

I thank Wally Block for sharing his experience and knowledge about non-Cartesian acquisitions. I thank Professor James Holden for his new ideas concerning projection reconstruction. Emilio Esparza has encouraged me to think about science internationally; Andrew Barger has shown me the power of taking work seriously. I also thank Oliver Wieben and Dean Skuldt for their encouragement and willingness to listen (to MR and to music!). I am indebted to Jason Polzin, Bryan Mock, Greg Wilson, Greg Cron, Jiang Du, Michelle Quigley, and Deitmar Cordes. I thank Sandra Fuller, Brett Borowski, Cathy Robichaud, and Al Rappe for their help.

I thank my brother Alan, and my sister Susanna, for their love and for the trips, conversations and criticisms. I thank my father for teaching me not to be afraid of science, or of life, or of trouble. I thank Jeremy, Paul, Ann Ivey, and Tom for their friendship. There are other friends whose help I feel I can never fully return, and they do not suspect how grateful I am.

I thank God for bringing me here. This thesis is dedicated to my mother, Margeret Peters, for her love and for teaching me to hope.

Contents

Abstract **i**

Acknowledgments **ii**

1 Introduction **1**

1.1 Motivation 1

1.1.1 X-ray Angiography 2

1.1.2 Contrast MR Angiography 4

1.1.3 The Interdependence of SNR, Imaging Time and Resolution 5

1.2 Outline 7

2 Background **9**

2.1 Nuclear Magnetic Resonance 9

2.1.1 Bulk Magnetization 10

2.1.2 The Bloch Equations 11

2.1.3 T1 and T2* 13

2.1.4 The Basic NMR Experiment 14

2.2 Fourier Encoding 15

2.2.1 The Fourier Transform 15
2.3 Spatial Encoding in MRI 19
2.3.1 Gradient fields 20
2.3.2 MRI Pulse Sequences 20
2.3.3 RF Excitation of spins 22
2.3.4 Spatial Encoding in X and Y 23
2.3.5 Conclusion 27
2.4 MR Angiographic Methods 27
2.4.1 Time-of-Flight 27
2.4.2 Phase-Contrast Imaging 29
2.4.3 Contrast-enhanced MRA 30
2.4.4 Diagnostic Purpose of MRA 31

3 Contrast-enhanced Angiography 32

3.1 Fast Gradient Echo Imaging 32
3.2 Description of Contrast Agents 35
3.2.1 Injection Protocol 36
3.2.2 Cost and Toxicity 36
3.2.3 Contrast Agent's Effect on Signal 37
3.2.4 The Relationship of the MR Signal to T1 38
3.2.5 Ernst Angle and Over-tipping 40
3.2.6 Dependence of SNR on Concentration 42
3.2.7 Influence of Injection Parameters on In-Vivo Concentration 44
3.2.8 Models of Contrast Agent Dilution 45
3.2.9 Equilibrium Concentration 54

3.2.10 The Outer Limits of Contrast Enhancement 56
3.2.11 Extravascular Contrast Agents 59
3.2.12 Intravascular Contrast Agents 60
3.3 Acquisition Order for Contrast-enhanced MRA: Theory 64
3.4 Acquisition Timing 65
3.4.1 Best guess 66
3.4.2 Dose timing scan 66
3.4.3 Automatic Bolus Detection 68
3.4.4 Fluoroscopic Triggering 68
3.4.5 Timing Methods: Breath-holding 68
3.5 Acquisition Orders 69
3.5.1 Acquisition Order Overview 70
3.5.2 Sequential Imaging 70
3.5.3 Centric order 71
3.5.4 Elliptical Centric View Order 72
3.5.5 3D-TRICKS 73
3.5.6 2D Projection Imaging 78
3.5.7 Multi-Frame Fast Imaging 79
3.6 Conclusions 79

4 Fast Imaging **81**
4.1 Low Resolution Methods 83
4.2 Unusual Trajectories 83
4.3 Short TR 84
4.3.1 Fractional Echo 85

4.3.2 Short Data acquisition Window 85
4.3.3 Short RF Pulses 89
4.3.4 Removing Non-essential Pulses 91
4.3.5 Use of Maximum Gradient Slew Rates 92
4.3.6 Conclusion 92
4.4 Acquisition Methods 93
4.5 Partial K-space Acquisition 94
4.5.1 Theory of Homodyne 94
4.5.2 Phase Detection 96
4.5.3 Filters for Implementation 97
4.5.4 Fractional Echoes 98
4.5.5 Partial Ky Acquisitions 100
4.5.6 Doubly Asymmetric Acquisitions 101
4.5.7 SNR and Resolution Changes Due to Homodyne Processing 104
4.5.8 Discussion of Homodyne 107
4.6 Reduced FOV 107
4.7 Sparse Sampling Schemes 111
4.8 Steady State Imaging 111
4.9 Conclusions 113

5 Limited Angle Projection Reconstruction 114

5.0.1 Outline 115
5.1 Small FOV concept: Theory and Simulations 116
5.2 Pulse Sequence Implementation 120
5.2.1 Disabled Acquisitions 121

- 5.2.2 Off-Center FOV 122
5.3 Contrast Enhanced Acquisitions with PR 124
- 5.3.1 ZIPR Acquisition Method 125
- 5.3.2 PRIZE Acquisition Method 126

5.4 Results: Phantoms 127
5.5 Results: Volunteer Studies 130
- 5.5.1 ZIPR Imaging in Volunteers 131
- 5.5.2 Interleaved ZIPR Methods 139
- 5.5.3 PRIZE Imaging in Volunteers 146
- 5.5.4 Renal Artery Imaging using PRIZE 147
- 5.5.5 Pulmonary Images Obtained with PRIZE 150
- 5.5.6 Carotid Artery Images Obtained using PRIZE 152
- 5.5.7 Conclusions: Contrast enhanced PR 156

5.6 Signal-to-Noise Ratio for PR 160
- 5.6.1 SNR for PR due to Ram-Lak Filter 160
- 5.6.2 Experimental Verification of SNR Factors 163
- 5.6.3 SNR in Undersampled PR 164
- 5.6.4 In-vivo SNR Measurements 165
- 5.6.5 Conclusion: SNR 167

5.7 Reconstruction Methods for PR 169
- 5.7.1 Filtered Backprojection 169
- 5.7.2 Regridding 173
- 5.7.3 Filters 174
- 5.7.4 Complex vs. Magnitude Backprojection 177

- 5.7.5 PR Homodyne 180
- 5.7.6 Projection by Projection Homodyne 184
- 5.7.7 Fractional Echo Artifacts 185
- 5.7.8 K-space Centering 186
- 5.7.9 Off-resonance Artifacts 187
- 5.7.10 Gradient De-warping for PR 190
- 5.7.11 Eddy Currents 192

5.8 Artifacts 193

- 5.8.1 Artifacts: Theoretical 194
- 5.8.2 Phantom Measurements of Artifact 205
- 5.8.3 In-vivo Measurements of Artifact 207
- 5.8.4 Artifact Removal Algorithm 212

5.9 Other Implementations of PR 217

- 5.9.1 Present Uses of Limited Angle PR 217
- 5.9.2 Future Uses of Limited Angle PR 217

5.10 Conclusion 220

Bibliography **222**

List of Figures

1.1 X-ray DSA image of the renal arteries. 3

1.2 For current MRI methods, SNR, imaging time, and spatial resolution are interdependent. 6

1.3 The link between imaging time and resolution is broken. 7

2.1 Aliasing in Fourier transform imaging. 18

2.2 An MRI pulse sequence diagram. 21

2.3 The phase of spins along the y direction during phase encoding. . 26

3.1 $Mz(n)sin(\theta)$ vs. the number of RF pulses, n. 39

3.2 Signal near the Ernst angle 41

3.3 Signal vs. concentration 43

3.4 Injection rate's influence on bolus shape. 51

3.5 Site dependence of concentration. 52

3.6 Signal vs. time in the carotids for 2 mls and 42 mls of contrast. . 53

3.7 Slices from a 3D volume of the heart. 62

3.8 A steady state MIP of the legs using intravascular agent. 63

3.9 Image slice and k-space representation. 70

3.10 K-space grid 71

3.11 Omnis k-space est divisa in quattor partes. 74

3.12 Arterial and mixed phases of the pulmonary vessels 77

3.13 Arrival of contrast into the pulmonary vessels. 78

4.1 One interleaf of an Archimedean spiral. 85

4.2 Projection reconstruction trajectory, showing 7 projections. 86

4.3 Pulse sequence timing diagram for the 3D fast gradient echo sequence. 87

4.4 0.5 ms truncated sinc RF pulse. 91

4.5 In partial k-space acquisitions, only a fraction of k-space is acquired. 94

4.6 Filter used for homodyne detection. 99

4.7 Spatial resolution improvement with homodyne compared to zerofilling 100

4.8 Phantom reconstructed with missing quadrants of k-space data. . 103

4.9 Slice profile of 1.28 ms minimum phase alpha pulse 104

4.10 The real and imaginary components of the point spread function with fractional k-space and zerofilling. 106

4.11 Result of de-aliasing with the Fredrickson-Pelc algorithm 110

5.1 The projection reconstruction trajectory. 117

5.2 Two objects provide artifact in the vicinity of each other. 120

5.3 The 3D projection reconstruction pulse sequence 122

5.4 Two acquisition orders, ZIPR and PRIZE. 126

5.5 Resolution phantom used to measure resolution. 128

5.6 Resolution phantom for 512 x 128 PR, 512 x 128 FT, 512 x 512 FT, and 512 x 400 FT. 129

5.7 A plot approximating the "MTF" of 128 PR, 512 FT, 128 FT and 400 FT. 130

5.8 MIPS from a contrast enhanced ZIPR study of the femorals using (clockwise from top left image) 400, 200, 100, and 50 projections for reconstruction. 132

5.9 A comparison of PR (left) and FT (right) for an identical slice (top) and the MIP (bottom) showing higher resolution for PR. 133

5.10 A contrast curve from a contrast enhanced ZIPR study of the pulmonaries, generated using Equation 5.7 134

5.11 A pulmonary MIP generated from a scan with unequally enhanced projections (left) and the same MIP after reweighting (right) . . . 135

5.12 Four frames from a multi-frame ZIPR exam of the femoral arteries. 136

5.13 Contrast curve generated by the projection data for the three frame ZIPR exam of the femorals 137

5.14 FT (left) vs. ZIPR (right) MIPs of the renal arteries. 138

5.15 Interleaved ZIPR acquisition, acquiring smaller sets of interleaved angles, over the entire angular range. 141

5.16 Two consecutive frames (32 projections each) and full set from an interleaved ZIPR exam of the renal arteries 142

5.17 Comparison of the contrast curves generated from the the dose timing scan and the projections of the ZIPR exam 144

5.18 Comparison of identically targeted MIPs from the first and second interleafs 145

5.19 Interleaved Pulmonary exam, two targeted MIPs from the second interleaf shown, 512 x 90 Np 146
5.20 Comparison of PR (left) and FT (right) both in slices (top) and MIPs (bottom) for 17 second scan 147
5.21 Obliquely reformatted MIPs of the left renal with PR and FT. . . 148
5.22 PRIZE MIPs of the renal and mesenteric arteries. 149
5.23 Single slice from pulmonary PRIZE scan 151
5.24 MIP comparison of PRIZE and FT in the pulmonaries 152
5.25 A PRIZE study of the carotid arteries. 153
5.26 PRIZE MIP of the carotid arteries 154
5.27 PRIZE MIP of the carotid arteries, sagittal acquisition. 155
5.28 SNR vs. SNR predictors 166
5.29 The process of obtaining projections of the object 170
5.30 The process of obtaining projections of the object. 171
5.31 The result of backprojection of a single bright pixel. 172
5.32 Resolution comparison of regridding and filtered backprojection. . 175
5.33 Backprojection vs. Regridding in a resolution phantom, a cross-section comparison. 176
5.34 Joseph's filter compared to the Ram-Lak filter. 177
5.35 a section of the resolution phantom acquired as 512 x 128 projections, and reconstructed with (left) the Pipe filter and (right) the Ram-Lak filter 178
5.36 Comparison of pulmonary MIPs using Pipe filter (left) and Ram-Lak filter (right). 179

5.37 MIPs of the renal arteries using phase-less and phase-sensitive reconstructions. 180

5.38 MIPs of the renal arteries using phase-less and phase-sensitive reconstructions. 181

5.39 Homodyne processing in PR. 184

5.40 QA phantom reconstructed by complex backprojection (a) and magnitude backprojection (b). 186

5.41 Midsection of the QA phantom with a series of k-space pixel shifts. 188

5.42 PR images acquired on-resonance and 300 Hz off-resonance. . . . 189

5.43 High bandwidth PR and FT are immune to off-resonance artifacts. 190

5.44 Grad Warp applied to the legs for PR. 192

5.45 Two Gaussian blobs, before and after undersampling. 195

5.46 The artifact from a Gaussian blob, analytical model. 198

5.47 The point spread function for 256 Nr and Np = 256, 128, 64, and 32. 199

5.48 Sampled points on the convolution kernel 201

5.49 Points on the convolution kernel that are sampled in the filtered back projection process. 203

5.50 The point spread functions for 512 Nr and Np = 64, for circular and elliptical rFOVs. 205

5.51 SNR vs. Np in the QA phantom. 206

5.52 QA phantom used to measure SNR vs. Np. 207

5.53 A equivalent slice from an PR (left) and FT (right) exam pulmonary exam. 208

5.54 Artifact due to large objects outside the FOV. 209

5.55 A slice from a 3D carotid exam before and during contrast infusion; noise was measured to increase in the ROI by 1.2. 211
5.56 The noise histogram before and after contrast enhancement 212
5.57 The artifact images from a contrast enhanced femoral artery exam, for 200, 100 and 50 projections. 213
5.58 Steps in the artifact removal process. 214
5.59 Artifact reduction algorithm applied to *in-vivo* image slices. . . . 216
5.60 A small FOV is prescribed with PR: aliasing is subtle. 219

Chapter 1

Introduction

> O socii–neque enim ignari sumus ante malorum–
>
> O passi graviora, dabit deus his quoque finem. Aeneid 1.198-199.

1.1 Motivation

This thesis presents new methods for diagnosing cardiovascular disease using contrast-enhanced magnetic resonance angiography. Cardiovascular disease is responsible for 40 percent of all deaths in the United States, and 17 percent of all deaths for people under 65. It is estimated that one quarter of the population has some cardiovascular disease [2].

An accurate diagnosis is necessary for treatment and prevention. The diagnosis relies on visualizing the blood vessels with enough detail to observe narrowings of the vessels (stenoses), completely closed vessels (occlusions), aneurysms, plaques in the vessels, and smaller vessels which have circumvented narrowed and occluded vessels (collateral vessels). **Angiography** is any method for visualizing the blood flow patterns in the body.

1.1.1 X-ray Angiography

The early days of angiography began with the discovery of x-rays in 1895. In 1896 the first angiogram was made using chalk as a contrast agent, and x-rays focussed onto an amputated hand. Since that time, the best quality angiograms have been produced using a method developed at the University of Wisconsin-Madison [3] [4]. This technique, called x-ray digital subtraction angiography (x-ray DSA) uses an iodinated contrast agent injection and x-ray imaging.

A catheter is threaded into the arterial system, until it reaches the target arteries. Then an iodinated contrast agent is squirted through the catheter into this arterial system, while x-ray images of the region are taken. The images with contrast agent present must be subtracted from baseline images to observe the vessels, a process called mask-subtraction. This method has been the "gold standard" angiographic technique for the past 20 years.

X-ray DSA provides images of extraordinary spatial and temporal resolution, and high signal-to-noise ratio. Figure 1.1 shows an x-ray angiogram of the renal arteries in a patient with a transplanted kidney. The entire arterial system of the transplanted kidney, a stenosis near the aortic bifurcation, and a femoral by-pass graft are all clearly shown in this angiogram.

The drawbacks to x-ray DSA are the invasiveness and risk of catheterization, the method's high cost, and the use of ionizing radiation and iodinated contrast agent. Furthermore x-ray DSA provides information limited to the projection of the vessels onto a plane. These projections can be misleading.

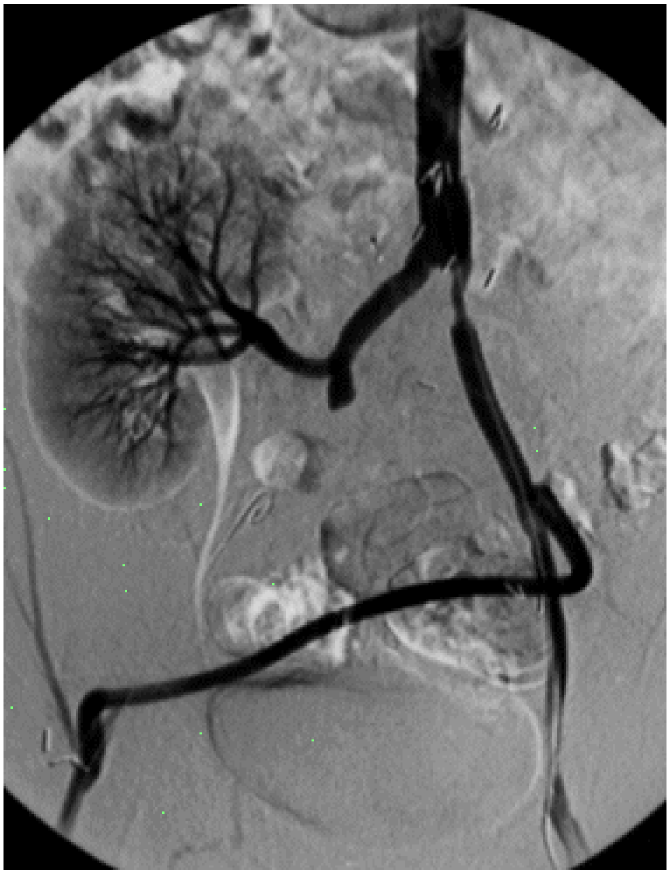

Figure 1.1:
X-ray DSA image of the renal arteries, for a kidney transplant patient with a bypass graft for the femorals.

The research to replace intra-arterial x-ray DSA with other imaging techniques has focussed on the use of intravenous x-ray DSA, ultrasound, computed tomography, and magnetic resonance imaging. These are competitive because they are less costly or less invasive, and sometimes can provide equal diagnostic information.

1.1.2 Contrast MR Angiography

In 1993, first-pass contrast enhanced magnetic resonance angiography (MRA) was introduced [6]. This consists of acquiring MRI data during the first passage of an MRI contrast agent through the vascular system, prior to dilution of the contrast agent concentration by mixing with the full blood volume. This technique is conceptually similar to that used in x-ray DSA. However, it has been found that the spatial and temporal resolution, and signal-to-noise are low relative to x-ray DSA.

There are a few identifiable reasons for this. The SNR in magnetic resonance imaging is linearly dependent on the voxel size of the final image:

$$SNR_{MR} \propto \Delta x \Delta y \Delta z \tag{1.1}$$

For x-ray the SNR depends only on the *square-root* of voxel size [1]:

$$SNR_{x-ray} \propto \sqrt{\Delta x \Delta y \Delta z} \tag{1.2}$$

Therefore, high resolution is easier to achieve in x-ray imaging, accompanied by acceptable SNR.

X-ray imaging is a faster imaging method than MRI. Scan time depends only on obtaining enough photon statistics for adequate SNR. Intra-arterial x-ray DSA can obtain an image with 0.3 x 0.3 mm voxel in about 30 milliseconds. In comparison, such resolution typically would require about 4 seconds for MR and the SNR would be unacceptably low. This comparison obscures many of the details of resolution, SNR, and imaging speed in MRI and x-ray DSA that depend on the specifics of the imaging procedure. However, it accurately reflects the orders-of-magnitude difference in speed between MRI and x-ray. The speed of x-ray imaging has a further advantage, since sub-millimeter resolution acquired over an extended time period, as with MRI, may have limited value when there is subject motion.

X-ray DSA is capable of imaging the presence of contrast in the arterial blood system alone, before the contrast agent had entered the veins. The appearance of veins is generally a hindrance to interpretation of an angiogram. The fact that the contrast reaches the veins 5 to 30 seconds after the arteries has never posed a problem in x-ray DSA, since image acquisition was so rapid. For MRA, which requires 5 seconds to minutes to obtain a 3D image, the appearance of veins in the images is not infrequent. A large amount of MRI research has focussed on their removal.

X-ray DSA benefits from an arterial injection, because the contrast agent is undiluted by mixing with the blood if injected at the imaging site. Contrast MRA does not benefit greatly from an intra-arterial injection, because the signal increase rolls-off at increased concentrations of contrast agent. There is very little SNR gain from intra-arterial injections for MRI [5].

1.1.3 The Interdependence of SNR, Imaging Time and Resolution

In spite of these real obstacles to obtaining a high quality MR angiogram, contrast MR angiography has the important benefits of lower cost and very little risk. Efforts have been made to improve the SNR, resolution and imaging time that characterize MRA.

There is a well known relationship between imaging time (Tscan), SNR, and resolution (voxel size, Δv). Roughly, the relationship is:

$$Tscan \propto \frac{1}{\Delta v} \tag{1.3}$$

$$SNR \propto \Delta v\sqrt{Tscan} \tag{1.4}$$

The scan time increases with decreased voxel size, because more data must be collected for finer resolution. The SNR is dependent on voxel size and scan time.

Using currently accepted MRA techniques, this triad, illustrated in Figure 1.2, forms an inexorable trade-off, in which any attempt to improve one degrades the others. For example, smaller voxels result in increased scan time, and decreased SNR. Many methods have been developed to improve imaging time, SNR, or resolution. But there have been few or no attempts to change the *dependencies* between these characteristics.

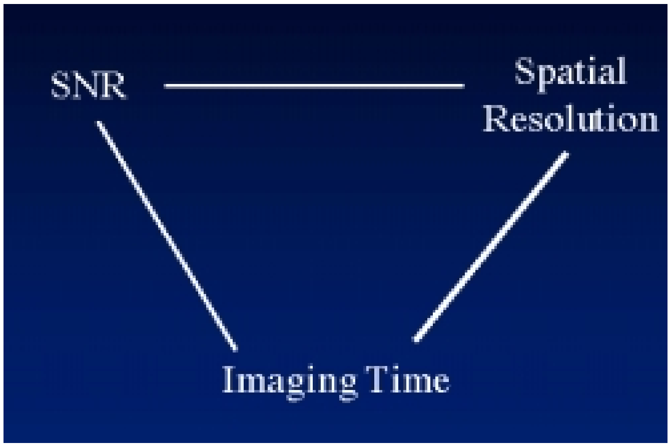

Figure 1.2: *For current MRI methods, SNR, imaging time, and spatial resolution are interdependent. The fixed relationships between SNR, imaging time and resolution causes any improvement in one image characteristic to result in worsening of the others.*

This thesis presents an MRI method that provides a new relationship between SNR, imaging time, and resolution, by breaking the link between resolution and

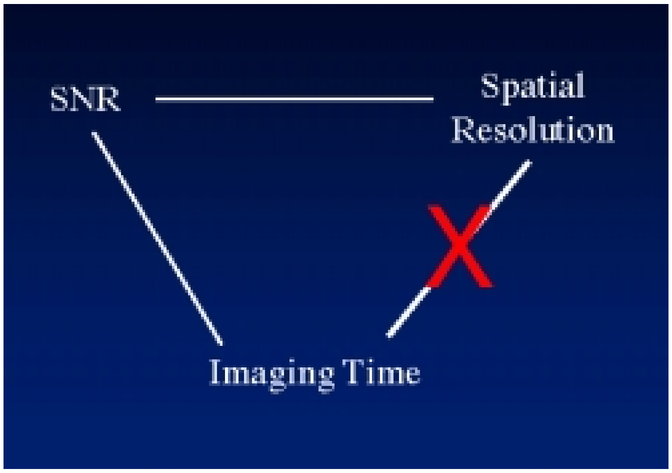

Figure 1.3: *In virtually all MRI methods, SNR, imaging time, and spatial resolution are interdependent. The topic of this thesis is a method that breaks the dependency between imaging time and resolution.*

imaging time (Figure 1.3). The technique presented in this thesis, called limited angle projection reconstruction, provides for image resolution which is fundamentally independent of imaging time. Acquisition of images with “arbitrarily high resolution” can be obtained, and are only limited by the associated artifacts and SNR loss, and not by imaging time.

1.2 Outline

Chapter 2 provides background information on MRI. Chapter 3 traces the developments of contrast-enhanced MRA, including its limitations. One of these limitations is the low spatial resolution obtainable during the short acquisition windows of peak arterial contrast. Chapter 4 discusses fast imaging methods for increasing the resolution. Chapter 5 presents a method for achieving higher spatial resolution during short scan times, using limited angle projection reconstruction. This method is applied to contrast-enhanced angiography, and very high resolution is obtained at the expense of artifacts.

Chapter 3 on contrast-enhancement and Chapter 4 on fast imaging contain a review of the literature along with some original methods and results of our research into fast contrast enhanced MRA.

The original contributions to contrast enhanced MRA are presented in Chapter 5. This thesis presents the first use of projection reconstruction for contrast-enhanced angiography. The usefulness of limited angle projection reconstruction is demonstrated for contrast-enhanced MRA. It was understood in the field of computed tomography that resolution is unchanged when the projection reconstruction acquisition is used in conjunction with a limited number of angles, although artifacts are generated. While these artifacts were unacceptable in computed tomography, they appear to be tolerable in contrast-enhanced MRA.

The sequence implementation and reconstruction method for projection reconstruction are described. Three methods of acquiring the projection reconstruction data during first pass of contrast agent are proposed and the results are presented. The tradeoff between spatial resolution, scan time, artifacts and signal-to-noise ratio are discussed for this method of MRA. The conclusion is that limited angle projection reconstruction does provide a new relationship between imaging time and resolution.

Chapter 2

Background

This chapter provides some background on the techniques of nuclear magnetic resonance (NMR), magnetic resonance imaging (MRI), and magnetic resonance angiography (MRA). A description of nuclear magnetic resonance is given, and methods for imaging are reviewed. Knowledge of MR methods for spatial localization are important for understanding Chapter 5, which describes the advantages of the projection reconstruction imaging method. A brief summary of the current techniques for MRA is given.

2.1 Nuclear Magnetic Resonance

The human body is made mostly of water, and it is the water which is detected in ^1H NMR. The hydrogens in the water molecules have a nuclear magnetic spin $\vec{J}$, and a nuclear magnetic moment $\vec{\mu}$ which is related to $\vec{J}$ by

$$\vec{\mu} = \bar{\gamma} \cdot \vec{J} \tag{2.1}$$

where $\bar{\gamma}$ is the gyromagnetic ratio, equal to 4250 Hz/G, $\vec{J}$ is the spin angular momentum. $\vec{J} = \hbar\vec{I}$, where I is the spin operator, quantized as Iz= +/- 1/2, and $\hbar$ is Planck's constant. (Note that an often used quantity, γ, is related to $\bar{\gamma}$ by: $\gamma = 2\pi\bar{\gamma}$.)

In NMR, the body is placed in a large magnetic field, B0. Our scanner operates at 1.5 Tesla. In the presence of a magnetic field B0, a magnetic dipole experiences a torque which is expressed as:

$$\vec{\tau} = \frac{d\vec{J}}{dt} = \vec{\mu} \times \vec{B}0 \tag{2.2}$$

which yields:

$$\frac{d\vec{J}}{dt} = \bar{\gamma}\vec{J} \times \vec{B}0 \tag{2.3}$$

This differential equation has a well known solution, which predicts that the nuclear magnetic moment precesses like a top at the precessional frequency:

$$\nu_0 = -\bar{\gamma} \cdot B0 \tag{2.4}$$

ν_0 is called the Larmour frequency. At 1.5 T, it is equal to 63.9 MHz.

2.1.1 Bulk Magnetization

In thermal equilibrium, the Boltzman distribution gives the relative number of spins which are aligned or anti-aligned with the magnetic field B0. The distribution is dependent on the energy difference between the two states, ΔE:

$$\Delta E = \Delta\vec{\mu} \cdot \vec{B}0 = \hbar\bar{\gamma}B0 \tag{2.5}$$

The ratio of spins aligned N^+ to those anti-aligned N^- is given as

$$\frac{N^+}{N^-} = \exp{(\frac{\Delta E}{kT})} \tag{2.6}$$

where k = 1.38 x 10^{-23} J/deg-k is the Boltzman constant, and T is the temperature in Kelvin. For T= 300 K and B0 = 1.5 Tesla, $\frac{\Delta E}{kT} \approx 10^{-5}$. The difference in number of spins that are aligned and anti-aligned is small. The bulk magnetization of the spins with magnetic moment μ is (following Sorenson [8])

$$M_{bulk} = \mu(N^- + N^+) \tag{2.7}$$

which can be evaluated using $e^x = 1 + x$ for $x \ll 1$, and that $N^+ \approx N^- \approx N/2$ to be

$$M_{bulk} = \frac{N(\mu)^2 B0}{2kT} \tag{2.8}$$

This shows the dependence of bulk magnetization and thus signal on B0, 1/T (the Curie law), μ, and the density of the target nuclei, N.

2.1.2 The Bloch Equations

Equation 2.3, after substituting $\vec{M}$, the bulk magnetization, for $\vec{J}$, a single spin's magnetization, gives the time dependence of the bulk magnetization:

$$\frac{d\vec{M}}{dt} = \bar{\gamma}\vec{M} \times (B0) \tag{2.9}$$

Phenomenological observation that the magnetization in z regrows with a time constant, T1, and that the magnetization on the x-y plane dephase with a time constant T2*, lead to the inclusion of this relaxation time dependence:

$$\frac{d\vec{M}}{dt} = \bar{\gamma}\vec{M} \times (\vec{B}0) - \frac{Mx}{T2*} - \frac{My}{T2*} + \frac{Mz}{T1} \tag{2.10}$$

where ν is the precessional frequency of the magnetization. The solutions to this vector equation are the famous Bloch Equations:

$$M_x = \exp\left(\frac{-t}{T2*}\right)[M_x(0)cos(\nu t) - [M_y(0)sin(\nu t)] \tag{2.11}$$

$$M_y = \exp\left(\frac{-t}{T2*}\right)[M_x(0)sin(\nu t) + [M_y(0)cos(\nu t)] \tag{2.12}$$

$$M_z = \exp\left(\frac{-t}{T1}\right)M_z(0) + (1 - \exp\left(\frac{-t}{T1}\right))M_0 \tag{2.13}$$

This time dependence of $\vec{M}$ can be converted into time dependence in the frame rotating at the Larmour frequency ν_0. The relationship between time dependence in the two frames is expressed as:

$$\left(\frac{dM}{dt}\right)_{lab} = \vec{\nu_0} \times \vec{M} + \left(\frac{\partial\vec{M}}{\partial t}\right)_{rot} \tag{2.14}$$

The Bloch equation solutions in the rotating frame are:

$$M_x = \exp\left(\frac{-t}{T2*}\right)[M_x(0)cos(\Delta\nu t) - [M_y(0)sin(\Delta\nu t)] \tag{2.15}$$

$$M_y = \exp\left(\frac{-t}{T2*}\right)[M_x(0)sin(\Delta\nu t) + [M_y(0)cos(\Delta\nu t)] \tag{2.16}$$

$$M_z = \exp\left(\frac{-t}{T1}\right)M_z(0) + (1 - \exp\left(\frac{-t}{T1}\right))M_0 \tag{2.17}$$

where $\Delta\nu = \nu - \nu_0$. These equations show the time dependence of the magnetization, once excited and tipped into the transverse plane. The longitudinal (Mz) magnetization regrows with a time constant T1, while the transverse (M_{xy}) magnetization dephases with a time constant T2*, and precesses at some offset frequency $\Delta\nu$ in the rotating frame.

Different tissues in the body have different T1 and T2 values. Since the magnetization of the spins is dependent on T1 (Mz) and T2 (M_{xy}), the signal strength from soft tissues in the body will be weighted by their T1 and T2 values: this creates contrast between tissues in MRI.

2.1.3 T1 and T2*

The T1 and T2* of the imaged sample are important quantities. In MRI, mainly T1 and T2* and proton density differences can be exploited to create contrast between tissues. For example, in contrast-enhanced MRA, the T1 and T2* are shortened by the contrast agent, and this creates signal differences between blood and tissue.

The T1 is called the spin-lattice time constant. It characterizes the return of the longitudinal magnetization to the equilibrium value, through energy loss to the lattice. The rate of transitions to equilibrium is dependent on the strength of magnetic fluctuations at the Larmour frequency. Thus T1 is set by the magnetic field fluctuations in the environment of the water protons.

T2* is the spin-spin time constant. When the spins are tipped into the transverse plane, they precess about the local main magnetic field. Because all the spins are in a slightly different environment, the precession rate is different, and the coherent signal gradually damps out, with a time constant T2*.

Furthermore, T2* can be separated into a fixed part and a random part. The fixed part of T2* is dephasing due to chemical shifts, B0 inhomogeneity, and susceptibility. This dephasing is constant in time, it is fixed. The remaining dephasing is due to random magnetic environment changes. T2* is the sum of the fixed and random contributions. T2 is the random part of T2*, while the fixed part is denoted $\bar{\gamma}\Delta B0$.

$$\frac{1}{T2*} = \bar{\gamma}\Delta B0 + \frac{1}{T2} \tag{2.18}$$

It is always true that $T2 \leq T1$, because 1/T1 is simply a component of 1/T2 [14]. This is important to remember, especially for contrast-enhanced imaging, when T1 is greatly decreased.

2.1.4 The Basic NMR Experiment

In the basic experiment, the sample's magnetization is tipped into the transverse (x-y) plane by an RF field which is rotating at the Larmour frequency in the presence of a main magnetic field B0. The transverse magnetization in the sample begins to precess and dephase and the longitudinal magnetization regrows, according to the Bloch Equations. A coil is used to detect the precessing transverse magnetization. A voltage is induced in the coil which is proportional to the magnetic flux change:$-\frac{d\Phi_B}{dt}$. The measured voltage is the NMR signal.

2.2 Fourier Encoding

Since this thesis deals with research on methods for obtaining greater spatial resolution, the standard methods for spatial localization in MRI are reviewed here. The factors which influence resolution and field-of-view (FOV) will be reviewed. Resolution refers to the separation distance between two objects at which the objects just barely appear distinct. The FOV gives the dimensions of an image, in three dimensions, x, y, and z.

2.2.1 The Fourier Transform

MRI is a unique radiological imaging modality because it acquires the Fourier transform of an object rather than acquiring image space information, as in ultrasound and x-ray.

The Fourier transform (FT) of a function f(x) is defined as

$$FT(f(x)) = F(k) = \int_{-\infty}^{+\infty} f(x) \exp{(-i2\pi kx)} dx \tag{2.19}$$

F(k) comprise the Fourier representation of f(x). x and k are conjugate variables, x is spatial distance, k is spatial frequency. F(k) can be Fourier transformed back to image space to obtain f(x):

$$FT(F(k)) = f(x) = \int_{-\infty}^{+\infty} F(k) \exp{(i2\pi kx)} dk \tag{2.20}$$

In MRI, the Fourier representation in two or three dimensions is usually obtained. The 2D Fourier transform is a simple extension of the 1D transform:

$$FT(f(x,y)) = \int_{-\infty}^{+\infty} \int_{-\infty}^{+\infty} f(x,y) \exp{(-i2\pi kx \cdot x)} \exp{(-i2\pi ky \cdot y)} dxdy \tag{2.21}$$

The Fourier transform is essential to MR Imaging. Here are some useful properties of the Fourier transform, where f(x) is a function in the spatial domain, whose Fourier transform is F(k):

- Area under a curve: $\int_{-\infty}^{+\infty} f(x)dx = F(k=0)$
- Addition: $FT(f(x)+g(x)) = F(k)+G(k)$
- Scaling: $FT(f(ax)) = \frac{1}{a}F(k/a)$
- Shift theorem: $FT(f(x-a)) = \exp(-i2\pi ka)F(k)$
- Convolution theorem: $FT(f(x)\cdot g(x)) = F(k)\bigotimes G(k)$
- FT of a rectangle (width a): $FT(rect(x/a)) = \frac{sin(\pi ak)}{\pi k} = a\cdot sinc(ak)$
- FT of a delta function: $\delta(x-a) = \exp(-i2\pi ak)$
- FT of a comb function: $FT(comb(k-n\Delta k)) = comb(x-\frac{n}{\Delta k})$

Field of View with Fourier Encoding

The data acquired in MR imaging system are the values of F(k), at discrete sampling points separated by Δk. This sampling distance is significant to MR imaging, in fact:

$$FOV = \frac{1}{\Delta k} \tag{2.22}$$

FOV is the field of view which can be reconstructed without "aliasing". Aliasing can occur because F(k) is sampled discretely. Discrete sampling is tantamount to multiplying F(k) by a comb function, consisting of delta functions spaced Δk apart.

$$F_{sampled}(k) = F(k) \cdot comb(k - \Delta k) \tag{2.23}$$

In the spatial domain, using the FT of a comb function, and the convolution theorem for FT (both given above):

$$f_{sampled}(x) = f(x) \bigotimes comb(x - \frac{1}{\Delta k}) \tag{2.24}$$

This image from sampled k-space is the true image convolved with a comb function, consisting of delta functions spaced a FOV ($FOV = \frac{1}{\Delta k}$) apart. The MR imaging acquisition always samples F(k) discretely. Aliasing will only result if the imaged object f(x) is larger than the FOV.

Figure 2.1 illustrates aliasing. The original object has non-zero signal outside of the FOV, as set by the comb function. This signal outside the FOV appears as signal inside the FOV, when the object is convolved with the comb function. Therefore to prevent aliasing, the sampling distance in k-space must be constrained so that:
$FOV = \frac{1}{\Delta k} >$ Object size.

Resolution with Fourier encoding

Now the factors influencing resolution will be reviewed. The resolution of the Fourier encoded image is expressed by its point spread function (PSF), the representation of a point object in the image. A delta function at x=0 has as its Fourier transform:

$$FT(\delta(x - 0) = F_{point}(k) = e^{(i2\pi 0k)} = 1 \tag{2.25}$$

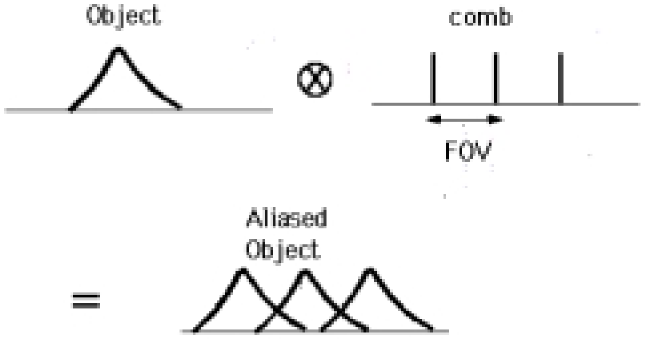

Figure 2.1: *Aliasing in Fourier transform imaging. The original object is larger than the FOV, as set by the spacing of the comb function. The result of their convolution is an object which has aliasing.*

The Fourier coefficients of this point object are a constant in k-space. When only a limited number of k-space samples are acquired, as happens in MR imaging, the spatial resolution is degraded. Consider the result of representing the point object by Fourier coefficients limited in k-space from -kmax to + kmax. This is equivalent to multiplying the k-space representation F(k) by a rectangle function, which is zero beyond +/- kmax. Then its image space appearance changes:

$$FT[F_{point}(k) \cdot rect(k/2kmax)] = \delta(x-0) \bigotimes \frac{sin(\pi 2kmax \cdot x)}{\pi x} \tag{2.26}$$

Thus, if the extent of sampled k-space is limited to +/- kmax, the result is this point object convolved with a sinc function. This sinc function reduces the resolution. Its first zero crossings are at +/- $\frac{1}{2 \cdot kmax}$. Furthermore the full width at half maximum of the central lobe of this sinc function is about $\frac{1}{2 \cdot kmax}$. This sinc convolution reduces the sharpness of the point object. Since an image consists of a series of point objects, the sampling of a finite extent of k-space limits the resolution of any object. The resolution of an image sampled from +kmax to

-kmax is equal to the width of the sinc function that convolves the image. This is the "Fourier resolution" or pixel size:

$$\Delta x = \frac{1}{2 \cdot kmax} \tag{2.27}$$

The relationship between pixel size and spatial frequency sampling can be explained by the Nyquist theorem for sampling k-space. To resolve two objects spaced Δx apart requires collection of spatial frequencies which sample at twice $\frac{1}{\Delta x}$. In order to increase the resolution, the extent of sampled k-space must be increased.

The spacing Δk is constrained as discussed above. Often the resolution can only be increased by increasing the number of sampling points, not by increasing the sampling spacing, because that would reduce the FOV. Increased resolution is only possible by acquisition of higher spatial frequencies, which in conventional MR imaging can increase scan times.

2.3 Spatial Encoding in MRI

The last section described properties of the Fourier transform of a function, and how the field of view and resolution are determined by the Fourier coefficients collected. This section shows how these Fourier coefficients are obtained in MRI for 3D tomography.

2.3.1 Gradient fields

In MR, magnetic fields whose strength varies linearly with position are used for imaging. These fields are called gradients, and they can spatially vary with x, y or z:

$$\frac{\partial Bz}{\partial z} = Gz \tag{2.28}$$

$$\frac{\partial Bz}{\partial x} = Gx \tag{2.29}$$

$$\frac{\partial Bz}{\partial y} = Gy \tag{2.30}$$

As indicated, they are all directed in the z-direction, the direction of the main magnetic field. These gradients are turned on and off in the pulse sequence for use in spatial encoding. They are used to spatially vary the precessional frequency of the spins. As discussed below, the Gz gradient is used for slice encoding, the Gx gradient is used for frequency encoding, and the Gy gradient is used for phase encoding. They can also be used to dephase the spins ("killers") or to encode non-spatial information into the image (for example velocity information).

2.3.2 MRI Pulse Sequences

The MRI pulse sequence consists of a sequence using gradients and radio-frequency (RF) pulses to affect the longitudinal and transverse magnetizations and their phases. The pulse sequence creates the contrast between tissues and the spatial encoding. Typical elements, shown in Figure 2.2, are the RF excitation pulse and slab select gradient, the frequency encoding gradient, and phase encoding gradient, all discussed below. These pulses are "played out" concurrently or sequentially in the pulse sequence. A pulse sequence is characterized by its repetition time, TR, the echo time, TE, and the flip angle of the RF excitation pulse (α), and a data acquisition (labelled A/D in Figure 2.2). The TE is the time between excitation of the magnetization and the collection of the central Fourier coefficients in x. During the TE time the signal can dephase with T2* dephasing, so TE should be as short as possible. The TR time is the time to collect one Fourier encoding line. Each pulse sequence also has a characteristic T1 and T2 weighting. The gradient amplitudes are modified each TR to acquire a specific spatial resolution in x, y, and z, for a given FOV in x and y, and slice or slab thickness in z.

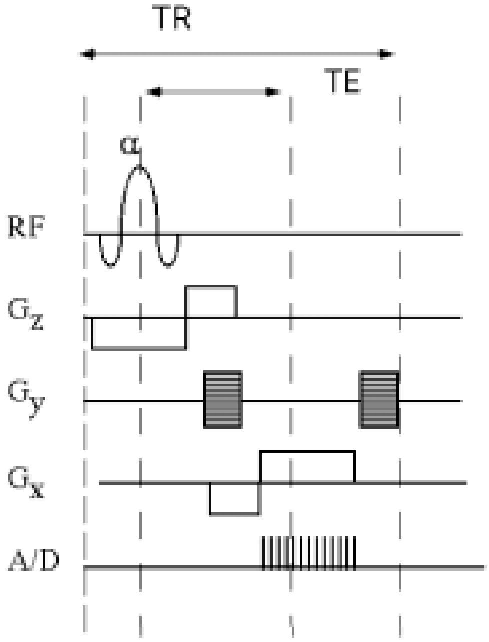

Figure 2.2: *An MRI pulse sequence diagram. The pulse shapes and amplitudes for the RF and the gradients (Gx, Gy, Gz) are shown, along with their relative positions in time. Some characteristics of a pulse sequence are the flip angle (α), the TR, and the TE.*

2.3.3 RF Excitation of spins

In order to detect the spins, they must be tipped into the transverse plane. The RF field, called B1, can flip spins into the transverse plane because it is rotating around the z-axis at the Larmour frequency, the same frequency as the transverse proton nuclear spins. Because of this, the nuclear spins in the rotating frame see an effective field of B1 alone. This is the resonance phenomenon. [9]. If RF pulse is time modulated, it can flip spins from a broader spectrum of frequencies.

Typically, a sinc modulated RF pulse is used to excite a rectangular band of frequencies. For example,

$$B1(t) = B1oe^{i2\pi\nu_0 t}sinc(t/to) \tag{2.31}$$

The Fourier transform of this RF field gives the spectral energy at each frequency [12]:

$$\int_{-\infty}^{+\infty}(B1(t))e^{-i2\pi t\nu}dt = rect(\nu to)\bigotimes\delta(\nu-\nu_0) \tag{2.32}$$

This sinc-modulated RF excites spins within a bandwidth of frequencies, $\Delta\nu = 1/to$. Normally, the spins precess at only the Larmour frequency, $\bar{\gamma}\cdot B0$. If a gradient is applied in the z direction (called the slice-select direction) direction, so that $\vec{B} = \vec{B0} + \vec{z}\cdot\vec{G}z$, the spin precession rate is dependent on its z position: $\nu = \bar{\gamma}(B0 + zGz)$. If the RF excites a bandwidth of frequencies, this will correspond to a range of space in the z-direction (the slice or slab thickness, Tsl): $Tsl = \frac{1/to}{\bar{\gamma}Gz}$. In this manner the RF excites a “slice” or “slab” instead of the entire object.

The B1 pulse tips the longitudinal magnetization into the transverse plane, with a flip angle, θ. After the B1 pulse, $Mz = M_0 \cdot cos(\theta)$, and $Mx = M_0 \cdot sin(\theta)$ where M_0 is the longitudinal magnetization prior to excitation.

2.3.4 Spatial Encoding in X and Y

This thesis presents a new application for the the original method for spatial localization in MRI, called projection reconstruction. This method was quickly replaced by "spin warp" techniques of localization which is used in virtually all of clinical MRI today. The spin-warp imaging method is described here. The projection reconstruction method of spatial localization will be described in Chapter 5. Spatial encoding consists of frequency encoding and phase encoding. These are described below.

Frequency Encoding

When an RF pulse is used to tip spins into the transverse plane, they begin to precess at the Larmour frequency. The acquired signal S(t) represents the integrated spin signal from the whole object.

In order to determine the distribution of spins along an axis, a gradient Gx is applied, which assigns to each x position a different precessional frequency:

$$\nu(x) = \bar{\gamma}B0 + \bar{\gamma}Gx \cdot x \qquad (2.33)$$

The acquired signal S(t) with this gradient on represents the collective signal from spins precessing at different frequencies. The frequency distribution of signal is determined by Fourier transforming the signal S(t):

$$M_{xy}(\nu) = \int S(t)e^{i2\pi t\nu}dt \tag{2.34}$$

M_{xy} is the magnetization strength at each frequency. The frequency encoding process assigns to each spatial position a frequency as in Equation 2.33, so that the frequency distribution is related by a scale factor to the spatial distribution of spins.

As an example, consider a single object at a position x1. Then S(t) will have only one frequency ($\nu_1 = \bar{\gamma}Gx(t) \cdot x1$) with spectral power. The Fourier transform of S(t) will localize the point. $M_{xy}(\nu) = \int (Soe^{i2\pi\nu_1 t})e^{i2\pi t\nu}dt$. This integral can be evaluated to be: $M_{xy}(\nu) = \delta(\nu - \nu_1)$.

More formally, the acquisition of signal under the influence of the gradient, Gx, results in a signal which is just the FT of the magnetization. The gradient causes an x-dependent phase-accumulation, so that the spins comprising the object, Mx, have a spatially dependent phase which increases with time. The signal acquired at time t is just the sum of all the signals in the object with different phase factors:

$$S(t) = \int M_{xy}e^{(i2\pi \int (\bar{\gamma}G \cdot x dt))}dxdy \tag{2.35}$$

Using the identification $\int \bar{\gamma}Gdt = k_x(t)$, the signal becomes

$$S(k_x) = \int M_{xy}e^{(i2\pi k_x x)}dxdy \tag{2.36}$$

Thus frequency encoding provides a signal $S(k_x)$ which is related to the object M_{xy} by the Fourier transform.

Phase encoding

Frequency encoding is used to localize the spins in the x-direction. Phase encoding is used to localize spins in the y-direction and for 3D methods in the z-direction. Phase encoding is analogous to frequency encoding, but the phase encodings are obtained in steps.

In frequency encoding, S(t) records the signal in time with a constant gradient Gx on, so that the signal at different levels of phase-accumulation is obtained through time.

Phase encoding differs because the gradient Gy is "blipped" – turned on for a short time, Tpe – causing a specific phase variation across the image. A frequency encoding is performed, with that phase-variation in place. Next, a slightly larger gradient Gy is turned on for the same time, creating a different phase-variation along y, and another frequency encoding is performed, and the signal is acquired again.

The phase accumulation of spins at position y due to the Gy gradient is:

$$\phi = (2\pi)\bar{\gamma} \int G_y(t) \cdot Tpe \cdot y \tag{2.37}$$

Figure 2.3 shows how this gradient causes the spins to be in and out of phase with each other. From top to bottom it shows the cosine of the phase across the phase encoding FOV for five values of Gy. If spins at different locations are in phase with each other, their signals add coherently, but if they are out of phase, the signals add destructively. Therefore each phase encoding step measures the coherence of the spins at a different spatial frequency. This intentional phase variation across the image provides the Fourier coefficients in the y direction.

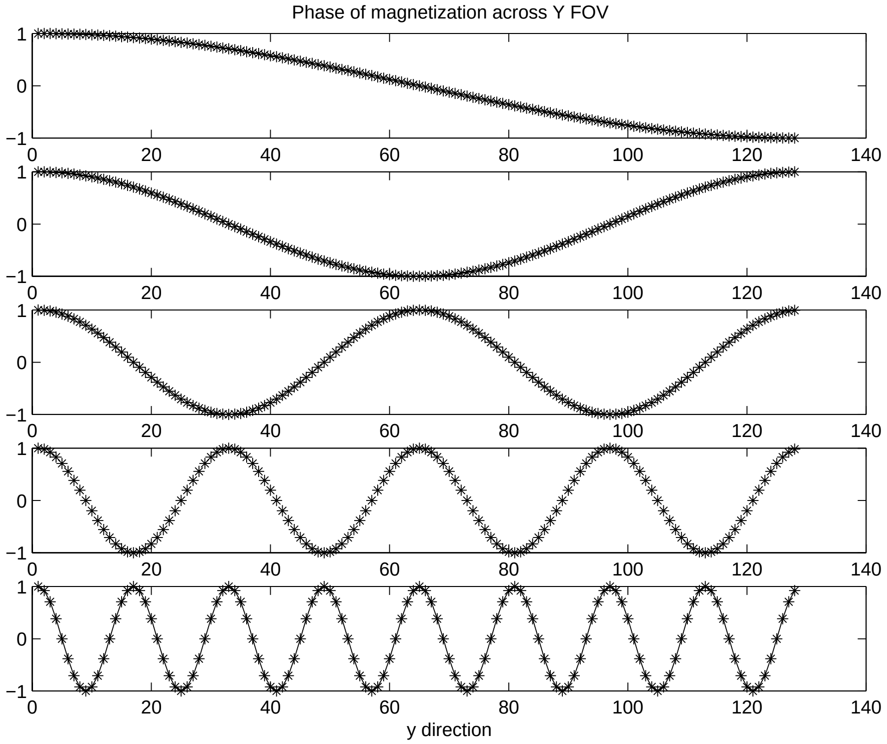

Figure 2.3: *The phase of spins along the y direction during the phase encoding process. The cosine of the phase is plotted. The series of plots shows the phase variation across the y FOV for the first five phase encoding steps. The* G_y *is played out for a time Tpe prior to frequency encoding. The* G_y *gradient creates the phase variation of the spins along y, given by Equation 2.37. The acquired signal strength is dependent on this applied phase variation.*

Each phase encoding step provides the signal with a different phase variation across y:

$$S(Gy) = \int M_{xy} e^{i2\pi(\bar{\gamma}Gy \cdot yTpe)} dydx \tag{2.38}$$

Here S(Gy) indicates that the y gradient strength is changing. Just as for frequency encoding, ky can be identified as $k_y = \bar{\gamma}Gy(ky)Tpe$. The signal can be identified as the FT of the image in y:

$$S(k_y) = \int M_{xy} e^{i2\pi k_y y} dx dy \tag{2.39}$$

2.3.5 Conclusion

Using slice-selection, and phase and frequency encoding, an image of the object is obtained with a specific resolution and FOV. The phase and frequency-encoding methods presented are characteristic of spin-warp imaging, by far the most common method of imaging in MRI. However, the acquisition of k-space points can be accomplished using gradients to traverse any k-space trajectory, and the principles are the same as described above.

2.4 MR Angiographic Methods

The three most common ways of obtaining contrast between flowing water in blood vessels and stationary tissue water are with time-of-flight, phase-contrast and contrast-enhanced imaging. Each of these methods has been the focus of extensive research in our group.

2.4.1 Time-of-Flight

Time-of-flight (TOF) techniques (descriptively called “inflow” techniques) rely on the velocity of blood for contrast. In these methods, selective RF pulses which tip a slab of spins into the transverse plane eventually cause saturation of the longitudinal magnetization, Mz, of stationary spins. After many RF pulses, the value of Mz is very small. But for fast moving blood, which enters the slice and only experiences a few RF pulses before exiting, Mz is large. This creates brighter signal for fast moving blood and contrast between blood and stationary tissue. The longitudinal magnetization after n RF pulses is determined by the TR, T1 and flip angle according to:

$$Mz_n \sin(\theta) = \frac{[1 - e^{(\frac{-TR}{T1})}][1 - (\cos(\theta) e^{(\frac{-TR}{T1})})^n]}{1 - e^{(\frac{-TR}{T1})} \cos(\theta)} (e^{(\frac{-TE}{T2*})}) \cdot sin(\theta) \qquad (2.40)$$

For fast flowing blood, the longitudinal magnetization is large because n is very small. However, the TOF method is susceptible to blood signal saturation due to slow or in-plane flow. When flow is slow or in-plane, the flowing spins experience a great number of RF pulses before exiting the slab. This causes the blood signal to fall.

TOF methods are also susceptible to intravoxel dephasing. The combination of a spread of velocities within a voxel and the use of gradients leads to a spread of phases within a voxel. This intravoxel dephasing results in signal loss. A spread of velocities is possible during laminar, turbulent or retrograde flow. Intravoxel dephasing may be reduced by using gradient moment nulling or flow compensation. This method places extra gradients into the pulse sequence which are designed to null the zeroth and first gradient moments. Another approach is to shorten the TE, since the phase-accumulation increases with TE. A third method is the use of small voxels, so that the spread of velocities is reduced.

The most straightforward implementation of the TOF method is the acquisition of multiple thin 2D slices, choosing the imaging plane to maximize inflow of fresh unsaturated blood. With 2D methods, inflow enhancement is excellent and venous suppression is achievable, but slices are often thicker than for 3D methods.

A 3D implementation is possible, acquired either as a single slab or using the multi-slab techniques [13], and has the typical advantages of 3D methods: shorter TEs, thinner slices, and higher SNR, due to averaging of the noise. But 3D techniques exhibit slab boundary artifacts due to progressive saturation of the spins as they flow through the slab and experience more RF pulses.

Furthermore, in TOF the scan times are very long, on the order of a few minutes, because the TR must be long in order to optimize the contrast and the SNR. The long scan times prohibit acquisitions during a breath-hold, and can result in motion artifacts.

Even with these limitations, time-of-flight techniques have high SNR, high resolution and possibility of venous suppression.

2.4.2 Phase-Contrast Imaging

Phase-contrast imaging uses gradients to impart a phase to the flowing spins of the blood and zero net phase is given to stationary tissue [10]. The phase is the phase of the transverse magnetization of the nuclear spins relative to stationary tissue spins. The gradient waveform G_{bp} establishes the phase difference. The phase of the spins is related to the gradient field and the spins' positions, $x(t) = x_0 + vt$:

$$\phi = (2\pi)\bar{\gamma} \int G_{bp}(t) \cdot x(t) dt \tag{2.41}$$

$$\phi = (2\pi)\bar{\gamma} \int G_{bp}(t) \cdot (x_0 + vt) dt \tag{2.42}$$

The gradient waveform G_{bp} is played out with a equally large positive and negative area (called a bipolar gradient), so that the net phase-accumulation for stationary spins is zero, but for spins with a velocity, the phase-accumulation is non-zero. To obtain a phase image which is purely sensitive to velocity, and not reflective of magnetic field inhomogeneity and susceptibility etc., the phase map is acquired without applying the velocity-encoding gradient [15]. This phase image reflects only incidental phase accumulations. The phase maps from the two acquisitions are subtracted, and the result is a “phase difference” image which is reflective of the velocities of the spins. Alternatively, the complex signals themselves are directly subtracted, resulting in a “complex difference” image.

Phase contrast imaging has the advantage of excellent background suppression and less susceptibility to blood signal saturation due to slow flow. Phase-contrast angiography has the drawback of long scan times for two reasons. First, TRs are long because of the velocity-sensitizing gradients. Second, at least four complete sets of phase encodings and frequency encodings must be collected, in order to obtain 3D velocity information.

2.4.3 Contrast-enhanced MRA

This thesis is a departure from the past research in our group. While still focussing on developments towards the diagnosis of cardiovascular disease, it presents recent advances with contrast agents for MR angiography, instead of non-enhanced angiography. Contrast MRA relies on injection of a contrast agent into the blood, so that contrast between blood and tissue is due to contrast agent presence, and not blood velocity.

2.4.4 Diagnostic Purpose of MRA

MRA is used to image the lumen of the blood vessels, and to show the presence of stenosis (narrowing of the vessels), or patency (open vessels). It also depicts collateral flow, in which smaller vessels are formed which circumvent a stenosed artery.

Radiologists use MRA every day to image the carotid arteries in the neck, the renal arteries which feed the kidneys, and peripheral arteries of the legs, among others. These regions make specific demands for resolution, scan time, and coverage in MR angiography.

Carotid artery stenosis indicates the possibility of stroke. Intra-arterial x-ray DSA methods are the standard for carotid artery imaging, but it is expensive and has risk. Renal artery stenosis is a cause of hypertension (high blood pressure). Cost effective treatments are available, so cost-effective diagnostic tools are important. In addition, MR imaging of the renal arteries can be performed without nephrotoxic contrast agents [7]. Peripheral vascular disease is caused by systemic athereosclerosis. It can threaten a limb, or cause chronic symptoms.

Many vessels are not commonly imaged with MRA, for example the pulmonary arteries and the coronary arteries, because of unacceptable image quality of MRA. Other vessels are not imaged with MRA because of cost.

Chapter 3

Contrast-enhanced Angiography

This chapter presents information on the advancement of MR angiography through use of contrast agents. Contrast agents are injected into the blood stream intravenously, where they can be imaged on T1-weighted images as a hyper-intense signal. They affect the T1 and the T2 of neighboring water nuclear spins. Martin Prince introduced imaging of the blood vessels using the first pass of contrast agent through the body, after intravenous injection [6]. Since then, contrast-enhanced angiography has advanced, and now often surpasses the other methods of MR angiography, like phase-contrast and time-of-flight, in accurately depicting vessel lumen. This chapter presents the methods used in contrast-enhanced angiography.

3.1 Fast Gradient Echo Imaging

In contrast-enhanced MRA, the pulse sequence most often used is a three-dimensional (3D) spoiled fast gradient echo pulse sequence using a spin warp acquisition. A 3D data set is advantageous so that the vessels can be viewed at any useful orientation. 3D methods can encode thinner slices than multi-slice 2D methods, because gradient amplitude limitations prohibit acquisition of very thin slices. Furthermore, the TE is shorter for 3D methods when thin slices are prescribed. 3D methods also have higher SNR due to averaging, although the effective TRs are shorter for 3D than 2D methods. The resultant slice images are used for diagnosis. Alternatively a maximum intensity projection (MIP) image can be constructed. The MIP processing involves projecting 3D data from multiple slices onto a single 2D projection, by retaining the brightest intensity encountered on the ray through the set of slices. In order to see the vessels, a series of MIPs projected at different orientations is useful.

Gradient echoes, as compared to spin-echoes, give T1-weighting. Gradient echo imaging also has short TEs and data acquisition times, making it less sensitive to flow artifacts. Imaging of flowing blood causes artifacts as the flowing spins move through the gradient field. Spoiled gradient echo imaging resolves this problem by acquiring the echoes quickly, and spoiling the residual magnetization.

Spoiling [49] refers to flipping down the longitudinal magnetization at random or carefully selected angles on the xy plane each TR. Without spoiling, residual transverse signal from previous “experiments” or RF pulses which have not yet dephased, due to T2* or due to gradient dephasing, will contribute to the current signal. Investigations of true FISP (Fast Imaging with Steady-state Precession) acquisitions are currently popular [20]. These methods do not spoil but instead use the residual transverse magnetization from previous RF pulses to gain SNR.

The theoretical dependence of T1 and T2* on contrast agent presence is given below. While the T2* of the blood is shortened by the contrast agent, most contrast-enhanced imaging exploits the signal increase of the T1-shortened blood on T1-weighted gradient echo images. Spin-echo imaging, because it involves a refocussing 180° flip angle has an inherently longer TR than gradient echo imaging. The 180° pulses also deposit more RF power into the body, so that safety limits prohibit short TRs in spin echo imaging.

The eponym “fast” means that the pulse sequence is very streamlined, including only the essential RF pulse and spatial encoding gradients. For example, flow compensation is not used.

The acquisition order is the manner in which the Fourier transform of the image is collected. It indicates the k-space acquisition trajectory, i.e. the k-space point collected and the time of collection. Spin-warp acquisition of frequency encodings and phase-encodings is the method of choice for most MR imaging, and for MRA. Spin-warp imaging is often performed using a single echo. Other acquisition methods which could be used in MRA are echo-planar imaging (EPI), which acquires multiple frequency encodings between RF pulses, spiral imaging, which acquires k-space points on a trajectory which spirals out to the edge of k-space with long data acquisition times, and projection reconstruction (PR), which acquires k-space in radial lines.

Contrast-enhanced MRA has been attempted with EPI, with mixed results [80] [83]. To date, no reports have been made concerning spiral acquisition during contrast-enhancement. One of the challenges is the long data readout times during which the signal can dephase [65]. This thesis presents the results of using projection reconstruction for MRA.

In these sequences, zero-filling is commonly used in the slice direction. Zero-filling reduces partial-voluming effects, and improves the apparent resolution without changing the SNR [31].

There is great uniformity of methods in contrast-enhanced MRA. Generally a 3D fast gradient echo spin-warp sequence is used. With these methods we are rapidly reaching the limits of resolution, SNR and speed.

Immunity to flow dephasing and strong T1- or T2-weighting seem to be the main requirements of any contrast-enhanced MRA sequence. Exploring the potential of other pulse sequences, and other acquisition strategies will provide fruitful results. In this thesis we present the results of using projection reconstruction for contrast-enhanced MRA.

3.2 Description of Contrast Agents

The advent of contrast-enhanced imaging in MRI has ushered in great advances in angiography. The MRI contrast agents can alter the T1 or T2* of the blood, which provide the weighting in MRI images. Contrast agents composed from the rare earth gadolinium decrease the T1. Gadolinium has 7 unpaired electrons in its outer shell and is highly paramagnetic. Its electronic magnetic moments align with main magnetic field. The large electronic magnetic moments rotate due to Brownian motion, and this causes a fluctuating magnetic field. If the frequency of the fluctuations is close to the Larmour frequency of the hydrogen nuclei spins, T1 relaxation of nearby hydrogen nuclei increases. The gadolinium increases the probability of transitions which tip nearby nuclear hydrogen spins up, towards the lower energy state, thereby increasing the regrowth rate of longitudinal magnetization (shortening T1)[24]. The T2 is also shortened. Other contrast agents mainly shorten the T2 through magnetic susceptibility effects. For example, Dysprosium DTPA (diethylene triamine pentaacetate) does not affect the T1 because its own relaxation is so fast, but it decreases the T2 of water protons by creating inhomogeneity of the magnetic field [25].

3.2.1 Injection Protocol

In contrast-enhanced MRA, a dose of up to 0.3 mmol per kilogram of patient weight (0.3mmol/kg) is chosen for the patient. This contrast is injected intravenously either by hand or by a commercial injector. (We use a commercial injector from Medrad, Pittsburgh, PA). The injection rate is chosen as discussed below. In actual injections a saline flush is used to push the contrast through the veins into the heart.

3.2.2 Cost and Toxicity

The cost of contrast at the time of this thesis (1999) is about 40 dollars for 10 milliliters of gadolinium contrast agent.

The toxicity of free gadolinium is very great. But chelated gadolinium agents have very high LD50 of about 10 to 30 mmol/kg. It is excreted by the kidneys with a half life of about an hour. A week after administration, less than 1 % of the agent remains in the liver [35].

3.2.3 Contrast Agent's Effect on Signal

T1 agents are signal enhancing because they increase the proton signal in T1 weighted images, while T2* agents are signal decreasing, because they decrease the signal of T2* weighted images. The T1 changes in inverse proportion to the concentration of contrast agent [26].

$$\frac{1}{T1} = \frac{1}{T1_o} + R1 * [Conc] \tag{3.1}$$

where $T1_o$ is the original T1 of the tissue or blood (about 1200 ms for blood), and R1 is the relaxivity in Liter/mmol-sec, and [Conc] is the concentration of agent in mmol/Liter. The R1 is the proportionality constant between $\Delta(1/T1)$ and [Conc]. The T2 changes similarly:

$$\frac{1}{T2} = \frac{1}{T2_o} + R2 * [Conc] \tag{3.2}$$

R2 is the proportionality constant between $\Delta(1/T2)$ and [Conc]. The $T2_0$ is about 250 msec for blood. For fast gradient echo sequences, the transverse relaxation rate of importance is T2*, which is related to T2 by:

$$\frac{1}{T2*} = \frac{1}{T2} + \bar{\gamma}\Delta B \tag{3.3}$$

where $\bar{\gamma}$ is the gyromagnetic ratio, and ΔB is the inhomogeneity around the spins. The ΔB represents the inhomogeneity in the magnetic field due to the magnet itself, the body, and other factors. In addition, when gadolinium contrast is present in blood, the susceptibility of the blood changes with concentration of gadolinium. Just as any paramagnetic substance changes the field around it, the gadolinium in the blood changes the main magnetic field [70].

Contrast agents decrease the T1 and T2. The R1 and R2 can be measured, and depend on the solute and the magnetic field strength. For Gd-DTPA in blood in a 1.5 T magnet, they have been measured to be [27]:

$R1 = 4.3 \frac{Liter}{mmol \cdot sec}$

$R2 = 5.2 \frac{Liter}{mmol \cdot sec}$

Another investigator reported measuring R2* (i.e. $\Delta(1/T2*) = [Conc]R2*$) as 30 L/mmol-sec [57] [68]. The conditions under which this measurement were made (which are not known to the author) are critical for interpreting the applicability of this value. Maki estimated that during gadolinium administration, $T2* \sim 0.66 \cdot T1$ [37].

3.2.4 The Relationship of the MR Signal to T1

The signal for a fast gradient echo sequence depends on the T1, the flip angle, θ, and the TR, TE and T2*. For completely stationary spins, the signal after the nth RF pulse is

$$Mz_n \sin(\theta) = \frac{[1 - e^{(\frac{-TR}{T1})}][1 - (\cos(\theta) e^{(\frac{-TR}{T1})})^n]}{1 - e^{(\frac{-TR}{T1})} \cos(\theta)} (e^{(\frac{-TE}{T2*})}) * sin(\theta) \qquad (3.4)$$

Figure 3.1 plots the evolution of the usable magnetization $Mz_n \sin(\theta)$ through 20 RF pulses, for three different T1 values of 10, 30, and 50 milliseconds which are typical for contrast-enhanced imaging. The TR was assumed to be 7 ms, and the angle is set at the Ernst angle (see below). No T2* effects were modeled. This figure shows the increased signal at progressively shorter T1s, and also how the equilibrium value is reached more quickly for shorter T1 values.

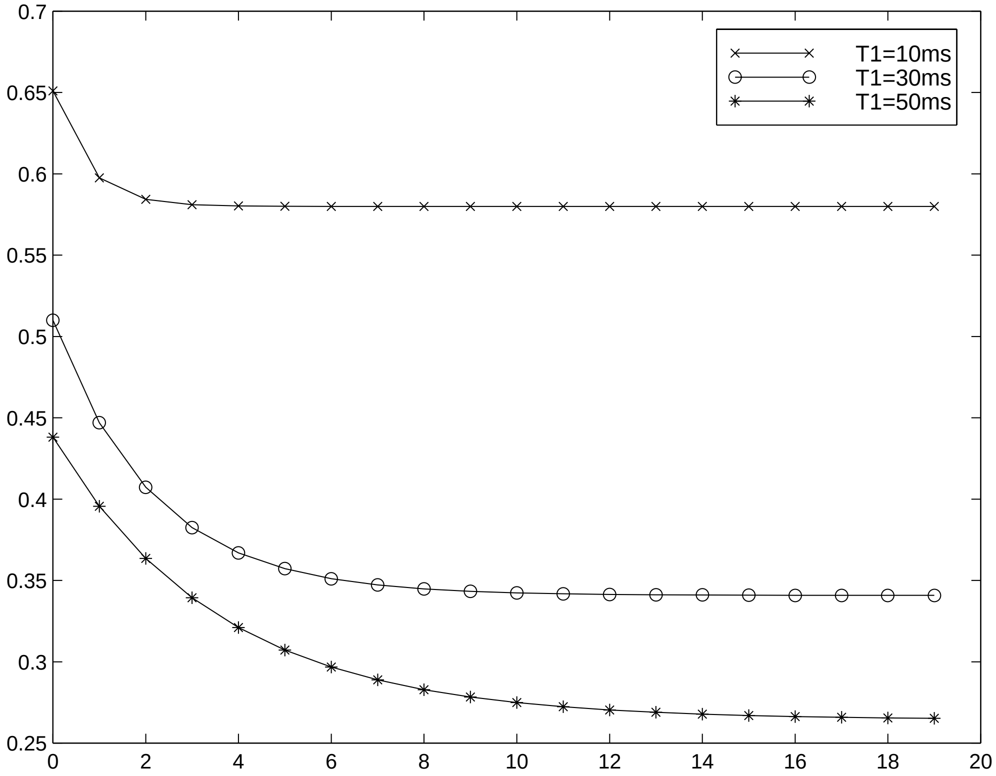

Figure 3.1: $Mz(n)sin(\theta)$ *vs. the number of RF pulses, n.*

After many RF pulses the spins are fully saturated, and the equilibrium signal becomes:

$$Mz_{\infty}\sin(\theta) = \frac{[1-\exp(\frac{-TR}{T1})]\sin(\theta)}{1-\exp(\frac{-TR}{T1})\cos(\theta)}(exp(\frac{-TE}{T2*})). \tag{3.5}$$

This is an important equation because in contrast-enhanced 3D gradient-echo imaging the RF pulses are repeated throughout the scan, without ceasing, so that the spins experience a very large number of pulses, and the signal is equal to the equilibrium signal. The number of pulses necessary to approach equilibrium depends on the flip angle and the TR/T1 ratio, lying in the range of about 8 to 30 RF pulses (see Figure 3.1). At large TR/T1 ratios, equilibrium is approached more quickly.

Usually, the factor involving T2* does not contribute to signal damping, because typical TE's are 1-2 msec, for fractional echo acquisition. The T2* value is not well known. At very high contrast agent concentrations, or for full echoes, damping might occur [37]. The T2 is always lower than the T1, and therefore the T1 value is an hard upper limit on T2. Thus, the signal depends primarily on TR, T1 and flip angle, and sometimes TE/T2*. The equilibrium signal (Equation 5.19) intensity for a given TR/T1 value is maximized by the flip angle called the Ernst angle, defined as the flip angle for which $\frac{dMz_{\infty}\sin(\theta)}{d\theta} = 0$. The Ernst angle is:

$$\theta_{Ernst} = \arccos(\exp(\frac{-TR}{T1})) \tag{3.6}$$

Maximizing the signal provides the highest SNR.

3.2.5 Ernst Angle and Over-tipping

The Ernst angle provides the highest signal. In contrast enhanced imaging, the T1 is not known exactly, but an estimate of T1 and thus the Ernst angle is possible. At times, it is desirable to "over-tip", meaning use a flip angle higher than the one which maximizes SNR. Over-tipping improves the contrast of contrast-enhanced anatomy compared to background tissue, because it saturates more strongly the background tissues that have longer T1s. Furthermore, near the Ernst angle, the derivative $\frac{dSignal}{d\theta}$ is not very large (by definition), and any flip angle near the Ernst angle provides similar signal. Thus the flip angle is set by two considerations. Firstly, maximum signal can be achieved with flip angle set near $(+/-10°)$ the Ernst angle. Secondly, the maximum contrast with background can be achieved with a flip higher than the Ernst angle.

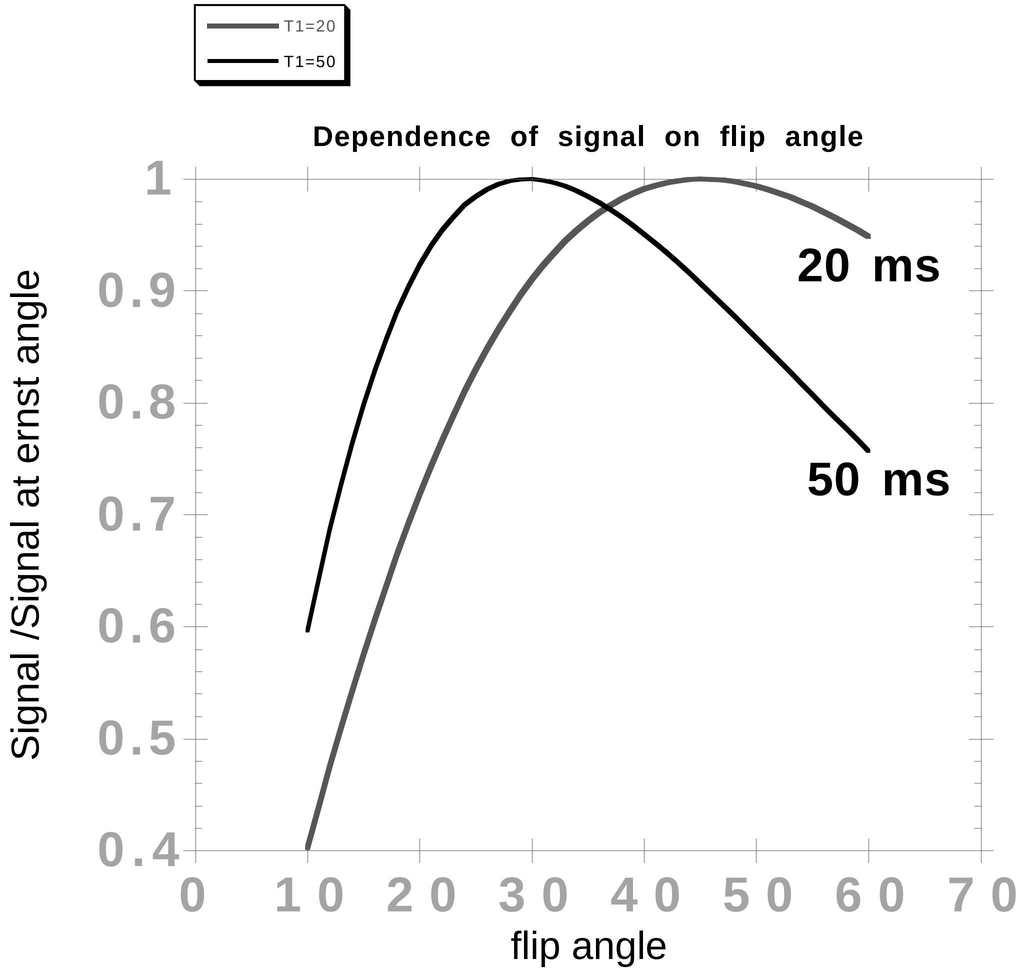

Figure 3.2: *Signal near the Ernst angle.*

Figure 3.2 illustrates these ideas. It plots the ratio of signal to the signal at the Ernst angle against flip angle. This graph illustrates that it is not necessary to know the true T1 in order to obtain the highest signal, because the signal is somewhat independent of flip angle, near the Ernst angle. The exact T1s obtained *in vivo* are not known, but using a flip angle from 30° to 60° will maximize SNR under most conditions, and over-tipping will improve contrast with the background.

3.2.6 Dependence of SNR on Concentration

Equation (5.19) relates signal to T1 and T2*. The relationships between concentration and T1 and T2 have already been described in terms of R1 and R2 in Equation (3.3) and Equation (3.1).

If these two equations are used together, estimates of the signal's dependence on concentration can be made, evaluating the signal at the Ernst angle. Figure 3.3 plots equilibrium signal (flip angle set at Ernst angle) for a huge range of concentrations, only assuming the R1, R2, T1o, T2o, TR and TE. (The model includes an R2* = 5.2.)

This graph shows how as the concentration increases, the equilibrium signal increase begins to roll off. The roll off is highly TE dependent. But even without TE effects, it rolls off when $T1 < TR$. Making T1 shorter than TR by more than a factor of 3 clearly is of no value, since full regrowth occurs after each RF flip. Thus the MR imager is a non-ideal gadolinium contrast agent concentration detector due to signal which rolls off with concentration. Currently, we are operating at about 3 to 15 mmol/L concentration ranges. A discussion on estimating contrast agent concentration is given below.

This plot of signal vs. concentration is limited in some ways. Firstly, as concentration increases, the T2* decreases. The signal damping due to T2* is only one of the effects of a short T2*. A potentially more serious effect is the dephasing of the k-space signal at short T2* [65]. Secondly, the T2* is not well known, since susceptibility effects due to increased concentration are also geometrically dependent [21] [67] [66].

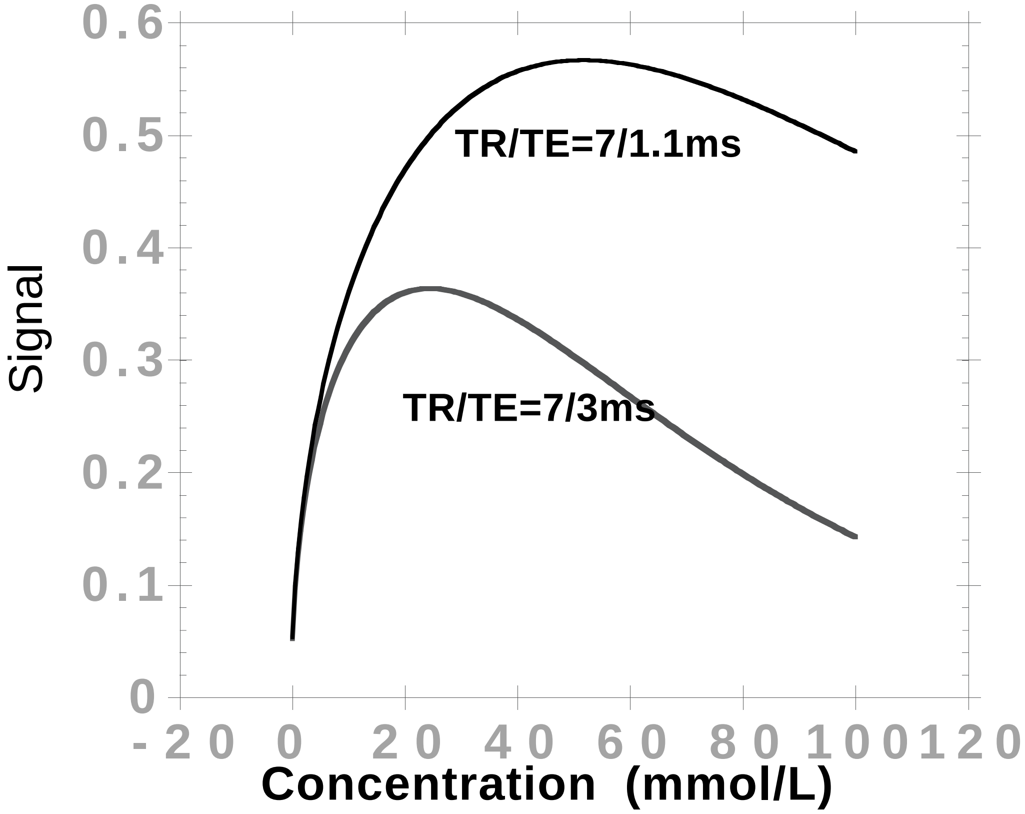

Figure 3.3: *Signal vs. concentration for a short and a longer TE, over a wide range of concentrations. This shows the roll-off of signal at high concentrations, due to T2* effects, and T1 < TR.*

From the graph of signal vs. concentration, it is observed that with current typical acquisition parameters (e.g. concentration of 12 mmol/L, TR/TE = 7/1.0 ms) the usable signal $Mzsin(\theta)$ is about 0.4. The maximum usable signal is

$Mzsin(\theta) = 1$. Therefore, the signal can not increase by more than a factor of 2.6. This is true for TRs of a 100 years, and TEs of 0ms, and concentrations of 1000 mmol/L. They will not improve the SNR by more than a factor of 2.6, compared to what is typically achieved today. That is the limit of contrast-enhanced imaging. When the usable magnetization is 1, then signal cannot be increased any further, except by other means, like coil improvement. Then the noise must be decreased, for example by bandwidth reduction, averaging. However, the SNR performance of pulse sequences vary. For example, currently $M_z \sin(\theta)$ is 0.4 at a TR of 7 ms. If $M_z \sin(\theta)$ is 1.0 at a TR of 7 ms in the future, an improvement could still follow, in which the $M_z \sin(\theta)$=1 for a TR of 1 ms. Furthermore pulse sequences have different requirements on bandwidths, and different scan efficiencies, both of which influence SNR.

3.2.7 Influence of Injection Parameters on In-Vivo Concentration

The importance of T1 for signal level has been explained, and the relationship between T1 and concentration has been shown. T1 is determined by concentration. There are two major factors which determine the concentration of the vasculature and tissue during a first-pass contrast-enhanced scan: the dose, or the amount of contrast injected, and the length of the scan. The amount injected is set by practical or FDA limits. The FDA limit for gadolinium agents is 0.3 mmol/kg of patient weight. The number of mmols injected is determined by multiplying this dose by the patient's weight. The length of the scan (Tscan) is determined by the TR, resolution, and coverage requirements, and patient motion considerations.

These two major factors, dose and scan time, determine the injection rate (Inj. R.), and ultimately the signal enhancements. This is because the injection should be long enough to cause enhancement of the blood signal throughout the scan. At the very least, the injection time is related if not equal to the scan duration. Roughly speaking, the injection rate (Inj. R.) is set by

$$Inj.R. = \frac{dose \cdot mass}{Tscan} \tag{3.7}$$

where mass is the subject's mass in kilograms, Tscan is the scan duration, dose is in mmol/kg, and Inj. R. is in mmol/sec. Inj. R. can be converted to ml/sec, if the initial concentration of the contrast agent is known (0.5 mmol/ml for Omniscan and Magnevist). Thus there are two constraints, dose and scan duration, and this determines the injection rate

Next the relationships between contrast concentration and injection rate, and patient physiology are explained.

3.2.8 Models of Contrast Agent Dilution

What is the relationship between concentration and injection parameters? In the 1980's, when X-ray DSA was being developed, this was a question of interest. Here a model developed for x-ray digital subtraction angiography (DSA) and iodinated contrast agent is presented. This provides a framework for estimating the contrast agent concentration. However, gadolinium contrast agent is not like iodinated contrast, in that it is not a blood pool agent, and it leaves the vascular system. For the first-pass of gadolinium contrast agent, the model provides a useful approximation.

Zierler, in his famous work on indicator-dilution techniques [23] provides a model of how concentration is related to injection rate. If an amount m of dye is injected into a flowing system, then all of it must eventually exit that system. This is a statement of conservation of mass. The amount which exits at any time t in the interval dt, is $dm = C(t)dV$, with dV the volume exiting at time t, in the interval dt. The amount dV of native fluid which exits in a time dt is related to the flow F of the fluid by dV=Fdt. Then dm=C(t)Fdt, which leads directly to the classical equation:

$$m = F \int C(t)dt \tag{3.8}$$

Here F is the flow of the system in Liters/s, m is the amount of contrast agent used in mmols, and C(t) is the concentration in mmol/L.

This model is applied to the concentration in the arterial system after an intravenous injection, which mixes blood with the contrast agent. The injection is performed in a vein, and the contrast travels from there to the heart, into the right atrium and ventricle, through the pulmonary arteries, veins, and capillary bed, and into the left atrium and ventricle. In the ventricles the contrast dose is mixed with the entire cardiac output of the heart. After exiting the left ventricle, the concentration of contrast material in any part of the vascular system follows Equation 3.8. Equation 3.8, sometimes called Fick's Principle, is used to calculate cardiac output, when a known amount of dye (m) is injected into the blood stream.

In contrast-enhanced MRA it can provide an estimate of the concentration, when a known amount of contrast agent is used, and the cardiac output (CO) is assumed (CO = 80 ml/sec). If the shape of the concentration curve is known, its scaling can be calculated by this equation. How is the shape determined?

If no knowledge about the shape of the contrast curve is available, it can be assumed to have some shape, for example a rectangular function. It is zero, increases quickly to some value Cmax for the length of the injection time T, and then returns to zero. Then the integral of Equation 3.8 can be evaluated to equal:

$$m \approx F C_{max} T \tag{3.9}$$

This leads to the well known rule of thumb: $C_{max} = \frac{m/T}{F}$ [16]. Intuitively, an amount of contrast m is mixed in a volume of blood T*F, which is just the amount of blood the heart pumps during the injection period. The blood before and after injection is not mixed with contrast in the first pass. This is expressed more simply for MRA using the injection rate (Inj. R.) in ml/sec of contrast agent, and the initial millimolar concentration (Co=500 mmol/ml) for gadolinium contrast agent.

$$C_{max} = Co \frac{Inj.R.}{F} \tag{3.10}$$

For a contrast curve of any shape Equation 3.8 still must hold.

In the absence of dispersion, an injection at a constant rate creates a rectangular concentration curve, with concentration height set by Equation 3.10. In the presence of dispersion, this rectangular concentration curve is convolved with a dispersion function, which is discussed next.

Dispersion of Contrast Agent: Verhoeven Model

Contrast agent concentration is determined by the injection rate and the cardiac output of the subject. It is also useful to predict accurately the shape of the contrast curve, its slope of increase and decrease and how concentration shape varies in different regions of the body. The contrast curve shape is useful in many aspects of contrast-enhanced angiography. The contrast curve can be used to determine how the acquired k-space will be weighted, and the enhancement and blur due to that weighting can be assessed. In subsequent sections, the weighting of k-space by the presence of contrast is discussed. Knowledge about the dispersion of the contrast (rise time of the concentration curve) allows the possibility of scanning during this upslope, improving utilization of the contrast agent. Another important quantity is time to peak concentration. When attempting to image the arteries in a region where the arterial-venous separation is small, it is beneficial to have short time-to-peak values, so that the arterial peak concentration does not coincide with some contrast agent in the veins. The shape of the contrast curve can be predicted by modeling the dispersiveness of the vasculature.

Verhoeven [63] formed a mathematical description of how the concentration of contrast agent varies with time, at a specific site, and following a specific injection protocol. Verhoeven's method was to consider the human body as system of impulse responses:

$$C(t) = \frac{m}{F}[x(t) \bigotimes h_1 \bigotimes h_2 \bigotimes h_3 ...] \tag{3.11}$$

x(t) is the injection pulse, and h_i's are the impulse responses. The x(t)and $h_i(t)$

functions are normalized, so that their areas are unity. The $h_i(t)$ give the dispersion of the bolus. This expression for concentration satisfies the equation of mass conservation (Equation 3.8). This equation must be rewritten in terms of injection rate (Inj. R.), and initial contrast concentration Co (in the bottle) and injection time Ti:

$$C(t) = \frac{CoTi(Inj.R.)}{F}[x(t) \bigotimes h_1 \bigotimes h_2 \bigotimes h_3 ...] \tag{3.12}$$

Next Verhoeven broke the impulse responses up into sections:

- Arm to right heart
- Right ventricle
- pulmonary artery and pulmonary vein
- Left ventricle
- arterial route to the site of interest

He developed expressions for dilution based on two physical descriptions.

1. Dispersion due to a blunted laminar flow in the vessels. This dispersion of the contrast material is due to a non plug-like flow. Because some portions of the blood move faster than other portions in a vessel, the contrast agent is dispersed.

2. Dispersion due to mixing and ejection in the heart. This dispersion is caused by the churning heart, which ejects a fraction of the total volume in the ventricles, the rest remaining behind for one or more heartbeats.

In the pulmonary capillary bed, he assumed no dispersion. Verhoeven's model leads to simple calculations of the contrast concentration at many physiological sites in the body. The important information that can be extracted is

1. dispersion of the injection when it reaches the imaging site.

2. the initial slope of the contrast concentration.

3. the peak contrast concentration.

The model provides the concentration vs. time for a given injection protocol and assumptions about physiology. The following demonstrates the insight provided by Verhoeven's model of contrast concentration in the body. The model was incorporated into Matlab code.

Verhoeven modeled the influences of injection rate, dose, cardiac output, and imaging site. Figure 3.4 uses his model to show how maximum concentration increases linearly with injection rate, and the concentration persists for shorter period of time. This model is for the carotid arteries, with 0.2 mmol/kg (28 mls) of gadolinium contrast agent. The injection times are equal to 28, 14, , and 5 seconds, for 1, 2,4, and 8 ml/s injections. The time of the rising edge is at about 11 seconds in Figure 3.4. The falling edge occurs about 26, 14, 7, and 4 seconds later, for the 1, 2, 4, and 8 ml/s injections respectively. There is maximal contrast present for slightly less time than the injection time, and contrast during an additional wash-in and wash-out times. If the injection time is shorter or about equal to the dispersion width (as for the 6ml/s, 5 second injection), then the peak concentration, Co(Fi/F) is never reached.

Figure 3.5 shows how the concentration changes with imaging site, for a

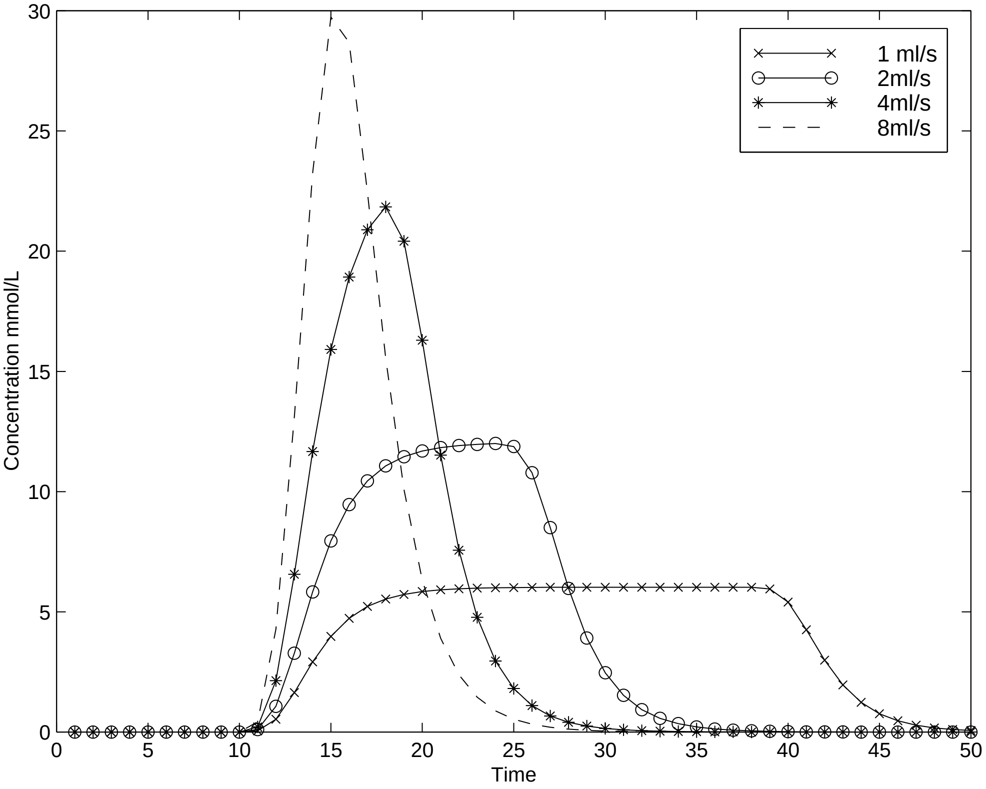

Figure 3.4: *Injection rate's influence on bolus shape.*

fixed injection rate and dose. The separate transit times for the carotid, renal, bifurcation and popliteal arteries are 0.7, 1.5, 2.6 and 5.6 seconds (These transit times are from the left ventricle to the region of interest through the arteries). The FWHM of C(t) changes very little except for case of the popliteal artery. The simulation included an injection rate of 1 ml/s, and a dose of 0.1 mmol/kg. The peak concentration is about the same for all imaging sites. The enhancement is progressively delayed.

Another use Verhoeven's model is to analyze the signal's time dependence related to dose, for a fixed injection rate. Figure 3.6 shows the predicted signal versus time curves in the carotid arteries for a dose of 2 mls and 42 mls of

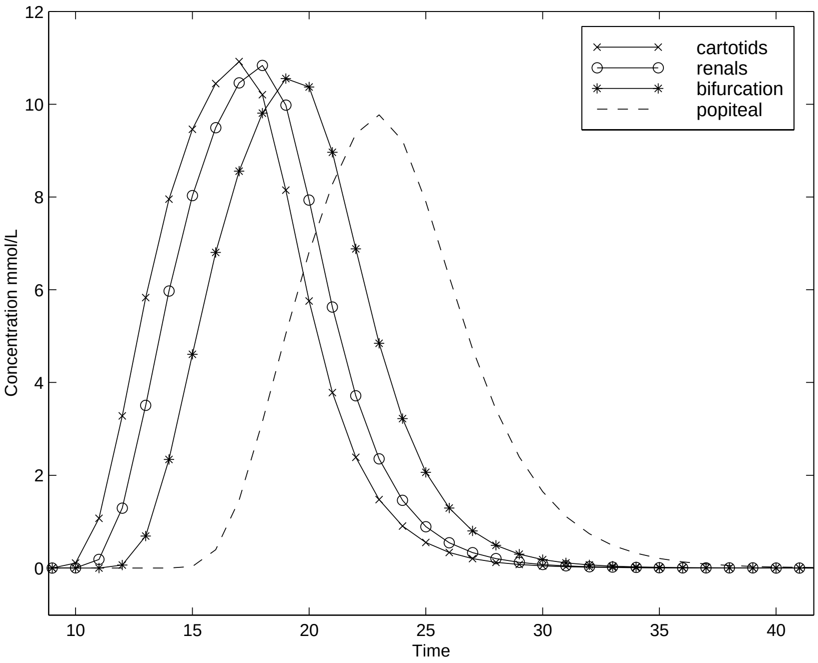

Figure 3.5: *Site dependence of concentration, showing concentration curves for the carotids, renals, the bifurcation and popiteal arteries, respectively.*

gadolinium contrast agent, both given at an injection rate of 1 ml/sec, with identical assumptions on scan parameters and physiological parameters. It is observed that the contrast does not reach its peak value when only 2 mls are injected. This shows that a dose timing scan using 2 mls will give ambiguous information when planning for a larger dose injection, because the time to peak is different for the two doses. The use of dose timing scans is discussed below.

Verhoeven's model, as stated above, was for first pass iodinated contrast agent. It must be cautiously used for extravascular contrast agents. MR imaging often extends into the venous and the recirculation phases. The pulmonary perfusion bed probably extracts some from the amount of contrast present in the blood during first pass imaging, since all venous blood passes through this vascular bed.

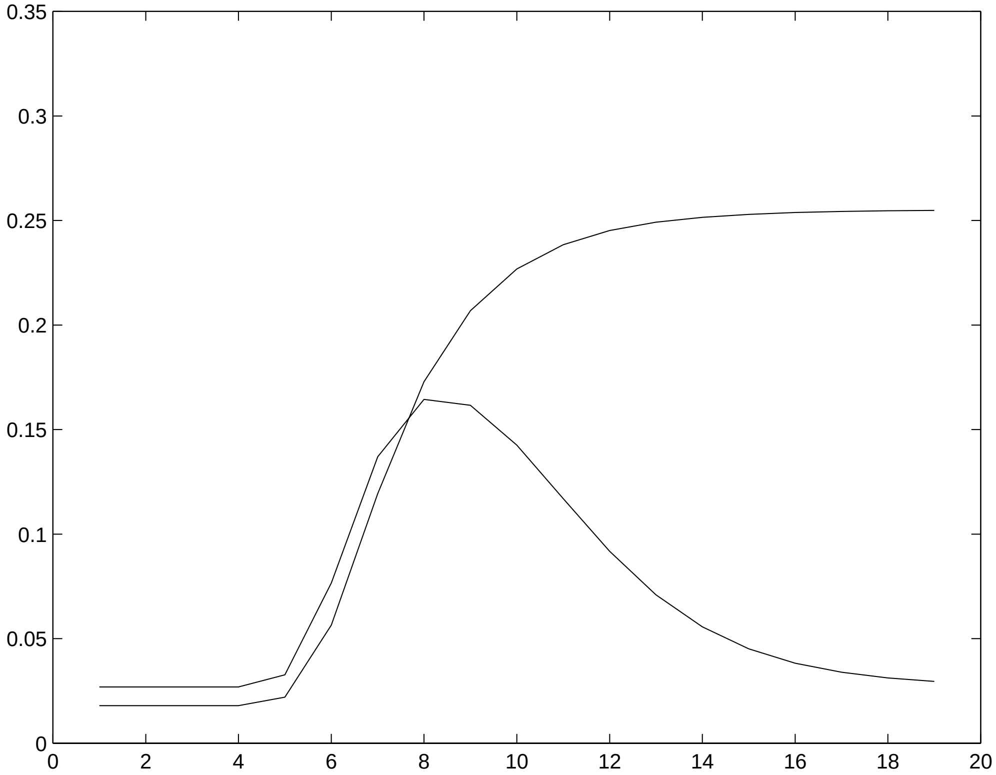

Figure 3.6: *Signal vs. time (seconds) in the carotids with a 1ml/s injection, comparing a 2 ml and a 42 ml dose of gadolinium contrast agent.*

To our knowledge this has not been studied for MR. Beyond that, extravasation in other tissues should not alter the situation during first pass MR imaging, compared to x-ray DSA. The slow acquisitions performed in MRA mean that some of the scan may be performed during the enhancement of veins and during recirculation. The concentration after a single recirculation may begin to equal the equilibrium concentration, which is discussed below. The simulated concentration curves above show concentration returning to zero. This does not happen, the agent is recirculated and extravasated and excreted.

In order to import Verhoeven's model into contrast-enhanced MR angiography, experimental verification in MR of the relationship between concentration or T1 and injection parameters is needed. While Verhoeven was able to verify the model for x-ray DSA and iodinated contrast, there are some differences in MR.

This model has been used in contrast-enhanced MR angiography to predict the shape of the contrast curve. Maki, whose work has concentrated on optimizing 3D contrast enhanced MR angiography with respect to timing of the acquisition of k-space, has used Verhoeven's model to predict concentrations of gadolinium contrast agent [37]. Other investigators have measured signal vs. time data from small test boluses, and used this as an impulse response function which must be convolved with the injection pulse, to estimate concentration curves of a full bolus of gadolinium contrast agent [46].

The new features which must be incorporated into Verhoeven's model for contrast MRA are:

- Recirculation concentration.
- Extravasation: how much of the contrast disappears during first-pass into the tissue.

When these characteristics have been incorporated into the model, and the model has been verified, it should provide more insight into contrast MRA.

3.2.9 Equilibrium Concentration

A simple estimate of equilibrium concentration is presented here. After the injection and first pass and equilibration of contrast agent, the concentration is about equal to the number of mmols injected divided by the total blood volume.

$$C_{equilib} = \frac{m}{5L} \tag{3.13}$$

This amount is the maximum concentration in the blood. Some of the gadolinium contrast agent has extravasated into the tissue beds. Some of it begins to be excreted by the kidneys.

In the absence of extravasation and excretion, the equilibrium concentration is 1 mmol/L to 4 mmol/L, for typical injection amounts spanning 10 to 40 mmol. This corresponds to T1s between 180 ms, and 45 ms. This means that even after first pass, extremely short T1s and signal enhancement persist, especially for large doses. This is surprising, because it is not common practice to obtain good angiograms in the post-contrast phase. If the T1 is truly this low after first pass, then this equilibrium period could be used for imaging.

One recent article reported that, measuring signal with a rapid 2D sequence during the first pass of 20mls injected at 3 ml/s, approximately 30% of the peak signal persisted in the arteries [53] after the first pass. Using some assumptions leads to an estimate of the post-contrast concentration:

1. $\frac{Signal_{post}}{Signal_{during}} = \sqrt{\frac{T1_{post}}{T1_{during}}} = 0.3$
2. $1/T1 \sim [Conc]$
3. $0.3 = \frac{Signal_{post}}{Signal_{during}} = \sqrt{\frac{[Conc_{post}]}{[Conc_{during}]}}$
4. $[Conc_{during}] \sim Co\frac{Inj.R.}{CO} = 500\frac{3}{80} = 19 mmol/L$
5. $.3 = \sqrt{\frac{[Conc_{post}]}{19}}$

6. $[Conc_{post}] = 1.7 mmol/L$

1.7 mmol/L concentration corresponds to 20 mls of contrast in about 6 L of blood. This concurs with the simple predictions for equilibrium concentration above.

To rapidly measure the signal during first pass using 2D methods may be misleading. The relationship between signal and concentration in a 2D sequence is not straightforward, because the slice profile of the RF excitation is non-ideal, and the tip angle is non-constant over the slice [64]. Furthermore, some of the post-injection increase in signal may be due to combined inflow and shortened T1.

3.2.10 The Outer Limits of Contrast Enhancement

With the use of contrast-enhanced MRA, researchers have begun to see its limitations. Heid [40], and Pelc [39] and Parker [27] have discussed the SNR of contrast-enhanced imaging in terms of dose, bandwidth, and voxel size only, starting from the conventional description of SNR as related to bandwidth, voxel size, and the number of encodings acquired.

To evaluate the SNR of a contrast-enhanced image, the conventional equation for SNR is used [8]:

$$SNR \sim Mz \sin(\theta) \frac{\Delta x \Delta y \Delta z \sqrt{NxNyNz}}{\sqrt{BW}} \tag{3.14}$$

where the voxel size is $\Delta x \Delta y \Delta z$, Nx, Ny and Nz correspond to the number of frequency encodings, phase encodings and slice encodings acquired, and BW is the bandwidth.

Equation (5.19) which gives $Mz\sin(\theta)$ is simplified when θ is the Ernst angle and $TR \leq T1$. Then, as Parker [27] has shown, the signal becomes:

$$Mzsin(\theta) = \sqrt{\frac{TR}{2T1}}exp(\frac{-TE}{T2*}) \tag{3.15}$$

If this evaluation of the usable magnetization is substituted into Equation (3.14), neglecting T2* decay, the result is

$$SNR = k\frac{\Delta x\Delta y\Delta z\sqrt{TRNxNyNz}}{\sqrt{BW \cdot T1}} \tag{3.16}$$

Here k is a constant. Heid and Pelc rearranged these terms, observing that TR*Ny*Nz is equal to the scan time, Tscan. 1/T1 is approximately equal to R1[Conc]. Nx/2BW is the Tadc, the duration of the readout.

$$SNR = k\Delta x\Delta y\Delta z\sqrt{[Conc] \cdot Tscan \cdot Tadc \cdot R1} \tag{3.17}$$

Recall that $[Conc] = Co\frac{Inj.R.}{C.0.}$. Thus $Tscan \cdot Conc \sim Tscan \cdot Inj.R. \sim dose.$ Therefore, $Tscan \cdot [Conc]$ can be replaced by dose in the above equation, yielding:

$$SNR = k\Delta x\Delta y\Delta z\sqrt{(R1)(dose)(Tadc)} \tag{3.18}$$

Heid and later Pelc showed how SNR dependence on T1 and Tscan is equivalent to dependence on dose. This means that SNR is constant with decreasing scan time, unless Tadc is changed. This shows that SNR is proportional to nothing but dose, the voxel size, and the Tadc. Thus the proportionality of SNR to scan time, or the number of encodings is gone.

Their insight on SNR in contrast MRA can be further interpreted. In MR, the SNR increases by the number of phase-encodings or slice-encodings, holding voxel size constant. In contrast-enhanced MR, if the number of encodings are increased, for equal scan time, the TR must be decreased, and SNR stays constant. If the number of encodings are increased by increasing scan time, the injection rate is lowered and consequently the $\Delta(1/T1)$ decreases. SNR is is about the same.

This SNR equation shows that longer TRs improve the SNR just as much as averaging does or scan time does. But this is only the case when Equation (3.15) holds, i.e. when $TR \leq T1$. Once the TR is increased beyond the T1, SNR again begins to depend on Ny, Nz, or scan time.

This new dependence of SNR on scan parameters does profoundly change the methods in contrast-enhanced MR angiography. Firstly, for constant voxel size, SNR is not dependent on scan time, but on the dose given. Thus a fast single volume scan can have equal SNR to slow single volume scans. Faster scans offer advantages in terms of patient motion, and arterial venous separation. However, as always, SNR improves with increased Tadc. Low bandwidth scans have better SNR than high bandwidth scans. With longer TRs, and resultant longer injections, lower bandwidths are possible. For contrast-enhanced imaging, the SNR is dependent on dose, not scan time. However, the best SNR will be obtained at low bandwidths, which usually result in long TRs and long scan times. Further discussion of the tradeoffs in fast imaging can be found in the next chapter.

3.2.11 Extravascular Contrast Agents

Extravascular agents perfuse through the vessels and leak out of the capillaries. They change the T1 and T2* of the vessels and the extravascular-extracellular space. MRI contrast agents do not enter cells. The measured T1 of a voxel is the average T1 of all water protons in that voxel. If it is a tissue voxel, then the water may have moved through the capillary, the cells, and the interstitial space during the TR, depending on the exchange rate of water between spaces. Such a proton will have experienced faster and slower regrowth environments. Equation (3.1) is only true for the "single compartment model", where the water proton experiences the effects of contrast agent of some concentration. For example, if there is water proton exchange between two compartments, one with contrast agent and another without, there are two T1s, one shortened by contrast, the other unchanged. The water's T1 is a weighted combination of the T1s of these two compartments, with weights related to the exchange rate between the compartments [28]. In tissues there are multiple compartments, while in large blood vessels imaged in angiography, there is only one compartment, the plasma. The plasma water is in fast exchange with the water in the blood cells [41]. There is evidence that there is not fast water exchange between the water in the capillaries and the water in the interstitial fluid, nor between the interstitial space and the cellular space [41].

Extravascular contrast agents, because they extravasate into the tissue, result in tissue enhancement in contrast enhanced MRA, which reduces the contrast between blood vessel and tissue.

3.2.12 Intravascular Contrast Agents

To date (1999), all FDA approved MRI contrast agents are extravascular agents which leak into the interstitial space and cause tissue enhancement. The concentration in the blood pool after the first pass is reduced, because some of the contrast resides in the interstitial space.

Many contrast agents are being developed which do not leave the blood pool. These are called intravascular agents. They are created by linking gadolinium chelate to a macromolecule, which is too large to pass through the capillary wall. Another intravascular agent which we have studied, Angiomark (EPIX Medical), binds to serum albumin. These agents are useful for a number of reasons.

For perfusion studies, which measure capillary blood flow to important organs like the heart and brain, intravascular agents might simplify the analysis of how signal intensity relates to blood flow. For extravascular agents, the transit time of contrast agents through the capillary bed is related to blood flow and to the extraction of the contrast into the interstitial space [58], but for intravascular agents the transit time is just related to the capillary network, and the capillary blood flow [59]. The intravascular agent does not leave the capillary, so measurement of its flow through the capillary network can be accomplished by measuring the signal time course in the tissue.

For contrast-enhanced MRA, these intravascular agents persist in the blood pool, causing T1-shortening for much longer than an extravascular agent because they do not extravasate into the tissue beds. The R1s are often greater than for gadolinium based intravascular agents because they are bound to large molecules. For example, for the Epix contrast agent Angiomark, the R1 varies from 45 $L \cdot mmol^{-1}sec^{-1}$ to 30 $L \cdot mmol^{-1}sec^{-1}$ for concentrations from 0.1 to 1 mmol/L, respectively, which is much higher than the R1 of the extravascular gadolinium contrast agents. However, the relaxivity of Angiomark is concentration dependent because as the Angiomark binds to the albumin sites in the plasma, these sites become saturated. The unbound agent has much less relaxivity. At typical first-pass gadolinium contrast agent concentrations of 5 to 10 mmol/L, the T1 shortening of extravascular gadolinium contrast agent may be equivalent to that of Angiomark. For steady state imaging at low contrast agent concentrations, Angiomark provides much shorter T1s for an extended period of time.

Our research group was involved in a research trial with Angiomark. One project was to image the coronary arteries using this agent in animals (pigs). During first pass the data was acquired using a ECG-gated, segmented, multiphase 3D fast gradient echo sequence, with a half FOV or the reduced FOV technique of Frederickson-Pelc [69] during a breath-hold [50].

Figure 3.7 shows the results of one such study, acquiring the data during first pass; two slices with large segments of the left anterior descending and the right coronary artery and a segmented MIP overlaying a slice are shown. Imaging parameters were: 256 (160 acquired) kx, 64 ky, 24 kz, rectangular FOV 24 x 12 cm, voxel size 0.9 x 0.9 x 2.0 mm, 288 ms temporal aperture. These slices show some segments of coronary arteries. They were the first 3D images of the coronary arteries with an intravascular contrast agent and among the first 3D ECG-gated images of the coronary arteries with with extravascular agents [17] [18]. However, currently many researchers are working in this area with greater success [62].

Equation (3.16) which states the SNR dependence: $//SNR = k\Delta x\Delta y\Delta z\sqrt{\frac{TRNxNyNz}{BWT1}}//$

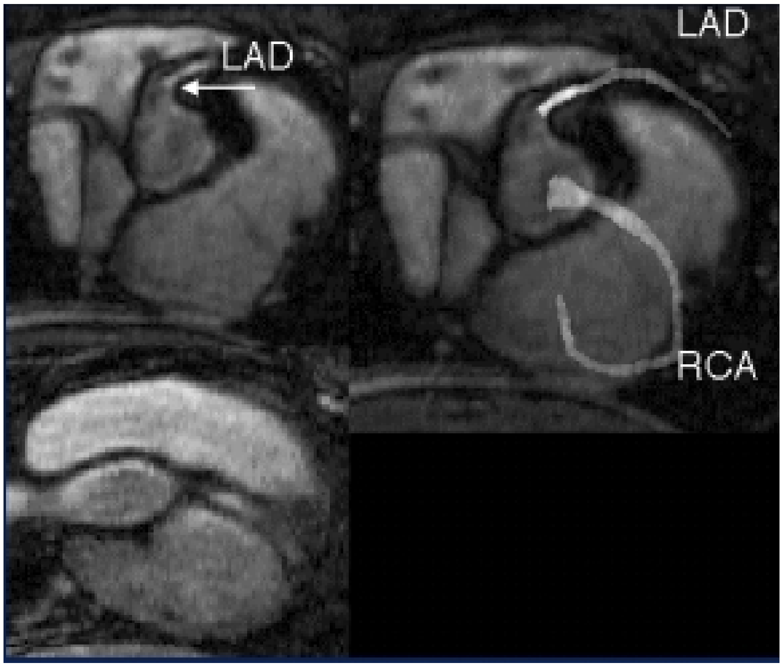

Figure 3.7: *Slices from a 3D volume of the heart, plus a segmented MIP overlaying a slice. See text for discussion.*

applies uniquely to the ongoing research on 3D breath-hold contrast-enhanced segmented cardiac gated coronary artery imaging. In cardiac gated sequences, a few phase-encodings and slice-encodings are obtained each cardiac phase. They are usually acquired with short TRs, within a small fraction η of each cardiac cycle, and during a breath-hold of about 30 seconds. In these scans the contrast is injected so as to be present for the entire 30 seconds, but the data is only collected for a fraction η of this time, equal to the fraction of the heart beat used. Now TR*Ny*Nz is not the scan time Tscan. TR*Ny*Nz is equal to η Tscan. Then, using $\frac{1}{T1} = R1 \cdot [Conc]$ and expressing [Conc] as $[Conc] = \frac{dose}{Tscan}$ and recognizing that $TR * Ny * Nz = \eta Tscan$ we obtain the SNR for a cardiac gated contrast-enhanced exam: $SNR = \Delta x \Delta y \Delta z \sqrt{(R1)(\eta(dose))(Tadc)}$.

This shows one drawback to cardiac gated contrast-enhanced imaging. Instead of having all the advantages of contrast imaging, it instead uses an effective dose that is only a fraction of the dose injected.

Another contrast agent which has been investigated by our group is NC100150 (Nycomed, Oslo, Norway). This is an ultra-small super-paramagnetic iron oxide contrast agent with an R1 of 20 $Lmmol^{-1}sec^{-1}$ measured at 0.5 T [48].

Steady state imaging with an intravascular agent provides high SNR high resolution images. We investigated Angiomark using high resolution steady state acquisitions, with good results [32]. An example of this research is given in Figure 3.8.

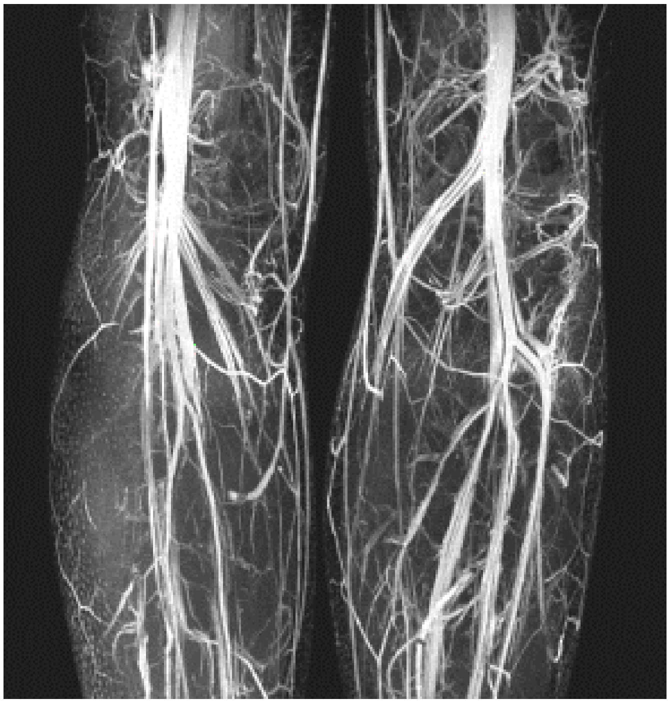

Figure 3.8: *A steady state MIP of the legs using an intravascular agent, Angiomark. Vessel detail is excellent, but veins are present in the image.*

One serious drawback to steady state imaging is venous enhancement, as can be observed in Figure 3.8. Artery-vein segmentation techniques for steady state imaging are the subject of investigation in our research group [43]. Another serious drawback is respiratory motion and other motions.

3.3 Acquisition Order for Contrast-enhanced MRA: Theory

When performing a contrast-enhanced acquisition, acquisition order and acquisition timing are essential. Several valuable techniques have been found for obtaining the best images with contrast. They will be reviewed here.

Contrast agent concentration is a function of time (C(t)), as discussed above. Thus the signal from the water spins is changing with time. Acquisition order refers to the specific temporal order in which k-space is collected. Each k-space point is acquired with a different bulk signal. This weights the k-space signals. The reconstructed image is affected by this k-space modulation:

$$Image^{'}(x,y) = Image(x,y) \bigotimes FT[W(kx,ky)] \tag{3.19}$$

where W(ky,kz) is the concentration-dependent weight. Various acquisition sequences and injection protocols differ in their resolution and contrast sensitivity due to the different k-space weightings they provide in accordance with Equation 3.19. It is advantageous for W(kx, ky) (hence C(t)) to be as large as possible to increase the signal. But secondly, ideally C(t) would be constant so that the image would be identical to the true image. These two aims sometimes conflict with each other. Thirdly, if it is not possible to have uniform k-space weights it is at least desirable to avoid discontinuities in the weighting function so that ghosts and ringing do not occur.

This goal is challenging because the concentration vs. time curve is not well known. Furthermore, due to limitations on contrast dose, contrast cannot be injected so as to create a maximum concentration over a very long time, to remove any issues of timing. But the most compelling challenge for CE-MRA comes from the desire to obtain an arteriogram without venous contamination. Most of problems stem from this goal. If this need could be circumvented, angiograms of higher quality could be easily obtained.

Many solutions that have been found to timing and acquisition order challenges are presented in the next sections.

3.4 Acquisition Timing

Many timing methods exist, by which the the relative timing between injection and the initiation of a scan is estimated.

- best guess
- test bolus injection
- automatic signal detection (MR SMARTprep)
- fluoroscopic detection (real time image monitoring)

Timing indicates the delay between the start of injection and the arrival of contrast in a region of interest. This delay includes the time for the contrast to transit the intravenous injection line, the time from the vein into the heart, and the time to the final region.

3.4.1 Best guess

The simplest way for timing an acquisition is to guess how long it will take for the contrast to reach the site of interest, based on experience. For example a recent report on contrast-enhanced MR pulmonary imaging [47] used a 5 second delay between the start of a 5 second 4ml/s manual injection of contrast, and the start of a 23 second scan. This report noted that a better timing method should improve the results.

These delays are effectively used, but they may vary. The time to peak aortic enhancement was measured as 34 +/- 5 seconds in one study [36]. To our knowledge no study has determined the contrast arrival variation within the same person. The best guess method is only appropriate for a scan which does not require timing accuracy. In sections below some acquisitions which can rely on best guess are presented.

3.4.2 Dose timing scan

Another method, advocated by Earls [54] and Grist [55], is to inject a small amount (1-4 ml) of gadolinium contrast agent at the same rate as planned for the imaging scan, followed by a larger amount of saline solution (20 ml). The injection is timed to coincide with the start of a 2D fast gradient echo scan which acquires one thick (30-80 cm) slice at a rate of 1 slice per second. The same slice is imaged each second. The slice is prescribed so that it contains anatomy which will be imaged during the contrast scan. Usually axial slices which have inflow-related enhancement are avoided, and coronal and sagittal views are acquired. Inflow enhancement, whereby spins that have experienced no RF pulses enter the slab and increase the signal, must be avoided because such enhancement mimics the arrival of contrast agent.

The timing scan can be improved by adding an RF pulse which inverts the spins by 180°, non-selectively. The acquisition of the center of k-space is then timed to occur when the longitudinal magnetization of unenhanced blood (T1=1000ms) is about zero. Then inflow of unsaturated blood will not mimic the appearance of contrast. In the time series of images, the arterial vessels of interest will enhance when the gadolinium contrast agent arrives into that region. The venous vessels will enhance soon after. Using the images, it is possible to assess the timing delay between start of injection, and arrival of contrast into a region of the body. This delay is the necessary information for timing the injection to match the 3D contrast-enhanced acquisition.

Timing scans have some potential shortcomings. Firstly, there is no validation that the contrast arrives at a region of interest in equal times for two different injections. Furthermore, it is known that variations in breath-hold can change the time of arrival, and breath-holds are performed in abdominal scans.

Another problem was discussed above. A small 2 ml injection may not portray the contrast dynamics, because maximal enhancement is never achieved. The simulation of Figure 3.6 shows that the concentration obtained with a 2 ml bolus indicates a time-to-peak which is about 5 seconds less than the 42 ml bolus indicates.

3.4.3 Automatic Bolus Detection

Another method for coordinating injection and k-space acquisition is through use of automatic signal detection. The full dose is injected and a region of interest is selectively excited and monitored for signal increase. When the signal increases above some user-specified base-line, the acquisition is initiated. This is now available on GE scanners as MR SMART-PREP [144], where the region is monitored with a spin echo sequence, using slab selective 90° and 180° pulses. The selected slabs are orthogonal, and their intersection defines a rectangular monitoring region.

3.4.4 Fluoroscopic Triggering

Another timing method, developed by the Mayo Clinic group, is called fluoroscopic triggering [52]. A full dose of gadolinium contrast agent is injected. Instead of monitoring a signal level in an user-specified rectangular ROI, they monitor a slice similar to that prescribed for the dose timing scan, except that it is reconstructed and assessed in real time. When there is visual detection of contrast by an operator, the operator switches to a contrast-enhanced 3D acquisition.

3.4.5 Timing Methods: Breath-holding

In all of these methods, abdominal imaging requires that a breath-hold be coordinated with the start of acquisition. The patient is instructed to suspend breathing either in real time (with fluoroscopically triggered timing or automatic contrast detection) or at the start of the scan (with test bolus timing).

3.5 Acquisition Orders

There are several possible acquisition orders which may be used, some of which do not require timing:

- Sequential acquisition
- Centric acquisition
- Elliptical centric acquisition
- 3D-TRICKS (variable rate k-space sampling)
- 2D Projection imaging
- Multi-Frame Fast imaging

The primary criteria for a good acquisition order has been discussed above: a smooth weighting of k-space, enhanced SNR, and venous rejection.

Figure 3.9 shows a contrast enhanced slice, and its k-space representation on a log scale. It has been observed from such images, that most of the image energy lies in the low spatial frequencies. In fact, the Fourier transform theory states that any object except a point object has most of its signal at low spatial frequencies. Using this simple concept all of contrast-enhanced imaging is driven to acquire the central region of k-space during the time of peak arterial concentration, and low venous concentration. This achieves high SNR, by acquiring central k-space at peak concentration and achieves venous rejection by only allowing high spatial frequency representations of the veins into an image.

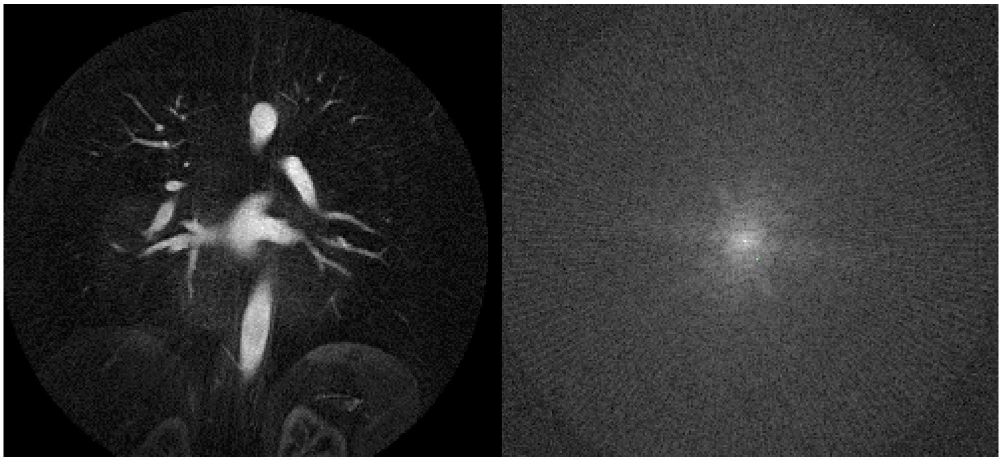

Figure 3.9: *Image slice and k-space representation on a log scale, showing that information is concentrated in the center of k-space.*

3.5.1 Acquisition Order Overview

Figure 3.10 shows the ky-kz-space with grid lines which indicate k-space data acquired during an acquisition. The center of k-space contains the most information. Acquisition orders are defined by how they collect the grid-points shown. A sequential acquisition starts at the top left corner, and proceeds to the bottom right corner, acquiring every point sequentially. A centric acquisition acquires points dependent on their proximity to the ky=0 line (ky-centric), or the kz=0 line (kz-centric), as shown by the vertical and horizontal arrows in Figure 3.10. The elliptical centric acquisition acquires k-space based on proximity to the point ky=0, kz=0.

3.5.2 Sequential Imaging

Sequential imaging can be used when arterial venous separation is not necessary or at least not challenging. In sequential imaging, the center of k-space is acquired

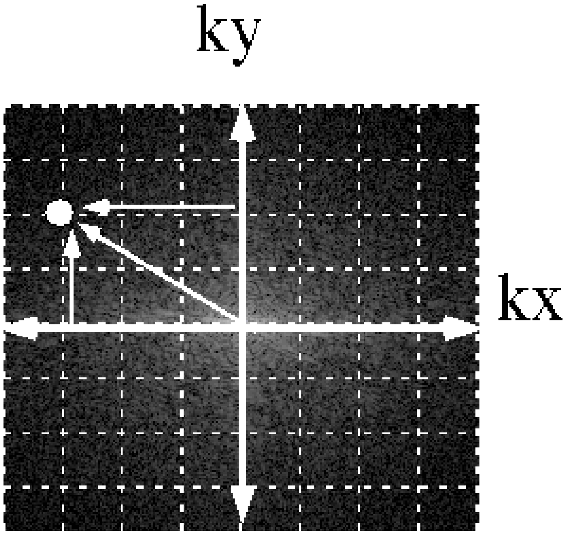

Figure 3.10: *k-Space grid, indicating acquired points, and showing how acquisition order is based on the proximity of a grid point to ky=0 or kz=0 lines, or the point (ky,kz)=(0,0).*

at the midpoint of the scan. Some researchers suggest acquiring the center of k-space at the midpoint of the contrast bolus [56].

3.5.3 Centric order

A centric acquisition acquires the ky or kz data in order of their proximity to the center of k-space. Centric ky encoding acquires all of kx and kz for the most central ky value, and then proceeds to the next most central ky value, until all the ky values have been collected. Centric kz encoding acquires all of the kx and ky points for the most central kz, before progressing to the next most central value.

Centric encoding achieves the goals of contrast-enhanced imaging by combining centric acquisition with accurate timing. The acquisition is timed to coincide with the onset of peak arterial enhancement. Because the arterial signal is at its peak, the central k-space is highly weighted, providing high signal and high SNR. Furthermore, because the veins have low signal during collection of central k-space, veins have low signal and SNR in the image. That is enough to suppress the veins and enhance the arteries. The weighting of kz or ky space (depending on whether centric ky or centric kz is used) is as smooth as the contrast bolus. The veins hopefully only enhance during collection of high spatial frequencies, and have inadequate weighting of low spatial frequencies. Only a high-pass filtered version of the veins appears.

When k-space is collected in a centric manner in breath-hold applications, the low spatial frequencies are collected immediately after the breath-hold occurs. Any mis-timing of the breath-hold could result in serious motion artifact. Studies have shown that in the early phase of the breath-hold some motion occurs. This may be a limitation.

3.5.4 Elliptical Centric View Order

Closely related to the centric acquisition is the elliptical-centric acquisition [29] [53]. This acquisition order is centric in ky and kz. It acquires frequency encodings for the smallest kr value, and then proceeds to the next smallest kr-value, where $kr = \sqrt{kz^2 + ky^2}$. (See Figure 3.10.) Arterial enhancement, venous rejection, and smoothness are achieved just as for the centric order.

In an elliptical-centric acquisition, the FOVz is determined by the slab select thickness, and not by aliasing concerns. The FOV in the z dimension is usually significantly less than in the y dimension. This means that $\Delta kz > \Delta ky$. The jumps in kz are much larger, so that an acquisition order based on radial proximity to the center of k-space would acquire many consecutive ky values, before incrementing its kz value. Because of this the elliptical-centric acquisition is similar to the centric kz acquisition. Elliptical-centric acquisitions are more “centric” than ky or kz-centric orders, so they are more effective at suppressing veins and enhancing arteries. But when (as often occurs) there are large disparities between z and y FOVs, elliptical-centric becomes similar to kz-centric.

The elliptical centric and the centric methods rely on small FOVs in y or z to jump out quickly to the edges of k-space. Centric acquisition (in kz or ky) also relies on a limited number of encodings in the other dimension (ky or kz), so that the low spatial frequencies are quickly acquired.

3.5.5 3D-TRICKS

The 3D-TRICKS technique (Time Resolved Imaging of Contrast KineticS) [30] developed at the University of Wisconsin, uses a k-space acquisition which for some applications greatly reduces the timing requirements. This is very different from the centric or elliptical-centric orders, although it relies on the concept that the central region of k-space must be acquired during peak arterial enhancement. Accurate timing is not necessary for 3D-TRICKS. In 3D-TRICKS, ky space is broken into multiple segments, for example four, called A, B, C, and D, as shown in Figure 3.11.

The A segment is the central-most portion of ky-space, while the D segment is the outermost region of ky-space. Then the acquisition proceeds as:
D C B A B A C A D A B A C A D ...etc..

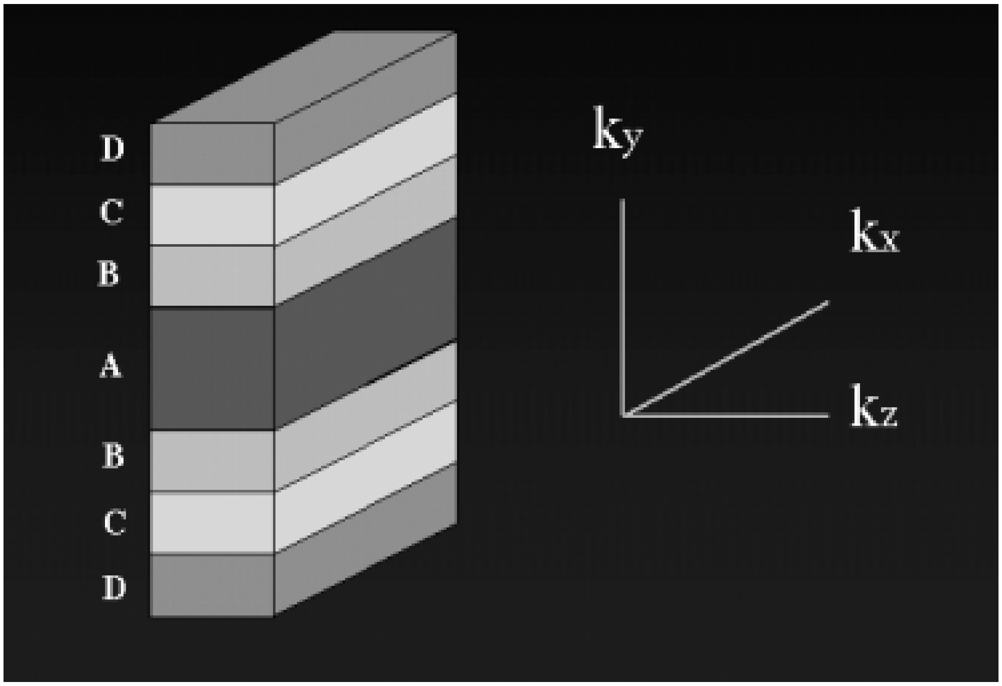

Figure 3.11: *Omnis k-space est divisa in quattor partes (All of k-space is divided into 4 parts)*

Acquisition of a segment means acquiring sequentially the ky-lines (both positive and negative ky values). For every ky value of the segment, all kz (slice-encoding) and kx (frequency encoding) values are acquired. Inspection of the acquisition order shows that A is acquired three times more often than B C or D. The acquisition samples a full mask data set (D C B A) and then acquires A (the central region) often enough to ensure that an A segment is obtained during peak arterial enhancement prior to venous enhancement. The reconstruction is performed by linear interpolation of the data, using either forward-looking, backward-looking, or nearest-neighbor linear interpolation. In other words, the A, B C, and D segments are needed to form a complete k-space, and they are obtained by using data that was acquired temporally closest to the A segment being used. Multiple temporal frames can be reconstructed. In fact a complete 3D volume can be created with a frame time equal to the time to acquire a single segment. For N segment 3D-TRICKS acquisition of Ny phase-encodings and Nz slice-encodings, the 3D-TRICKS frame time T_F is:

$$T_F = TR \cdot Nz \cdot \frac{Ny}{N} \tag{3.20}$$

$$\tag{3.21}$$

The temporal aperture (T_{app}) is defined as the temporal window in which all the data (e.g. A B C and D) used in reconstruction of an image volume is collected. For four segments, inspection of the acquisition order shows that the temporal aperture, T_{app} is:

$$T_{app} \geq 5(FrameTime) \tag{3.22}$$

There are tradeoffs with this method, compared to the centric methods. One advantage of 3D-TRICKS is that multiple frames can be reconstructed instead of a single frame. Thus the passage of contrast through the vasculature can be observed. In the case of disease, any late filling vessels can be observed in later frames. This is not possible for a centric acquisition which produces a single 3D volume. The second advantage of 3D-TRICKS is that timing is unnecessary for non breath-hold applications, since the center of k-space is repeatedly acquired. Timing is required for breath-hold imaging, so that the subject suspends respiration during the the peak arterial phase of the injection. The main disadvantage is that during the most valuable time period, which starts at onset of peak arterial gadolinium contrast agent concentration and depreciates from there, the central

A region is collected 1 or 2 times more often than is absolutely needed, so that from 1/5 to 1/3 of the most important time is not used efficiently, either for collection of more high spatial frequency information, or for increased TR, decreased bandwidth acquisitions. The "depreciation" of k-space with time is not so severe, and a D region acquired 10 seconds past the arterial phase may still be acceptable. These tradeoffs have been carefully examined [126]. Another drawback is the uneven modulation of ky-space due to the acquisition of discrete ky-space blocks. The 3D-TRICKS acquisition was initially applied to ky-kz space, instead of ky space [61] [60].

One region which challenges the 3D-TRICKS ability to obtain a pure arterial frame is in the pulmonary vasculature. Here the separation time between artery and vein enhancement is about 4 seconds. Figure 3.12 shows two time frames from a modified 3D-TRICKS acquisition of the pulmonary region. The acquisition parameters were: TR/TE/flip = 4.5/1.9/25°, 36 cm FOV, 256 x 256, 8 - 10 mm slices, full echo, partial Fourier acquisition, a frame rate of 1.4 seconds, and a temporal window of 7.2 seconds.

The image shows a true arterial frame. The low SNR, blurriness and lack of coverage result from the tradeoffs made in order to achieve a frame rate of 2 seconds. The tradeoff with image quality makes this arterial-venous separation unattractive. Arterial-venous separation is never achieved in contrast-enhanced MRA of the pulmonaries, unless resolution is compromised or 2D imaging is used. Recently, some promising pulmonary arteriograms have been obtained using fast imaging and multiple short injections and severely truncated data [42].

Figure 3.13 shows four time frames of a single slice from a 3D volume of the

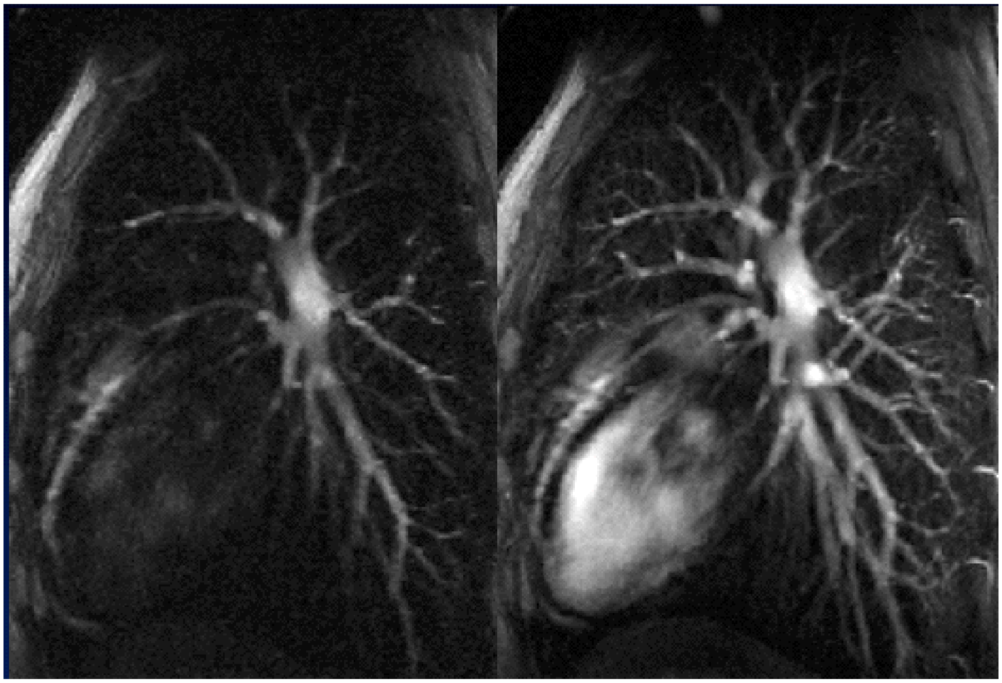

Figure 3.12: *Arterial and mixed phases of the pulmonary vessel.*

pulmonary vessels using a modified 3D-TRICKS acquisition. The scan parameters were: TR/TE/flip = 4.5 ms/1.9 ms/30°, 36 cm FOV, 256 x 256,10 mm slices, 8 slices, full echo, partial Fourier acquisition, a frame rate of 1.4 seconds, and a temporal window of 7.2 seconds. The passage of contrast through the pulmonary vessels is observed.

With an arterial-venous separation time of seven seconds, the carotid arteries are still a great challenge, but have been more successfully imaged. The renal arteries are usually imaged at our site with a centric acquisition, because in the abdomen a breath-hold must be coordinated with the acquisition, so a timing method is required. Therefore, acquisition methods which rely on timing scans are used in the abdomen.

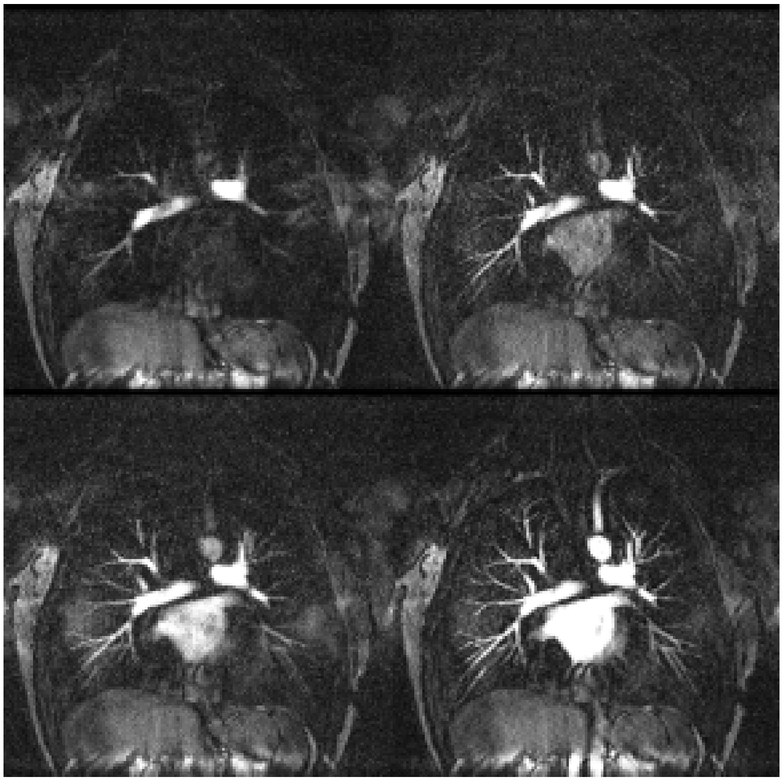

Figure 3.13: *Time series of single slice from a volume, showing the arrival of contrast into the pulmonary vessels. The frame rate was 1.4 seconds.*

3.5.6 2D Projection Imaging

Another method for obtaining contrast-enhanced images with good temporal resolution is thick-slab projection imaging [16] [22]. The images are projections of all the signal throughout the thick slab. This is analogous to the method for obtaining images in x-ray DSA. MR has different properties from x-ray imaging, that put this method at a disadvantage. The thick voxels are a summation of spins which may have different phases, due to precessional frequency variations across the slab. Thus there may be signal cancellation. Furthermore, the background signal, even if small, may dominate the signal in a pixel with a thick z-section. Finally, it is a very fast imaging sequence, with consequently poor SNR. Often complex subtraction of the mask image is used to remove the problem of background signal [16]. This has been shown to be better than magnitude mask subtraction for thick slab imaging.

3.5.7 Multi-Frame Fast Imaging

In multi-frame acquisitions, all of the k-space is acquired during a short temporal window [19]. This method does not require timing and provides vein-free images, if the temporal aperture is short. The coverage, resolution and TR are decreased in order to achieve short temporal windows. The acquisition of k-space proceeds sequentially and is repeated multiple times. The disadvantage of this method is the tradeoff of coverage, resolution and SNR to obtain a vein-free image.

3.6 Conclusions

Contrast-enhanced imaging depends on the temporary T1-shortening properties of contrast agents to provide high signal from the enhanced arteries. The relationship between signal and contrast concentration has been discussed. The relationships between contrast concentration and injection protocol have been elucidated. Many successful acquisition methods employed in contrast-enhanced MRA have been reviewed. It has been observed that there is a limited acquisition window for imaging the first pass arterial phase. In this short window, the resolution obtainable is low relative to that of other modalities, for example x-ray DSA. This leads to the discussion of fast imaging methods found in the next chapter. Fast imaging techniques can provide higher resolution for acquisitions during the first pass of contrast.

Chapter 4

Fast Imaging

Fast acquisition methods are central to MR research. This chapter reviews the developments in fast imaging, and presents results obtained in the investigation of fast imaging methods.

The current methods for fast acquisitions of k-space include methods for shortening the TR, like increasing the bandwidth, acquiring lower resolution, using shorter RF pulses, or removing unnecessary pulses. Other methods reduce the number of TRs needed by partial Fourier acquisitions, reduce the volume coverage, or use sparse sampling techniques. Still other methods acquire data in novel trajectories that acquire more of k-space per TR, for example the spiral and the echo-planar trajectory. Finally, some redefine the meaning of acquisition time to mean the time to acquire only the center of k-space. All of these methods have been the subject of research in fast imaging, and will be reviewed here.

Rapid acquisitions are necessary when the entire scan must be acquired within a 15 to 30 second breath-hold. Breath-holding is used when imaging the abdomen or lungs. A breath-hold reduces respiratory motion, although not completely [78].

Rapid acquisition is also required for cardiac imaging. In cardiac imaging, ECG-gating is used to stop the motion of the beating heart. In order to reduce cardiac blurring, only a fraction of the heart beat is used for imaging. For example, a scan which requires 30 seconds of ungated scan time will take 3 minutes, if only one sixth of the cardiac cycle is used for acquiring data. Even this would be acceptable, except that respiratory motion requires cardiac imaging during a breath-hold. Breath hold and ECG-gating in combination are not possible without fast imaging.

Rapid acquisitions are also needed for any imaging which requires high temporal resolution to obtain a time course. Examples include perfusion imaging, functional imaging, and imaging of the uptake and inflow of contrast in the brain, tumor or myocardium, or vessels.

In contrast scans, as has been discussed above, the presence of veins in the image degrades image quality. Thus fast imaging is necessary for acquiring as much as possible of the central portion of k-space before venous enhancement. Aside from concerns about motion and venous suppression, fast imaging is not required during the first pass of contrast. Any lengthening of the data acquisition time (slower imaging) can be met with a lengthened injection time, without sacrificing, and often improving SNR (through bandwidth reduction).

This chapter presents a review and research in fast imaging. The research discussed in this chapter was motivated by our experience with contrast enhanced coronary artery imaging. This experience led us to attempt to shorten scan times by any possible means, faced with the requirements of ECG-gating, contrast passage and breath-holding. Many of the methods in this chapter produce incremental improvements for MRA. In the next chapter, a wholly novel method is presented for fast imaging, undersampled projection reconstruction.

4.1 Low Resolution Methods

One method for fast imaging is acquisition of low resolution images. For example, while a typical scan has 256 Nx (x-resolution) and 128 Ny (y-resolution) in a 30 cm FOV, a 128 x 64 matrix could be acquired in about 1/4 of the time.

4.2 Unusual Trajectories

Usual trajectories are those which collect the k-space data with frequency encodings and phase encodings, acquiring one frequency encoding line per TR interval. Many of the *unusual* trajectories were designed specifically for fast imaging.

One promising method for fast imaging is with the use of echo-planar imaging (EPI) [80] [81]. In this acquisition method, the RF flips spins into the transverse plane, where they are made to form multiple echoes using either spin echo or gradient echo techniques. Multiple frequency encoding lines at different phase encoding values are collected before a new excitation pulse is applied. The major difficulty in EPI is the T2* dephasing of magnetization caused by the long times in the transverse plane [83] [65]. The k-space data are amplitude and phase modulated. Because multiple echoes are collected, the signals from later echoes have greater phase and amplitude modulation. The collected signal is affected by the phase modulation due to the acquisition gradient, the phase encoding gradient, dephasing due to T2*, and dephasing due to flow. The extra dephasing time results in worse image quality in EPI compared to single-echo imaging.

Two well known non-Cartesian acquisition methods are spiral imaging [94] [84] and radial projection reconstruction imaging. Spiral imaging acquires a greater portion of k-space during each TR, so that fewer TRs are required to obtain an image. The spiral trajectory can be implemented as a more rapid method than Cartesian FT imaging [94]. The signal readout time can be very long (10 ms or more), so that the image quality is extremely sensitive to off-resonance effects. The spiral trajectory of one spiral interleaf is shown in Figure 4.1; many interleafs are acquired to fully sample k-space. Projection reconstruction acquires radial lines of k-space, as shown in Figure 4.2. Although it is not inherently faster than Cartesian acquisitions, projection reconstruction can provide more resolution per unit time than Cartesian acquisitions. That is the focus of the next chapter.

4.3 Short TR

Short TRs decrease scan time, which is always proportional to the TR time. The improvement in scanner gradient strengths and gradient slew rates has resulted in shorter TRs. Figure 4.3 shows a pulse sequence timing diagram for a 3D fast gradient echo sequence. TR can be shortened by shortening the TE, the data acquisition window, Tadc, the RF pulse width, or reducing the areas of the optional rewinders and killers. The phase encoding and slice encoding gradient areas cannot be reduced. However, the pulse widths of the gradients may be reduced by using high gradient slew rates and maximum gradient amplitudes.

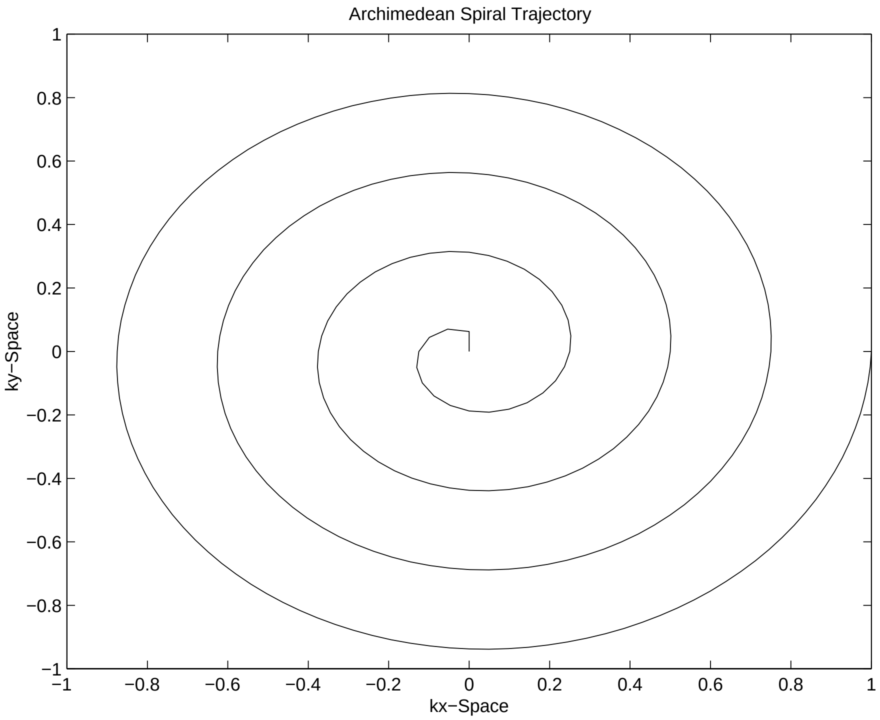

Figure 4.1: *One interleaf of an Archimedean spiral. Many interleafs are required to sample k-space fully.*

4.3.1 Fractional Echo

Acquiring k-space in fractional echoes shortens the TR, by acquiring only a fraction (typically 60% to 75%) of the kx-space desired. The rest is synthesized, in a manner described below. Fractional echoes are primarily used to reduce the echo time (TE) by reducing the readout time before the echo, and the prephasing time for the readout gradient. They also result in shorter TRs.

4.3.2 Short Data acquisition Window

One method for fast imaging is using shorter data acquisition times (Tadc), by increasing the receiver bandwidth, and increasing the gradient strength. The time

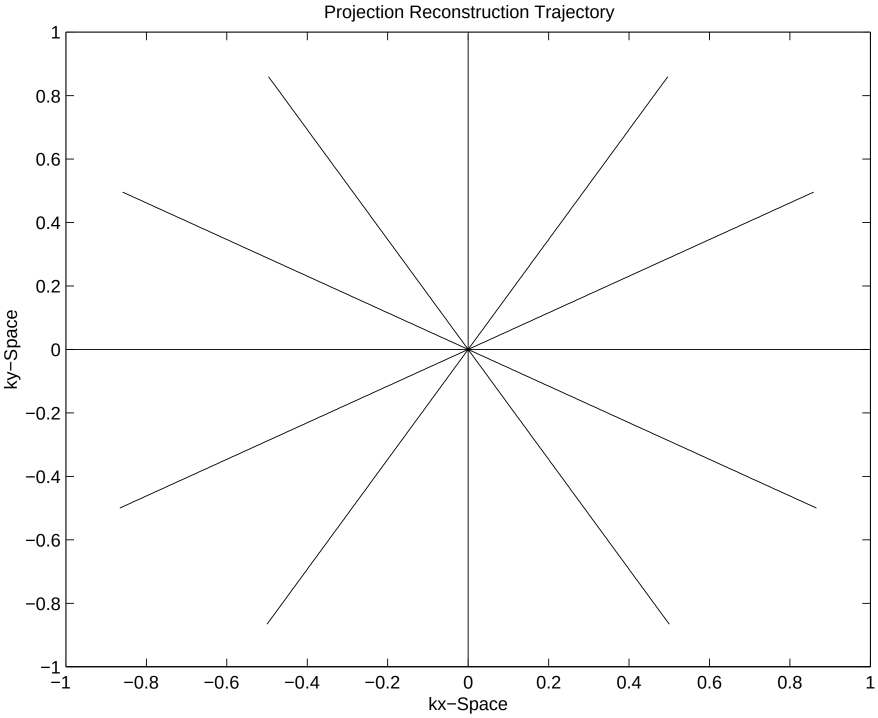

Figure 4.2: *Projection reconstruction trajectory, showing 7 projections.*

evolution of kx-space trajectory is related to the gradient strength G_x by:

$$k(t) = \bar{\gamma} \int G_x(t)dt \tag{4.1}$$

This shows that the velocity with which k-space is obtained, $\dot{k}(t)$, is proportional to G_x, so that increasing the readout gradient amplitude shortens the acquisition of kx-space.

Since the gradient causes the Larmour frequency of the spins to vary by $\bar{\gamma} G_x FOV_x$, from one edge of the FOV to the other, then the receiver bandwidth (BW) must be set accordingly:

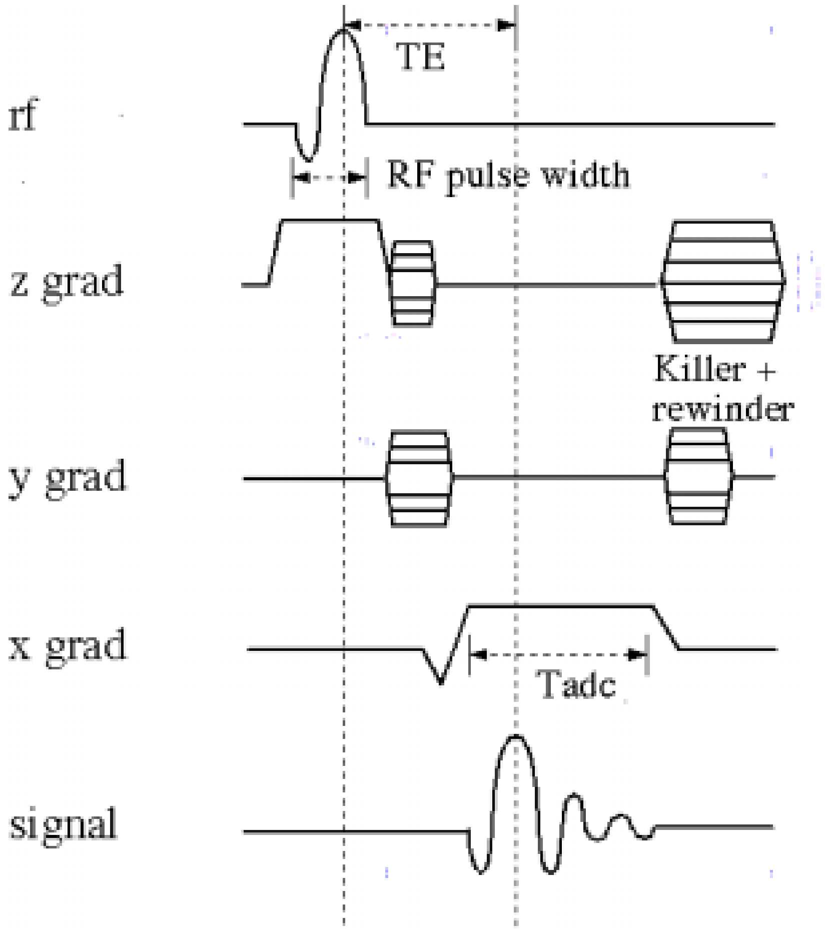
TE
rf
RF pulse width
z grad
Killer +
rewinder
y grad
x grad
Tadc
signal

Figure 4.3: *Pulse sequence timing diagram for the 3D fast gradient echo sequence. The Tadc, the RF pulse width, the TE time, and the killer time can be shortened for fast imaging.*

$$2 \cdot BW = \bar{\gamma} \cdot G_x \cdot FOV_x \tag{4.2}$$

(Note that it is conventional to define bandwidth, BW, so that 2BW is the span of frequencies across the FOV during frequency encoding.) The inverse of this bandwidth, $\frac{1}{2BW}$ is equal to the seconds per kx-space point acquired. Finally, the data acquisition time (Tadc) is equal to

$$Tadc = \frac{Nx}{2 * BW} \tag{4.3}$$

To shorten the Tadc, the bandwidth is increased, and the gradient strength is increased.

With the past hardware constraint on GE scanners of 0.5 G/cm (in the early 1990's), and using a typical 24 cm FOV, and $\bar{\gamma} = 4250 Hz/G$, the maximum required receiver bandwidth was 25 kHz. Currently, on the LX cardiovascular scanner, the maximum gradient strength is 4 G/cm, so that the highest required receiver bandwidth is 200 kHz. Increased maximum gradient strengths have allowed for higher receiver bandwidths, and thus decreased the Tadc.

The TR is shortened because the Tadc is shortened. At low receiver bandwidths, the Tadc time is often a large portion of the total TR time. At high bandwidths, the Tadc is a smaller portion of the total TR. Table 4.1 gives the Tadc, TE, and TR at various x-resolutions, bandwidths, for full and fractional echoes. These times were recorded for the 3D fast gradient echo sequence on the GE Horizon scanner equipped with maximum gradient strengths of 2 G/cm and a 288 μs rise time to full scale.

Consider the values for a minimum echo acquisition. For a 256 matrix, an increase of bandwidth from 16 kHz to 32 kHz reduces the TR by $\frac{6.1}{8.7} = 0.7$. With a 128 matrix, a change of bandwidth from 32 to 64 kHz only changes the TR by $\frac{4.1}{4.7} = 0.87$. This illustrates an important consideration in using bandwidth increases for fast imaging. Bandwidth increase has a greater effect for large matrix sizes and low initial bandwidths than for small matrix sizes or high initial bandwidths.

Increasing bandwidth does shorten TR through reduction of Tadc, but it also

Xres	Bandwidth	TR_{min}	$Tadc_{min}$	TE_{min}	TR_{full}	$Tadc_{full}$	TE_{full}
512	64 kHz	6.0	2.5	1.3	8.2	4.1	3.6
512	32 kHz	8.5	5.1	1.7	12.3	8.2	5.7
256	64 kHz	4.8	1.3	1.2	5.8	2.0	2.2
256	32 kHz	6.1	2.6	1.4	7.8	4.1	3.2
256	16 kHz	8.7	5.1	1.8	11.8	8.1	5.2
128	64 kHz	4.1	0.64	1.0	4.6	1.0	1.5
128	32 kHz	4.7	1.3	1.1	5.4	2.0	1.9
128	16 kHz	6.0	2.6	1.3	7.5	4.1	2.9

Table 4.1: *Table of values for typical TR, Tadc and TE values for different resolutions and bandwidths. Values are shown for full and minimum echoes.*

reduces the SNR. Recall from Chapter 3 that SNR is proportional to $\sqrt{TR \cdot Tadc}$ for contrast enhanced imaging, so that the scan time reduction comes at a cost of lost SNR due to both TR and Tadc decreases. Since increasing bandwidth by 2 decreases Tadc by 2, and decreases TR by some amount less than 2, SNR is lost more quickly than just $\sqrt{T_{scan}}$ [27]. This makes increased bandwidth a method of last resort. For full echoes, the TR is shortened by a greater percent by bandwidth increase. Ideally, the bandwidth should only be increased to shorten TE, and not as a primary means for fast imaging.

4.3.3 Short RF Pulses

Increased bandwidth discussed above is a primary method for reducing TR. Besides this, the RF pulse can be shortened. In 3D MR imaging, the RF pulse width can be shortened without concern for exceeding the maximum gradient strength. The gradient strength of the slice select pulse must satisfy $\frac{1}{tp} = \bar{\gamma} \cdot V_{thick} \cdot Gz$, where $\bar{\gamma}$ is the gyro-magnetic ratio, V_{thick} is the slab thickness excited, Gz is the required z gradient strength, and $\frac{1}{tp}$ is the RF bandwidth, which determines the RF pulse width. The maximum gradient strength of 2 G/cm does not prevent reduction of RF pulses for any reasonable slab thickness.

However, the RF amplifier cannot produce the required power to flip the spins during short RF pulses. The RF amplitude needed to achieve a flip angle θ is set by $\theta = \gamma \int (B1(t)dt$, which can be simplified to be $\theta = \gamma B1_{max}(pw_{eff})$ where pw_{eff} is the effective pulse width, (the pulse width of the RF pulse if it were a rectangular pulse of the same area). The maximum RF amplitude is related to the RF power by:

$$Power \sim (B1_{max})^2 = \frac{(\theta)^2}{(\bar{\gamma} pw_{eff})^2} \tag{4.4}$$

This pw_{eff} is much smaller than the pulse width for a pulse with many sinc cycles (i.e a pulse with good slab profile). The power required can exceed the capabilities of the RF amplifier, when the RF pulse width is reduced.

For example, the commercially provided minimum phase alpha pulse used in the 3D fast gradient echo sequence has a pulse width of 3.2 ms, although the pw_{eff} is only 0.1005 ms. This pulse has a much smaller effective width than actual width. This pulse has been modified to work at 1.28 ms, using the same shape and thus the same slice profile. The pulse width cannot be reduced further, because the RF amplifier is incapable of providing enough power to achieve the desired flip angle. To circumvent this, pulses with larger effective pulse-widths are used, for example a truncated sinc pulse with very few lobes. In some sequences a 1.5 or a 0.5 ms truncated sinc pulse is used. The 0.5 ms truncated sinc has a non-ideal slice profile, as shown in Figure 4.4.

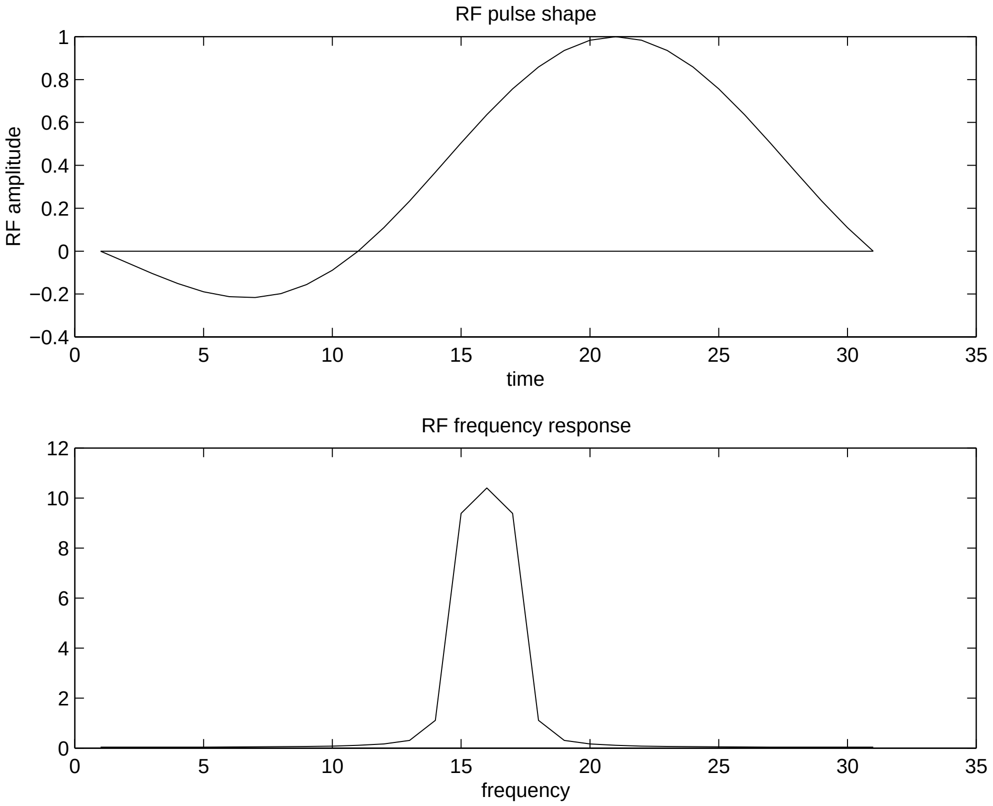

Figure 4.4: *0.5 ms asymmetrically truncated sinc RF pulse (top), and frequency response (bottom).*

Because of the poor profile of a truncated sinc pulse, we have often chosen to use the minimum phase alpha pulse, and accept a longer TR.

4.3.4 Removing Non-essential Pulses

Gradients which only improve the image quality incrementally can also be eliminated. The "killer" on the z-axis contributes to spoiling by dephasing along z. It is turned on at the end of the data acquisition. Often the area and thus the pulse width of the z-killer can be reduced. The area is determined by the number of phase wraps desired through the slab. If the RF spoiling is sufficient, then the z-killer should be removed. Furthermore, the slice encoding and phase encoding rewinding gradients may be removed, to decrease the TR. Initial studies of how their removal affects image quality were inconclusive.

4.3.5 Use of Maximum Gradient Slew Rates

Another method for decreasing the TR is by use of the maximum gradient slew rates. Our scanner is equipped with gradients with specifications of 2 G/cm, and slew rate of 188 μs to full strength. In commercial sequences, the 2 G/cm gradients are utilized, but the maximum slew rate is not used. Instead a 288 μs to full scale slew rate is used. Our experience shows that use of maximum slew rates can shorten the 3D fast gradient echo sequence TR by about 400 μs. Maximum slew rates may be unusable if they exceed the FDA $\frac{dB}{dt}$ limits.

4.3.6 Conclusion

Sometimes the minimum TR achievable cannot be realized on the scanner, because the scanner has insufficient time to perform calculations or write data to memory. When the bandwidth is increased to shorten TR, this results in a lower duty cycle, Tadc/TR. Other methods of fast imaging involve an improved duty cycle for the sequence, that is an increased Tadc/TR. The increase in duty cycle leads to the best SNR [95].

The TR can be successfully shortened. For example, TRs of 3.8 are obtained using full-echoes, 160 x-resolution, a shortened RF pulse, and a 64 kHz receiver bandwidth [88].

4.4 Acquisition Methods

Some methods for obtaining resolution quickly are accomplished through novel k-space acquisition orders and a redefinition of acquisition time. The acquisition time is redefined as the time to acquire the central portion of k-space data, which contains most of the information.

A pioneering method of this kind is the keyhole method [38], which acquires the outer k-space data once, and repeatedly acquires the central k-space data rapidly. Temporal volumes are reconstructed by combining the updated central k-space data with the outer k-space data. While this sacrifices the temporal resolution of the high spatial frequencies for the temporal resolution of the low spatial frequencies, it is a powerful method and has been a rich source for new variations.

Two methods based on the importance of central k-space were discussed in the last chapter, elliptical centric acquisition and 3D-TRICKS. These are considered fast imaging methods, because they redefine the meaning of temporal resolution to mean the time for acquisition of the central k-space lines only. They were discussed in Chapter 3 in relation to contrast enhanced imaging. Another such method is BRISK [82], which is used for cardiac imaging.

4.5 Partial K-space Acquisition

4.5.1 Theory of Homodyne

Figure 4.5 shows partial k-space data. Collecting only part of k-space reduces scan time by either shortening the TR or reducing the number of required acquisitions for a given resolution. In partial k-space acquisitions, about half of k-space data is acquired. All of the central k-space data is obtained for purposes explained below.

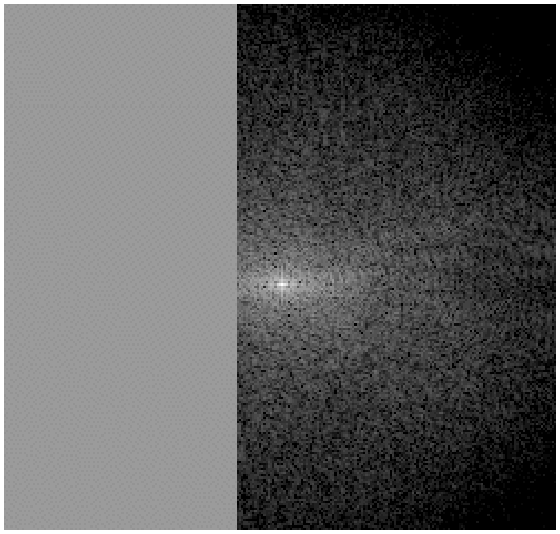

Figure 4.5: *In partial k-space acquisitions, only a fraction of k-space representation is acquired, using zeroes for the missing data. Note that a little more than half of k-space is collected.*

The homodyne method was introduced in 1985 by Paul Margosian, but was used earlier in other disciplines. It relies on the Hermitian nature of k-space to synthesize half of the data. Because an MR image portrays a real object, neglecting field inhomogeneities, chemical shifts and other imperfections which impart phase, its Fourier Transform is Hermitian, i.e. $S(-k) = S^*(k)$, where

$S^*(k)$ denotes the complex conjugate of S(k). This is easy to see:

$$S(k) = \int M(x)e^{(i2\pi x(k))}dx \tag{4.5}$$

$$S(-k) = \int M(x)e^{(i2\pi x(-k))}dx = S^*(k) \tag{4.6}$$

This is only true if $M^*(x) = M(x)$ (i.e. one has a real image). By Hermiticity, only half of k-space must be measured, the other half can be calculated. Consider a 1D line of k-space, which represents a 1D object in image space; the line consists of S(k) values. If S(k) is known, S(-k) is also known.

Now suppose the we know the k-space point S(a) and lack the point S(-a). Then S(-a) is just its complex conjugate. S(a) is represented as

$$S(a) = (Sr(a) + i \cdot Si(a))\delta(k - a) \tag{4.7}$$

where Sr and Si are the real and imaginary components, and the delta function represents the position of S(a) in k-space. S(-a) is the complex conjugate of S(a):

$$S(-a) = (Sr(a) + -i \cdot Si(a))\delta(k + a) \tag{4.8}$$

The Hermitian nature of k-space means that if S(a) is measured, then S(-a) is known. The following shows how the FT of both points is represented by the FT of just one. The FT of S(a) is

$$FT((Sr(a) + i \cdot Si(a))\delta(k - a) = (Sr(a) + i \cdot Si(a))e^{-i2\pi(ax)} \tag{4.9}$$

making use of the fact that $FT(\delta(k-a)) = e^{(-i2\pi ax)}$. The FT of [S(a) + S(-a)] is:

$$FT((S(a) + S(-a)) = (Sr(a) + i \cdot Si(a))e^{-i2\pi(ax)} + (Sr(a) + -i \cdot Si(a))e^{i2\pi(ax)} \tag{4.10}$$

Equation 4.10 can be evaluated, after the substitution $e^{(i2\pi ax)} = cos(2\pi ax) + isin(2\pi ax)$, to yield:

$$FT(S(a) + S(-a)) = 2Real(FT(S(a))) \tag{4.11}$$

Equation 4.11 indicates how the FT of both points is obtained from the FT of just S(a). It provides the homodyne implementation: to obtain the unknown k-space values, the known conjugate k-space values are doubled, k-space is Fourier transformed, and the imaginary part is discarded.

4.5.2 Phase Detection

The process of taking the real part of the FT of the k-space data requires knowledge of accidental phase accrual across the image. In practice, this phase is measured by acquiring more than half the data, as shown in Figure 4.5, acquiring all of the low spatial frequencies on both sides of k=0, so that a low resolution phase image can be made. See Figure 4.6(top) for the filter used to create the low-passed phase image. The phase is calculated as

$$\Phi(x) = tan^{-1}(\frac{Imag(I_L(x))}{Real(I_L(x))} \tag{4.12}$$

The image $I_L(x)$ is only the *low-passed* representation of the true image, since the high spatial frequencies are not acquired on both sides of k-space.

It is important to note that if the phase map were constructed by using asymmetrically truncated k-space data, the phase map would be in error, because the partial k-space data is equal to full k-space data multiplied by an asymmetric step function. It is well known that the FT of a function that includes an odd component is complex. Convolution of the true image with a complex function adds phase to the image thus produced, so that the phase can not be estimated using the FT of all of k-space.

The low frequency phase-estimate can be used to remove the phase of the image, after which the imaginary part is set to zero. The phase will be accurately determined if it is a slowly varying function in image space. This assumption may not hold at sudden interfaces into different magnetic environments. The validity of the phase correction for contrast enhanced images has not been carefully studied in literature to this date.

4.5.3 Filters for Implementation

Noll's paper sets forth the theoretical and practical aspects of homodyne processing [119]. In the reconstruction code, asymmetric k-space data is carefully centered, and then a 1D FT is performed along the fully sampled k-space dimension. The k-space is filtered along the other dimension with two filters, a low pass filter (wl(k)), which removes the high spatial frequencies, and a 3-step filter (wh(k)) which approximates:

$$wh(k) = \begin{cases} 0 & \text{if } k < -f \cdot kmax \\ 1 & \text{if } -fkmax < k < +f \cdot kmax \\ 2 & \text{if } k > +f \cdot kmax \end{cases} \tag{4.13}$$

wh(k) weights the acquired high spatial frequencies by two, as is required by Equation 4.11. Here f is the fraction of k-space acquired on the truncated side of the echo. For example, for a 60% echo, f=0.2. The actual filters have smooth transitions and are given as

$$wl(xres - j) = \frac{1}{1 + \exp(\frac{(j-j2)}{hnw})} - \frac{1}{1 + \exp(\frac{(j-j1)}{hnw})} \tag{4.14}$$

$$wh[xres - j] = 2.0 - \frac{1}{1 + \exp(\frac{(j2-j)}{hnw})} - \frac{1}{1 + \exp(\frac{(j1-j)}{hnw})} \tag{4.15}$$

In the above equations, j1 is the position marking the start of data collection, j2 is the identical point on the opposite side of k=0, and hnw is the transition width for the smooth transitions. For example, for a 62.5% echo of 256 k-space points, j1= 96 , j2 = 160, and hnw=2. For this case, the filters are plotted in Figure 4.6.

Homodyne can be used in synthesizing the missing data in fractional echoes, partial ky or kz acquisitions, or a doubly asymmetric acquisition, in which fractional echoes and partial ky-space are acquired. These will be reviewed in turn.

4.5.4 Fractional Echoes

The most common application for homodyne is for fractional echo acquisitions. Fractional echoes start collection of k-space data at about 10% of -kmax, then

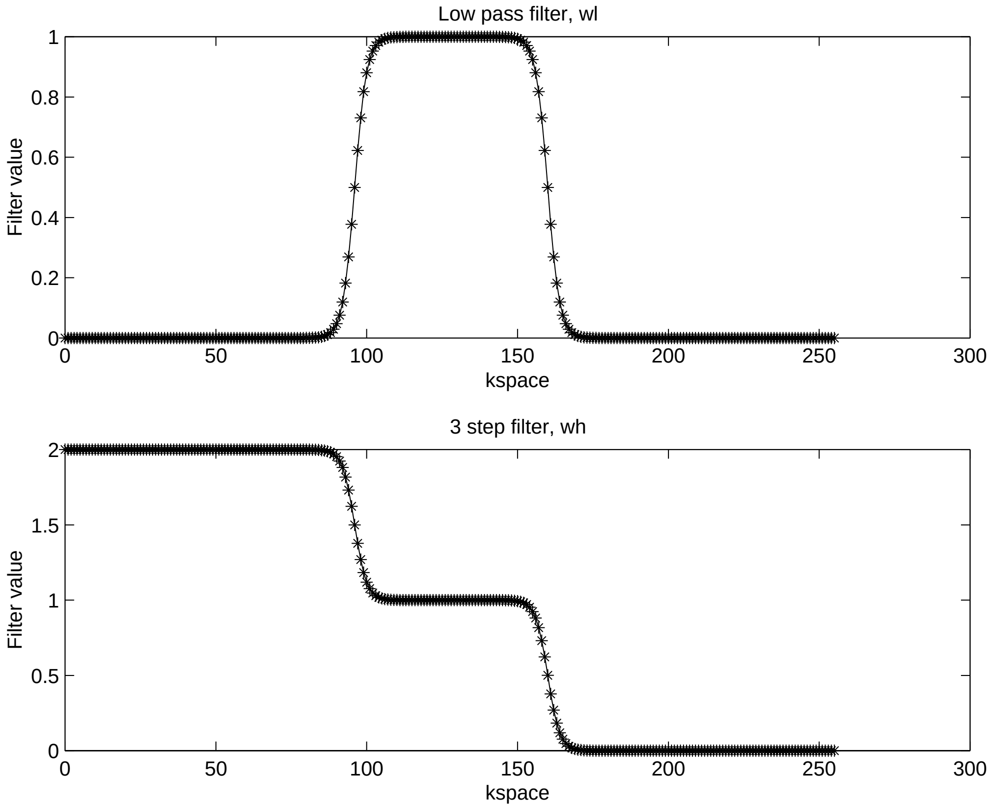

Figure 4.6: *Filters used for homodyne detection. wl(k) (top) is for low-pass filtering the data to reconstruct the phase estimate, and wh(k) (bottom) is for weighting the acquired high spatial frequencies by 2. The filters are shown for a 256 matrix, with a 160 acquired points. The transition points are j1=96 and j2=160.*

acquire through 0 to +kmax. They are used to shorten the time (the TE) between RF excitation of the spins, and the acquisition of the central lines of kx-space. A short TE time reduces artifacts due to flow dephasing, T2* dephasing, and inhomogeneities of the field.

Figure 4.7 shows a contrast enhanced slice from a 3D coronary artery volume, acquired with fractional echo and reconstructed either by zero-filling or homodyne. The matrix size was 256 x 128. 160 kx points were acquired. Zero-filling is the technique of filling in zeroes for the missing k-space data, and it improves the apparent image resolution compared to Fourier transforming non-zero-filled k-space [71]. In practice, k-space is always subject either to zero-filling or homodyne. The sharper image quality in the homodyne processed image is evident.

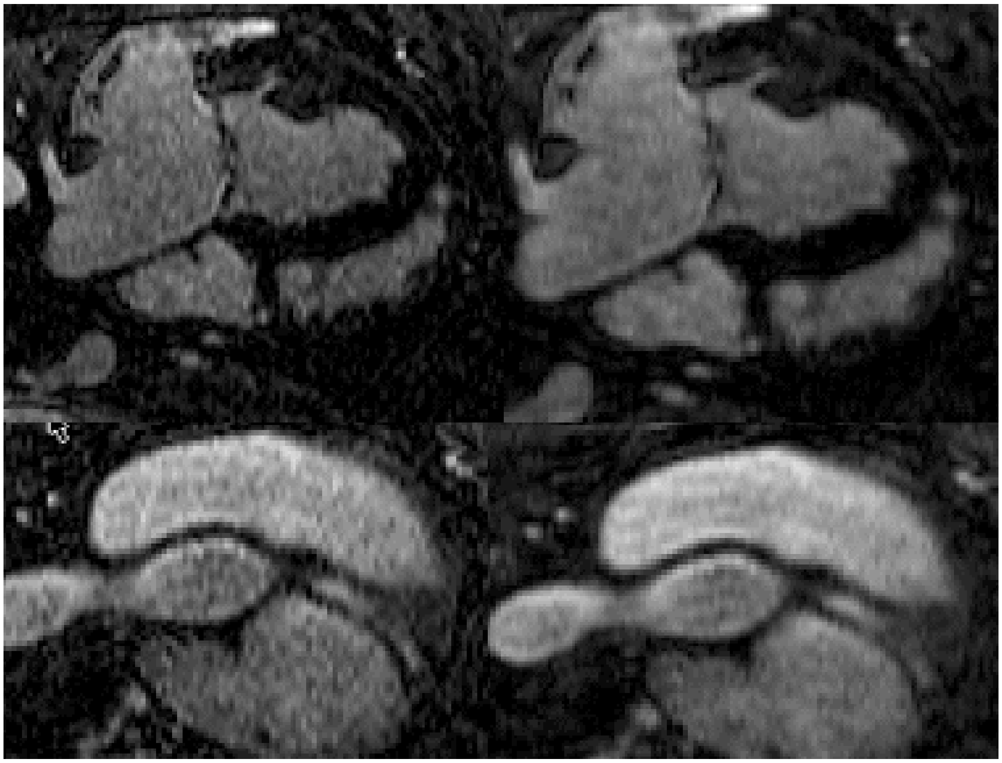

Figure 4.7: *Spatial resolution of homodyne processed image compared to zero-filling. Two slices are shown from a contrast enhanced coronary artery imaging volume. 160 kx-space lines were acquired in a fractional echo, and either zero-filled (right) to 256 or subject to homodyne detection (left).*

4.5.5 Partial Ky Acquisitions

If a full echo is acceptable, than the partial ky (called half Nex by GE) can be used to increase the speed of an acquisition. All points in kx-space are acquired, but only 60% of the ky values are obtained. Homodyne detection synthesizes the remaining data as discussed above. In this case, the ky data must be synthesized.

Since contrast is a susceptibility agent, the stability of the phase map during contrast infusion is a concern; the phase map may change throughout the acquisition of phase encodings, because of the changing presence of contrast. The phase is related to TE by $\phi \propto TE$. Because of the short TEs used in fast gradient echo sequences, the phase map should not change greatly. The phase changes due to contrast at large TEs have been measured [77].

Partial ky imaging is useful for fast acquisitions. The ratio of imaging times of partial ky space to a fractional echo acquisitions is:

$\frac{(f/2+0.5)\cdot Ny\cdot TR(1)}{Ny\cdot TR(f)}$

This determines whether partial ky acquisitions will improve the imaging speed, where TR(f) is the shortened TR due to fractional echo of fraction f, and Ny are the number of phase encodings, (f/2+0.5) of which are acquired for partial ky acquisitions. Referring to Table 4.1, the ratio can be evaluated as 0.89 at 512 matrix and 32 kHz, but 0.70 at 128 matrix and 64 kHz. So for small matrix sizes and high bandwidths, partial ky acquisition is helpful to reduce imaging time, but for low bandwidths and large matrix sizes, the gain is small and the problems created by a long TE are greater.

In addition to partial ky, it is possible to acquire partial kz data.

4.5.6 Doubly Asymmetric Acquisitions

Some groups, including our own, have experimented with the idea of doubly asymmetric acquisitions. It is such an attractive idea that GE commercial sequences allow it (in a very limited way), even though it has inherent flaws. The idea is to acquire one quadrant, by obtaining a *fraction* of the phase encodings as *fractional* *echoes*, and then attempt to synthesize the other three quadrants of the data in kx, and ky. Theoretically, since only one quadrant of k-space is known, S(kx,ky), only the opposite quadrant can be created, S(-kx, -ky). The quadrants S(-kx,ky) and S(kx,-ky) are completely unobtainable. This leads to anisotropic resolution, highest at one 45° angle in image space, and lowest in the direction orthogonal to that. We have tested doubly asymmetric acquisition and reconstruction.

Figure 4.8 shows the GE phantom. The full k-space was acquired, and the phantom was reconstructed using 1) all of k-space, 2) only 1 quadrant, 3) two quadrants which are related by Hermiticity (e.g. S(kx, ky) and S(-kx,-ky) 4) one quadrant with homodyne synthesis of the opposite quadrant. Comparison of the phantoms reconstructed with 1 quadrant and reconstructed with 1 quadrant acquired and the other homodyne synthesized, shows success in creating the other quadrant. The images reconstructed with two quadrants shows higher resolution than that from one quadrant. In this study, by luck, we have the important quadrants for resolving the comb-like object in the lower right corner of the images. Any objects with spatial frequency content in the other quadrants will be blurred. In humans, the synthesis process has not been as successful as in this phantom study.

Figure 4.9 compares a full k-space image to a two quadrant image of a contrast enhanced pulmonary vessel slice. The comparison shows that the resolution is similar between the two. The original data was acquired with fractional ky space data, and synthesized, and the 2 quadrant image was generated by zeroing out part of the full k-space data. The difference image shows the expected loss of detail in the direction at 45 ° angle.

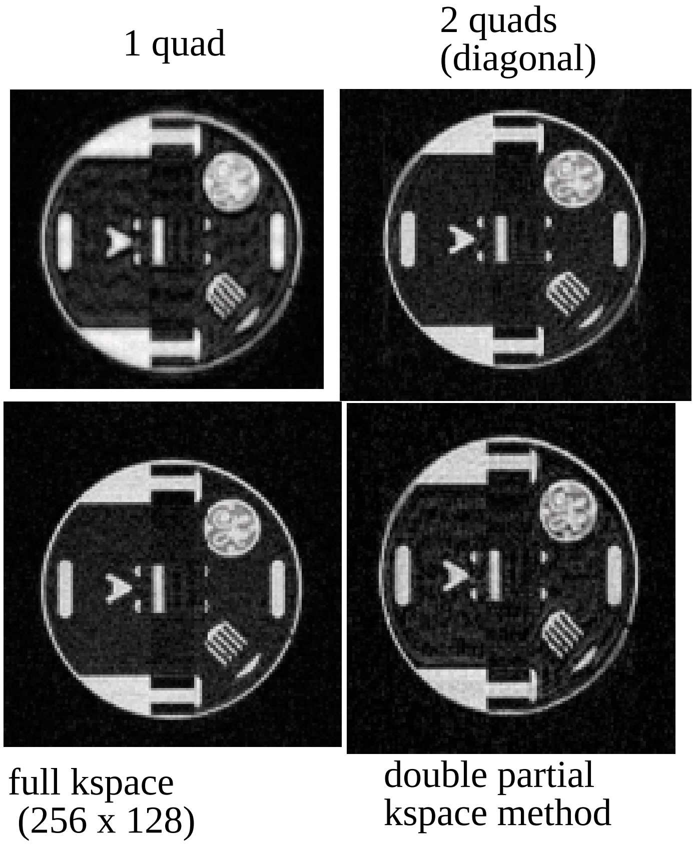
1 quad
2 quads
(diagonal)
full kspace
(256 x 128)
double partial
kspace method

Figure 4.8: *Phantom reconstructed with 256 x 128 k-space points, compared to images reconstructed with only 1 quadrant of k-space, 2 diagonal quadrants, and 1 quadrant used and the other quadrant synthesized.*

In sequentially acquired contrast enhanced fractional echo acquisitions used in MRA, often the earliest phase encodings are acquired before the arrival of contrast, so that the central phase encodings are weighted with peak arterial contrast. This means that a double partial k-space acquisition is obtained unintentionally, with resultant loss of detail for these acquisitions.

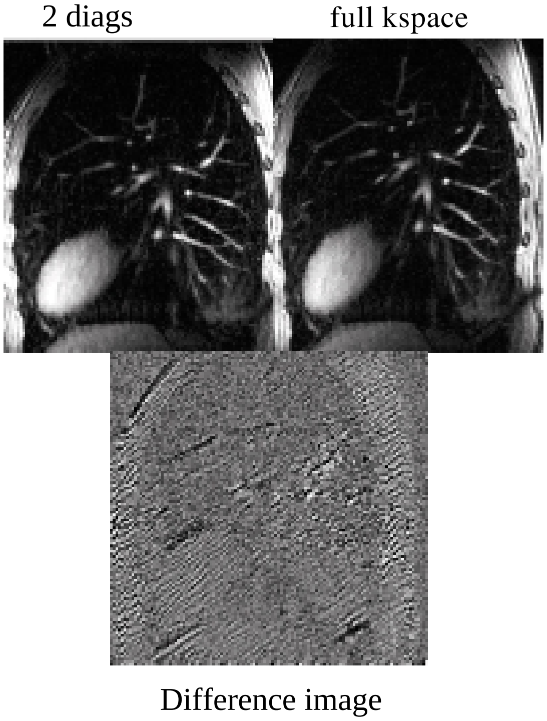

Figure 4.9: *Comparison of a slice through the pulmonary vessels, reconstructed from full k-space and 2 diagonal quadrants. The difference image shows vessel detail missing in the direction of 45°.*

4.5.7 SNR and Resolution Changes Due to Homodyne Processing

The SNR of a homodyne-processed image is less than that of a full k-space image and that of a zero-filled image.

Hurst [71] discusses the SNR difference between fractional k-space data and full k-space data. The signal is unchanged, since most of the signal occurs at the center of k-space. However the noise variance is decreased for fractional k-space by the factor

$$\sigma^2_{frac} = (f/2 + 0.5) \cdot \sigma^2_{full} \tag{4.16}$$

where f is defined above. Thus the SNR ratio between full and fractional k-space images is

$$\frac{SNR_{full}}{SNR_{frac}} = \sqrt{f/2 + 0.5} \tag{4.17}$$

It is expected that the low frequency SNR of the image after homodyne will be worse because only the high frequency signal is increased through homodyne weighting, and the noise is increased.

Similarly it is expected that the SNR of a fractional echo-homodyne processed image will be worse than a full echo image, by the decreased number of acquired kx points, if all else is equal. Noll [119] reports the SNR ratio between full and homodyne processed k-space: $\frac{SNR_{full}}{SNR_{homod}} = 1.32$, using a step filter and a 62.5 % fractional acquisition. This SNR ratio is obtained using the same reasoning as above. The signal is unchanged, but the variance is increased by the weighting of k-space, by wh(k) (see Figure 4.6). The noise in the homodyne processed image increases by

$$\sigma^2_{frac} = \sigma^2_{full} \int_{-.5}^{0.5} (wh(k))^2 dk \tag{4.18}$$

Since wh(k) is known, this can be evaluated to be $\sigma^2_{frac} = 2 - 2f$. Thus the ratio is:

$$\frac{SNR_{full}}{SNR_{homod}} = \sqrt{2 - 2f} \tag{4.19}$$

This results in Noll's reported loss of about 1.32 in SNR.

The resolution of the homodyne-processed image should be equivalent to the resolution for a full k-space acquisition. However, the resolution of zero-filled asymmetric k-space isn't easily expressed. Hurst has shown that the because half of the high spatial frequencies are collected, the high spatial frequencies are represented at half the signal level. The point spread function for partial k-space is shown in Figure 4.10, separated into real and imaginary components. Hurst showed that the imaginary component does not degrade the resolution very much, compared to the loss of half the high frequency signal in the real channel.

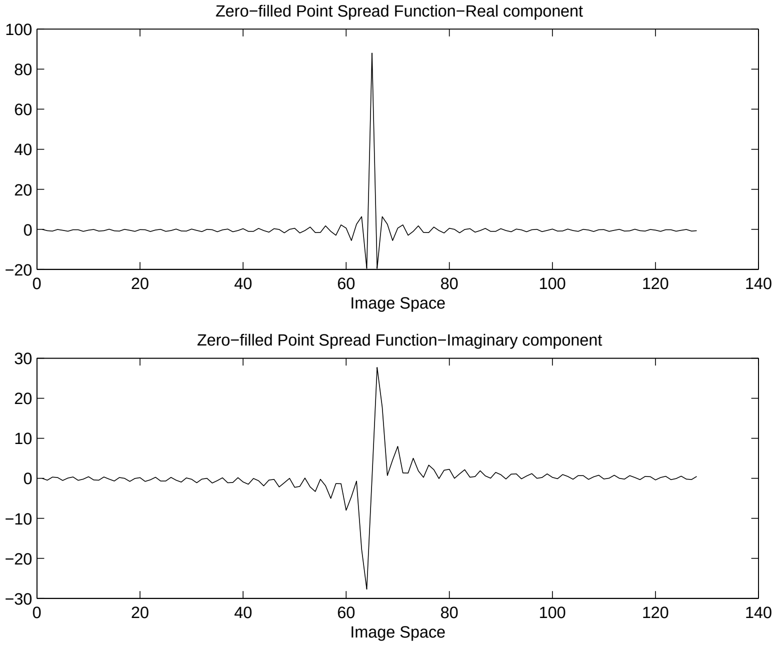

Figure 4.10: *The real and imaginary components of the point spread function with fractional k-space and zerofilling.*

Thus zero-filling fractional echo data retains some of the high spatial frequency information, and does not corrupt the image. Often fractional echoes are acquired and not subjected to homodyne, since SNR is reduced through homodyne.

4.5.8 Discussion of Homodyne

The homodyne methods discussed here have all been implemented using C code for the reconstruction of MR data. Homodyne is not the only method for reconstructing partial k-space. The Cuppen-POCS [74] method is also frequently used, and performs similarly. In this method, the image is reconstructed from fractional k-space, and the image data is constrained to have the phase of the low-passed image, in an iterative manner.

The homodyne method is routinely used and very useful for fractional echo acquisitions. The partial ky-space approach to reducing scan time has had some success [88]. The double partial k-space approach is used but results in loss of resolution [75] [42].

4.6 Reduced FOV

Another method for fast imaging is to image with reduced FOV. In 2D FT imaging, the resolution is determined by $\Delta y = \frac{FOVy}{Ny}$ while scan time T_{scan} is $T_{scan} = TR \cdot Ny$. This shows that resolution can be increased by either increasing Ny and thus scan time, or by reducing the FOV in y. Reducing the FOV is possible only if it does not incur aliasing that obstructs important anatomy. In the frequency encoding direction, aliasing does not pose a problem, because encoding is done so that at each x-position there is a different precessional frequency. Then a bandpass filter removes any signal outside of the FOV. In the phase encoding direction, the Δk_y must be set to be as large as the FOV in y.

One reduced FOV method is the use of 2D selective RF pulses [90]. No aliasing occurs because outside of the FOV no spins are excited into the transverse plane. This has the disadvantage of using a RF pulse of long duration. Another method uses a gradient insert that dephases spins in regions proximal to it, effectively reducing the FOV [93].

Another method is the Hu and Parrish [76] reduced FOV method, later refined by Fredrickson and Pelc [69] and developed by Madore [91]. The reduced FOV method works in increasing temporal resolution in anatomy which contains a static unchanging part of the FOV and a dynamically varying part of the FOV. For example, in cardiac imaging, the heart is rapidly moving, but the rest of the chest is stationary during a breath-hold. In this method, the complete set of phase encodings with given Δky and kymax are broken up into even and odd encodings. The even encodings, spaced $2\Delta ky$ apart, provide data to reconstruct an image with half the FOV and identical resolution, as do the odd encodings. The FT of the even and odd k-space data result in an image with aliasing from outside the reduced FOV. The even and odd encodings reconstructed together provide the full FOV. In the reduced FOV method, the odd encodings are acquired at least once as a reference, and then the even encodings are acquired multiple times during the cardiac cycle. The even (or odd) encodings provide an aliased image. If the even and odd encodings are reconstructed together, the full FOV is obtained, but the heart is blurred, because the temporal aperture has increased. The steps for the Fredrickson-Pelc reduced FOV method are:

- 1. Reconstruct the full FOV image by combining even and odd encodings.
- 2. Zero-out the dynamic inner half of the image.

- 3. FT (2) zeroed-out image to k-space.
- 4. From (3) retain only the odd (even) k-space points.
- 5. Subtract (4) from the odd (even) points acquired at each phase of the cardiac cycle, to remove aliasing of the static outer half of the image.
- 6. FT the result (5) into image space for a half FOV image without aliasing.

This method improves the acquisition speed of multi-phase cardiac imaging, because the heart only occupies half of the FOV occupied by the body, for example in the axial view. The Hu-Parrish technique acquires the even encodings once as a reference, and then acquires odd-encodings. The Fredrickson-Pelc technique acquires the odd and even encodings in an interleaved way. Madore's technique allows for dynamic central and outer regions of the FOV.

We have implemented the Fredrickson-Pelc reduced FOV technique to obtain better temporal resolution in single breath-hold contrast enhanced 3D multi-phase cardiac imaging [50]. Figure 4.11 shows an example of the reduced FOV technique in a 3D contrast enhanced study of the heart. In this example the de-aliasing is not perfect. The reason for imperfect de-aliasing is due to magnetization which was larger in the first cardiac phase than the second phase, resulting in unequal signal strengths. This was remedied by simply using more disabled acquisitions, which apply RF pulses to saturate the magnetization to its equilibrium value.

Mazaheri from our group has experimented with a variation of this method, by acquiring the central k-space with a full FOV, but the high spatial frequencies with a reduced FOV [44]. In other words, high spatial frequencies are undersampled, while low spatial frequencies are adequately sampled. This provides high

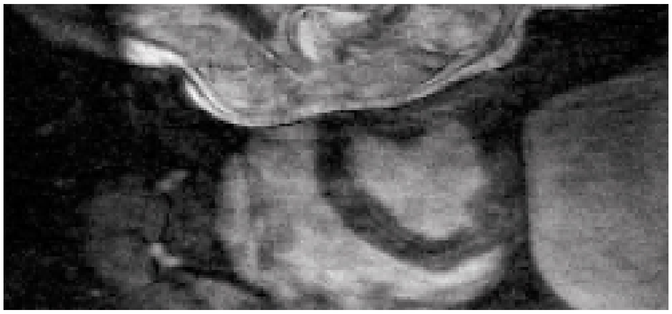

Phase 1 shows aliasing

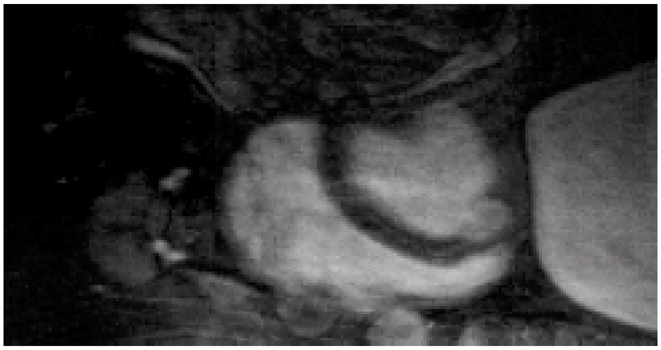

Phase 2 after de-aliasing with
Fredrickson-Pelc algorithm

Figure 4.11: *Result of de-aliasing with the Fredrickson-Pelc algorithm. This shows myocardium in two phases of the cardiac cycle. Information from the first phase was used to de-alias the second phase. Here the de-aliasing is not perfect.*

spatial frequency aliasing, similar to a method advocated by Lauzon and Rutt in connection with sampling on concentric rings [92]. It is akin in spirit to the method presented in the next chapter, limited angle projection reconstruction.

The advantages of reduced FOV are great, but special methods are needed to obtain FOVs in y that are smaller than the object extent.

4.7 Sparse Sampling Schemes

Sparse sampling refers to acquiring less k-space data than conventional FT sampling requires. One recent method for sparse sampling is called SMASH [85]. It relies on multiple receiver coils placed along the body. If a series of phase encodings are obtained, then intermediate phase encodings can be obtained by weighted addition of the signals from spatially consecutive receiver coils. Thus large steps in ky space are traversed.

Another method permits sparse sampling when there are multiple non-adjacent regions of signal within an otherwise empty FOV. This is called multiple region MRI (mrMRI) [79]. It applies the Fourier sampling thereom which specifies Δk necessary to support each region, but too small to support the full FOV. It obtains images which are composites of all the regions, aliased onto the small FOV, but the aliasing pattern is varied by collecting signals at shifted k-space grid points. Enough k-space data is acquired to de-alias the image and reconstruct the full FOV. Conventional Fourier imaging is just a special case of this method.

Wavelet encoding is another method of sparse sampling [86].

4.8 Steady State Imaging

The reasons for fast imaging listed in the beginning of this chapter included vein suppression and imaging during a breath-hold. Steady state imaging refers to imaging after equilibration of a contrast agent. This imaging suffers from venous contamination and motion artifacts if performed post-contrast in the abdomen without a breath-hold. However high quality images could be obtained if these problems were solved, because of the long scan times possible. Long scan times allow low bandwidths, long TRs, averaging, and any desired resolution [32].

Navigator echoes [87] are one method for circumventing motion artifacts, due to respiration. Navigators are performed by exciting cylinders oriented in the superior-inferior direction, which cross the diaphragm. A frequency encoding is acquired along this cylinder in this S-I direction, and the position of the diaphragm with time is monitored. The navigators are obtained repeatedly during an image acquisition. They guide the acquisition by indicating temporal windows in which the diaphragm is in a desired position for acquisition of data. They can provide information about the S-I shift of the abdomen for post-processing correction. Anyone who has ever breathed knows that navigators suffer because breathing is not reproducible. They also increase scan times by about a factor of 5. With navigators, the challenges posed by motion due to breathing might be solvable. Navigators have often been used to image the coronary arteries, where the combination of cardiac and respiratory motion conspire to reduce resolution.

Steady state imaging may be more easily applied to areas outside of the abdomen, like the peripheral arteries, and the carotid and cerebral arteries, where respiratory gating is not needed.

Venous contamination could be removed from an image using some arterial-venous segmentation scheme [21] [43]. There are no clinically utilized methods thus far.

4.9 Conclusions

I have reviewed some of the recent methods for fast imaging. Fast imaging often compromises signal-to-noise ratio or creates artifacts. Fast imaging is necessary in contrast enhanced MRA to increase the spatial or temporal resolution obtainable during first-pass of contrast.

The next chapter presents a new a way of obtaining high resolution within short scan times, at the expense of diffuse artifact, using projection reconstruction methods with a limited number of angles.

Chapter 5

Limited Angle Projection Reconstruction

Projection reconstruction (PR) imaging was one of the earliest imaging techniques in MRI [103] and lately is the subject of renewed interest. Investigators have shown the utility of PR in reduction of motion artifacts [104]. Its characteristic of sampling some high and low spatial frequencies in each acquired projection has been exploited for dynamic imaging of moving objects by several investigators. Rasche et al. used undersampled PR to image joint motion [105] using a sliding window reconstruction. Another recent application is undersampled PR for catheter-tip tracking [107] [106]. PR also permits FID imaging of short T2* anatomy [108] [109] because it is conducive to short echo times.

In PR, low spatial frequency data are accumulated with a higher density than high spatial frequency data. This results in a factor of $\frac{\pi}{2}$ increase in the data collection time required for artifact-free reconstruction for a FOV and resolution comparable to FT imaging.

Spin-warp methods [111], also known as Fourier transform (FT) or Cartesian methods, generally provide images of higher quality than PR because of their immunity to off-resonance effects and k-space trajectory errors [101].

Chemical shift and Bo inhomogeneity cause blurring in PR but not in FT methods, although short data readout times for each projection (large bandwidth-per-pixel), possible today because of stronger gradient strengths, reduce the blurring in PR.

Some investigators [113] [116] have recently applied the techniques of Hu and Parrish [76], and Fredrickson and Pelc (discussed in Chapter 4) [69] to PR [112] [113] to improve resolution over a small field of view (FOV). In those studies the goal was to acquire high resolution images rapidly in a small dynamically changing FOV within a larger static FOV. We have recently reported [115] [125] [114] potential resolution advantages throughout the FOV using undersampled PR for MR angiography. Our initial work suggested that the spatial resolution that can be acquired in a given acquisition time using undersampled PR is uniform throughout the FOV and is similar to that normally associated with reduced FOV techniques. This increased resolution is accompanied by artifacts which appear to be tolerable.

5.0.1 Outline

In this chapter limited angle projection reconstruction is presented. The theory and reasons that limited angle projection reconstruction provides greater resolution per unit time than Cartesian (a.k.a. spin-warp and heretofore called Fourier transform, FT) acquisitions will be explained. Our interest was to acquire high resolution contrast enhanced angiograms in reasonable scan times. This initial insight, that reduction of the number of projection angles resulted in diffuse artifact rather than loss of resolution, resulted in the work presented in this chapter. The acquisition pulse sequence and reconstruction code did not exist formerly at our MR site. Their development is described here. Two acquisition orders, PRIZE and ZIPR, for obtaining the k-space data during contrast infusion will be described.

This chapter also presents the results of using limited angle PR for angiography. Phantom experiments are shown to verify that PR provides higher resolution per unit time than FT. Then the results of applying limited angle PR in contrast enhanced human studies is presented. The improvement in resolution and the appearance of undersampling artifacts are discussed.

The best applications of PR for MRA are deduced based on these experiences with PR. Sections on reconstruction methods, undersampling artifact, and signal-to-noise ratio are included as essential areas of research.

5.1 Small FOV concept: Theory and Simulations

It is well known in FT imaging that the FOV that can be reconstructed without aliasing is inversely proportional to the k-space sampling interval. This was discussed in Chapter 1. Because of this relationship, higher resolution per unit time can be obtained when the FOV is decreased. For a fixed pixel size, larger k-space step size permits faster traversal of the required k-space. However, often larger k-space steps are not possible, because objectionable aliasing will occur.

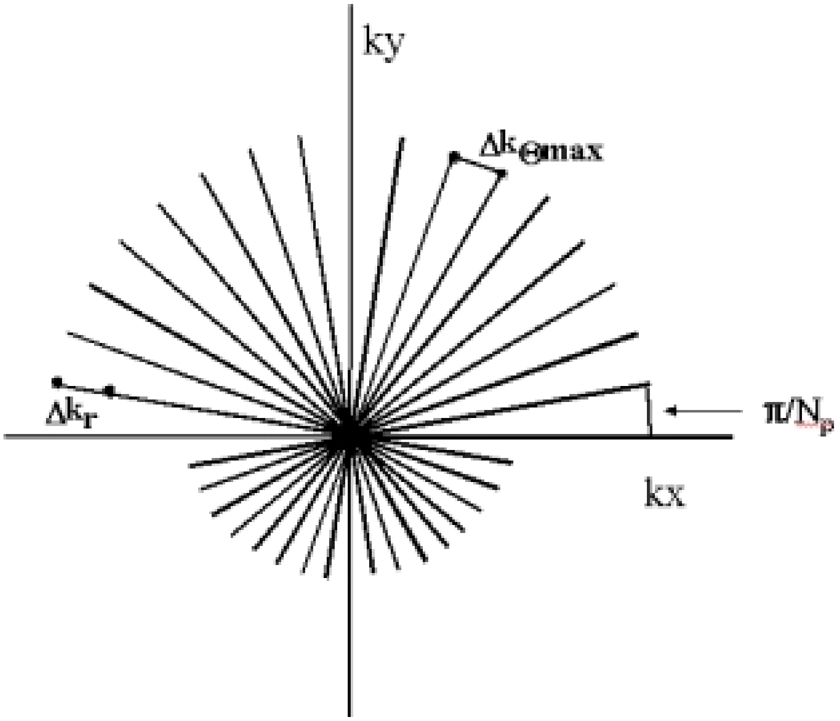

Figure 5.1: *The projection reconstruction trajectory. The spacings of* Δkr *and* $\Delta k\theta_{max}$ *are shown. The angular spacing is* $\Delta\theta = \frac{\pi}{Np}$. *Aliasing will occur if* $\Delta k\theta_{max} > \Delta kr$.

The case of limited angle projection reconstruction is illustrated in Figure 5.1. k-Space is acquired in radial lines, at multiple projection angles. Suppose that the radial k-space sampling interval Δkr would be sufficient to reconstruct Nr pixels along a distance D:

$$D = \frac{1}{\Delta kr} \tag{5.1}$$

When the number of projections Np is just sufficient to ensure that the maximum distance between k-space samples, $\Delta k\theta_{max}$ is no larger than Δkr, a FOV of diameter D is properly reconstructed. However, when Np is reduced, the k-space step-size $\Delta k\theta_{max}$ (see Figure 5.1) in the azimuthal direction exceeds Δkr and artifact-free reconstruction is only possible within a field of view of reduced linear dimension, d. This is given by the inverse of the arc length $\Delta k\theta_{max}$

$$d = \frac{1}{\Delta k\theta_{max}} = \frac{1}{(\frac{\pi}{Np})(\frac{\Delta kr \cdot Nr}{2})} = \frac{2Np}{\pi \Delta kr Nr} \tag{5.2}$$

Therefore, the reduced field of view, rFOV, supported by Np projections is related to the full FOV supported by the radial sampling as follows:

$$\frac{rFOV}{FOV} = \frac{d}{D} = \frac{2Np}{\pi Nr} \tag{5.3}$$

The condition for rFOV=FOV is: $Np = Nr(\pi/2)$. For this reason fully sampled projection reconstruction requires scan times $\pi/2$ times longer than conventional FT for the same matrix. Fewer projections will result in artifacts, due to inadequate sampling and aliasing of high spatial frequencies.

In the image domain, an undersampled PR image of a point object (the point spread function) anywhere in the image has a well reconstructed region rFOV, centered at the object. Even when the rFOV is significantly smaller than the overall image FOV, the spatial resolution is determined by the radial readout resolution and is fairly independent of Np. Artifacts due to the point object are negligible within the rFOV. Radial streak artifacts, emanating from the object, become apparent outside the rFOV. These artifacts contribute to the signal at distant points within the image. Similarly, the signal at each point within the image contains artifacts from all points separated from it by rFOV or more.

This is illustrated in Figure 5.2 which shows simulation results for the case of two objects reconstructed on a 256 x 256 matrix using only 64 projections. The input image is shown in Figure 5.2a. As shown in Figure 5.2b and Figure 5.2c, when either object is separately reconstructed with undersampled PR, the object is surrounded by an artifact-free region with a diameter one sixth of that of the full FOV. However, the object contributes artifacts to the rest of the FOV. In Figure 5.2d, both objects are simultaneously reconstructed. Since the reconstruction process is linear, the artifacts produced by each object appear in the region of the other object. Nowhere is the reconstruction artifact-free.

Provided that these artifacts can be tolerated, undersampled PR rapidly produces high resolution images throughout the FOV. The number of projections used is equivalent to the number required in artifact-free reduced FOV imaging. As the number of projections is reduced, the spatial resolution, which is determined by the radial readout resolution (Nr), remains essentially unchanged and exists throughout the FOV. Note that this is very different from the situation in conventional spin-warp imaging. In that acquisition method, the resolution in the phase encoding direction depends directly on how many phase encoding lines are acquired.

This property of limited angle PR, of having resolution which is independent of the Np, and only dependent on the readout resolution, allows images of greater resolution to be obtained using projection reconstruction than FT for equal scan times.

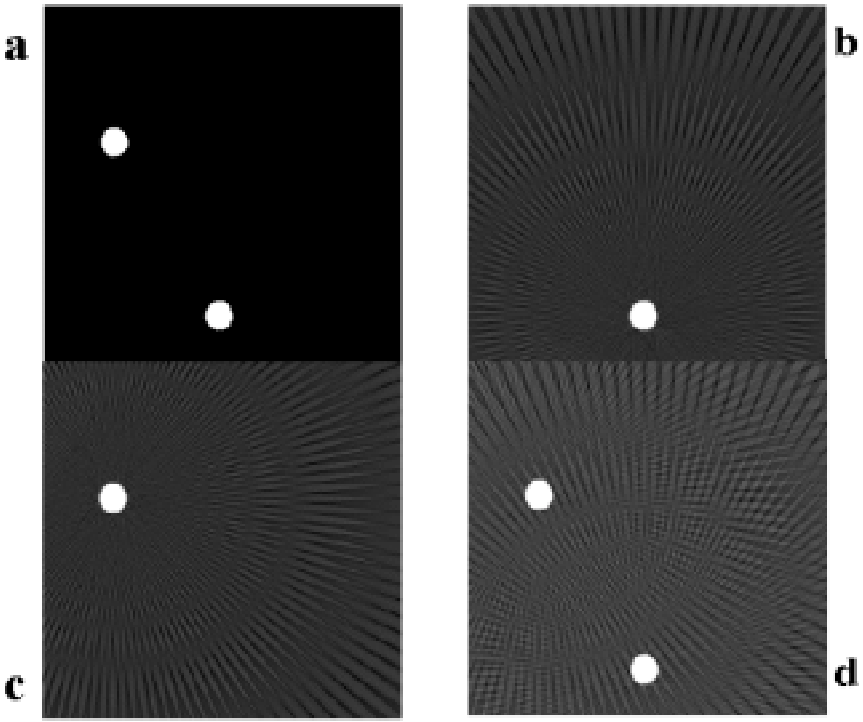

Figure 5.2: *a. Two original objects. b. one object reconstructed using 64 projections and 256 radial resolution. c. the other object. These objects have a alias-free zone around them, providing artifact in all other regions of the FOV. The resolution is unchanged. d. When the objects are reconstructed together, each object provides artifact in the vicinity of the other.*

5.2 Pulse Sequence Implementation

A commercially provided fast 3D gradient echo sequence was modified to collect projections in the kx-ky plane. Fourier-encodings in the kz direction are used for 3D imaging. The pulse sequence is shown in Figure 5.3. The RF is a shortened conventional minimum phase pulse of 1.28 ms duration. Alternatively, a slab-selective asymmetrically truncated sinc RF pulse of 0.5 ms duration was used as shown in Figure 5.3. The z gradient is used for slab selection and phase encoding in the kz-direction. The x and y gradients shown are for prephasing and fractional-echo readout. Also shown are optional gradients to rephase the varying phase accumulation from the readout gradients for each projection angle. High bandwidths (+/-64 kHz) are commonly used to reduce blurring due to off-resonance spins. Since fat is a bright off-resonance signal, undersampling artifacts from this source are reduced by fat suppression. Fat suppression is accomplished using a chemically selective presaturation pulse followed by gradient dephasers, played separately (TR_{fat} = 10 ms) every few TRs. Figure 5.1 shows the radial k-space path. TRs are reduced to their lowest values possible using a Signa Horizon 1.5 T scanner equipped with slew rates of 120 mT/m/sec and 22 mT/m maximum gradient strength. The projections were acquired as fractional echoes at angles through 180 degrees. Flip angles were set near the Ernst angle for T1-shortened blood. At the start of the scan, RF pulses were played out with all gradients on and acquisition disabled.

5.2.1 Disabled Acquisitions

In 3D fast gradient echo sequences, “dummy” RF pulses are played out at the start of the scan to allow the magnetization to equilibrate during these excitations. The signal is not acquired during these disabled acquisitions. In PR, we have found it important to not only play out the RF pulses to saturate the longitudinal magnetization, but also set the gradient amplitudes and cycle the gradient waveforms just as in the beginning of the scan. This is believed to be important due to eddy current effects. Typically about 10 disabled acquisitions are played out.

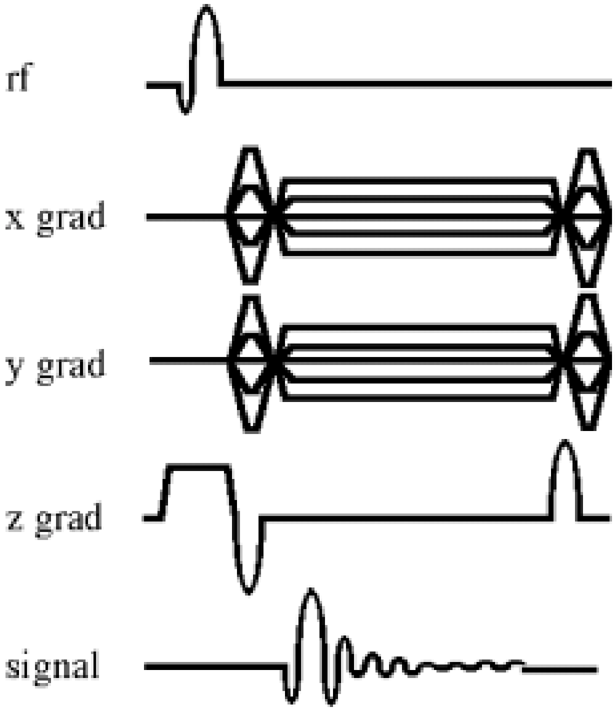

Figure 5.3: *The pulse sequence used for 3D projection reconstruction with slice-encoding in the z direction. The projections are obtained as fractional echoes in the x-y plane.*

5.2.2 Off-Center FOV

With PR sequences, when the center of the FOV (in x-y plane which is resolved with projections) is prescribed away from the physical center of the magnet, the carrier frequency of the receivers must be modified, similarly to changes for FT sequences with off-center FOVs in x. The readout gradients encode the readout position of spins by causing the spin precessional frequency in the readout direction to vary linearly across the FOV from a frequency +BW off the Larmour frequency at one edge of the FOV, and -BW at the other edge. The frequency of spins at a distance d away from the gradient center along the readout direction is $f = \frac{2BWd}{FOV}$.

The center of the FOV is located where the gradient field is zero, and it is fixed in the MR scanner coordinate system (with directions anterior-posterior or AP, right-left or RL and superior-inferior or SI). In the SI direction, the table can be moved so that the prescribed center is placed at the physical z=0 position. Prescribing off-center in SI does not result in an off-center FOV, because the scan table moves instead. However, to prescribe off-center in the A-P or R-L directions, the receiver frequency and phase must be modified.

In order to acquire an F0V centered at an offset point (x0,y0) for a projection at the angle θ the receiver's center frequency is shifted by:

$$\Delta f = \frac{2BW(x_0cos(\theta) + y_0sin(\theta))}{FOV} \tag{5.4}$$

This modification of the receiver frequency is performed in the pulse sequence. For magnitude backprojection this is effective, but it has been found that for complex backprojection, that the reconstruction does not work. This is because the offset receive frequency, while correctly shifting the projection center in image space from (0,0) to (x0,y0), also adds a phase which is constant over the frequency readout, but differs from projection to projection. The receiver is set to receive this frequency offset from the Larmour frequency, and the time between the setting of the receiver frequency and the acquisition of the central k-space point, T_{delay}, creates a phase shift which is applied to the k-space projection:

$$\phi(\theta) = T_{delay}\Delta f(\theta) \tag{5.5}$$

The k-space data for each projection is scaled by the complex number $e^{i\phi(\theta)}$, which causes a projection angle dependent phase error.

T_{delay} is a pulse sequence dependent and scanner dependent quantity: the time between the hardware setting of the receive frequency, and the center of the gradient echo. For the current (1998) Waisman Center scanner, a GE 5X Signa Horizon, for a 3D FGRE sequence, T_{delay} is equal

$$T_{delay} = 106\mu s + Trd1a \tag{5.6}$$

Trd1a is the time between the start of the readout and the echo center.

In summary, when off-center FOVs are prescribed, the receiver frequency must be adjusted as given by Equation 5.5. This shifts the FOV center, but also induces a phase error in each k-space projection. This phase error is projection angle dependent, but independent of kr. It must be removed by multiplying each projection by the constant $exp(-i\phi(\theta))$. This can be performed off-line in reconstruction code, or on the scanner using the routines to set receiver phase. Karl Vigen and Walter Block from our research group have investigated this aspect of off-center FOVs.

5.3 Contrast Enhanced Acquisitions with PR

For contrast enhanced imaging, we present two approaches. As illustrated in Figure 5.4, both approaches acquire projections in the kx-ky plane and slice-encodings in the kz-direction. The two approaches differ only in the order in which k-space data are collected.

5.3.1 ZIPR Acquisition Method

In the first method, ZIPR (kZ-encodings Inside PRojections) (see Figure 5.4), all of the slice-encodings are acquired for each projection prior to incrementing the projection angle. The projection angle is incremented as in spiral x-ray CT. The projections are collected at sequential angles. Acquisition proceeds for a time longer than that required to acquire a single time frame. Multiple time frames can be formed using a sliding temporal window to choose complete sets of projections for reconstruction [105]. Because all kz information is acquired for each projection, typically in 80-200 msec, there is very little contrast-induced modulation in the kz direction. Projection data can be modulated by the contrast curve resulting in angular variations in signal in the x-y plane.

ZIPR data contain an estimate of the average contrast enhancement in the FOV throughout the scan, because a projection is just the sum of all the signal in the FOV. Following the FT in the radial and kz direction, each projection can be used to obtain the total signal in each slice. Except for variations produced by anatomy not present in all projections, this sum is a constant for all projection angles, in the absence of contrast enhancement, i.e.

$$\int P(r,\theta)dr = const.\forall\theta \tag{5.7}$$

If there is contrast infusion, this sum changes with time. Therefore the ZIPR acquisition provides an estimate of the contrast curve with a temporal resolution of $Nz \cdot TR$ (the time between successive projections), typically 150 msec. This provides useful information about the arrival time of the contrast, and indicates

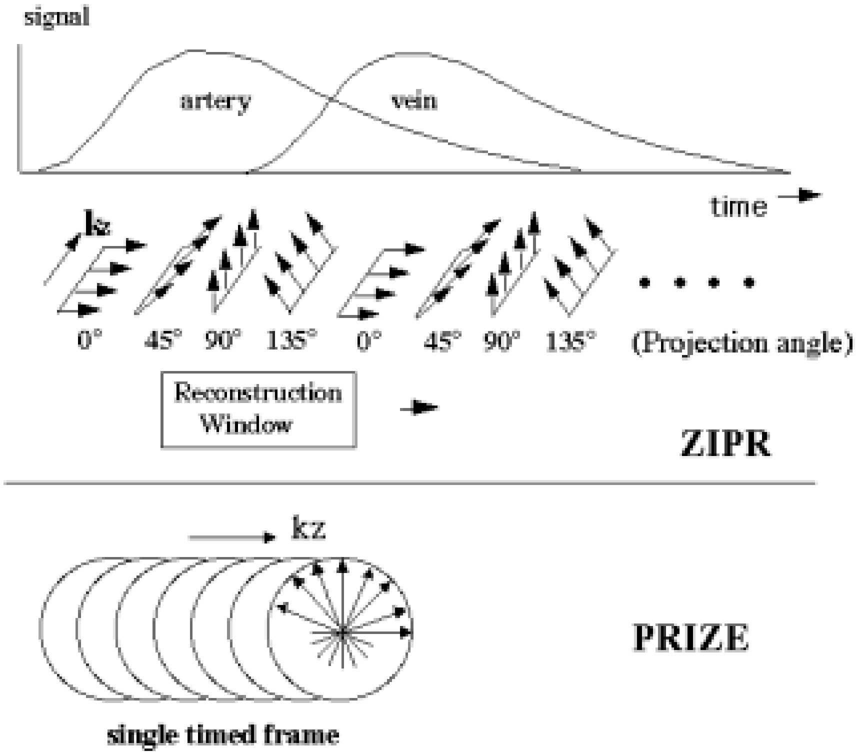
signal
artery
vein
time
kz
0°
45°
90°
135°
0°
45°
90°
135°
(Projection angle)
Reconstruction Window
ZIPR
kz
PRIZE
single timed frame

Figure 5.4: *Two acquisition orders, ZIPR and PRIZE, for 3D PR during first pass of contrast. These acquisition orders were designed for collecting k-space during the infusion of an MRI contrast agent.*

which reconstructed time frames might be optimal.

5.3.2 PRIZE Acquisition Method

In the second method, PRIZE (PRojections Inside kZ-Encodings) (see Figure 5.4), all of the projections are collected for each sequential slice-encoding. Because the entire set of projections is collected for each slice-encoding, there is little contrast modulation in the kx-ky plane; all substantial modulation occurs in the kz-direction. Therefore, contrast-induced artifacts, if present, will appear in the slice direction.

It is essential to time the PRIZE acquisitions so that the center of k-space is acquired during peak arterial contrast, as in conventional FT. This reduces venous contamination and contrast-induced artifacts [117]. In PRIZE, centric kz encoding may be used.

For contrast enhanced PR, weighting of k-space due to contrast passage differs from FT methods because the radial k-space path of PR acquires some high and low spatial frequencies with each TR. For FT imaging, the artifacts caused by modulation of k-space signal due to contrast passage can be serious and have been investigated [117]. They have not been examined previously for PR. Here are presented the results of applying undersampled PR to contrast enhanced MRA using two schemes for acquiring data during contrast infusion.

5.4 Results: Phantoms

To attempt to quantitate the resolution improvement and test our hypothesis that the resolution is independent of the number of projections, we performed resolution phantom experiments. The resolution phantom is shown in Figure 5.5.

A resolution phantom imaged with 512 readout resolution and 128 projections was compared to conventional FT images with 512 readout resolution and 512, 400 or 128 phase encodings. The phantom's smallest pattern contained dots of 0.5 mm width, spaced 0.5 mm apart, the subsequent patterns had spacing and widths of 0.75, 1.0, and 2.0 mm. Magnified views of the resolution pattern displaying resolution in the phase encoding (right-left) direction are shown in Figure 5.6. The undersampled PR image has resolution roughly equivalent to the 512 x 512

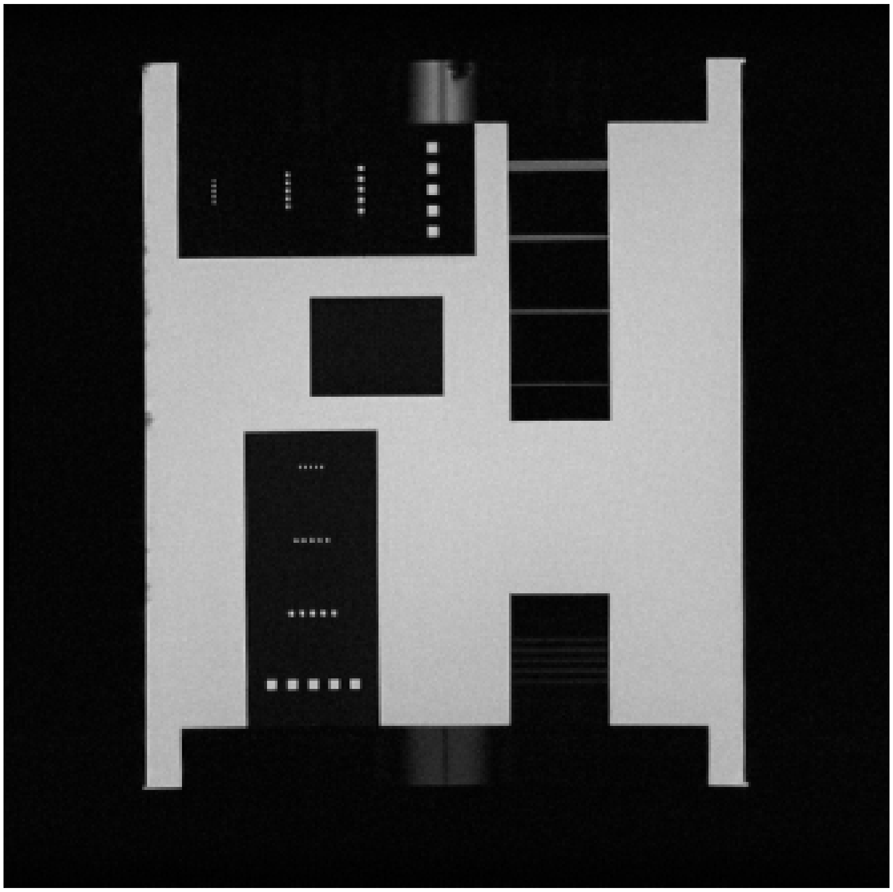

Figure 5.5: *Resolution phantom used to measure resolution. The bar patterns contain squares of width and spacings of 0.5 mm, 0.75mm, 1.0mm, and 2.0mm.*

FT image, even though it was acquired in one fourth of the scan time.

The PR data was reconstructed with regridding, to use the improved MTF of regridding, compared to Backprojection [92]. The FT data was reconstructed without the Fermi-filter (a k-space filter which rolls off high spatial frequencies). However, the comparison is between FT resolution in the phase encoding direction compared to PR, in which all directions are frequency encoded. It is well known that the resolution in the phase encoding direction is higher than the frequency-encoding direction, if all else is equal, because of T2* decay. This may affect the